Experimentelle Physik

Coherence and Perturbed Dynamics in Magnon Bose Einstein Condensates

Inaugural-Dissertation
zur Erlangung des Doktorgrades
der Naturwissenschaften im Fachbereich Physik
der Mathematisch-Naturwissenschaftlichen Fakultät
der Westfälischen Wilhelms-Universität Münster

vorgelegt von
Patryk Nowik-Boltyk
aus *Grudziadz, Polen*
2014

Dekan:	Prof.Dr. Markus Donath
Erster Gutachter:	Prof.Dr. Sergej O. Demokritov
Zweiter Gutachter:	Prof.Dr. Carsten Fallnich
Tag der mündlichen Prüfung:	
Tag der Promotion:	

Zusammenfassung

Die vorliegende Arbeit behandelt intrinsische sowie dynamische Eigenschaften eines Magnon Bose-Einstein Kondensats. Das Kondensat wird erzeugt indem, durch parametrisches Pumpen erzeugte, zusätzliche Magnonen in das thermische Magnonen Gas injiziert werden. Die darauffolgende Thermalisierung dir zusätzlichen Magnonen führt zu einem neuen thermischen Gleichgewicht und resultiert Schlussendlich in der Erzeugung eines Bose-Einstein Kondensats. Als Medium für die Magnonen dient, aufgrund seiner besonders langen Magnon Lebensdauer, ein epitaktisch gewachsener, dünner Yttrium Eisen Granat Film. Brillouin Licht Streuung und magneto-optische, zeitaufgelöste Magnetometrie werden eingesetzt, um die örtliche und zeitliche Verteilung der Magnonen zu bestimmen.

Das erste Experiment dieser Arbeit beweist eindeutig, dass die starke Überbesetzung des Grundzustandes tatsächlich als Bose-Einstein Kondensation identifiziert werden kann. Zu diesem Zweck wurde eine neuartige stroboskopische Methode, basierend auf einer zeitaufgelösten magneto-optischen Magnetometrie, mit einer zuvor unerreichten Frequenzauflösung von unter $200Hz$, angewendet um das Kondensat zu untersuchen. Dieses Experiment hat gezeigt, dass das Kondensat einen hohen Grad an Kohärenz und eine Linienbreite von $2MHz$ bei einer Frequenz von etlichen GHz aufweist, was mit den Eigenschaften, die von einem Bose-Einstein Kondensat erwartet werden, übereinstimmt. Diese Messungen waren notwendig, da alle Messungen die bislang an einem solchen System gemacht worden sind mittels Brillouin Licht Streuung vorgenommen wurden. Diese Methode bietet eine vergleichsweise schlechte Frequenzauflösung. Somit war es bislang nicht möglich zu bestimmen, ob die Magnonen sich tatsächlich im Grundzustand sammeln oder ob sie lediglich Zustände in der Nähe des Grundzustandes besetzen.

Im zweiten Experiment wird der Einfluss der zweifachen Entartung des Magnonen Grundzustandes, in einem dünnen ferromagnetischen Film, auf die räumliche Verteilung des Kondensats untersucht. Die Beobachtung einer inhomogenen räumlichen Verteilung des Kondensats ist ein weiterer Beweis seiner Kohärenz, darüber hinaus belegt dieser Befund die Existenz eines Mechanismus der dafür sorgt dass die Phasen, der beiden Komponenten des Kondensats, eine zeitunabhängige Beziehung zueinander haben. Das Erscheinen stationärer, quantisierter Wirbel legt eine suprafluide Natur des Magnonen Kondensats nahe. Ein phänomenologisches Modell zeigt auf, dass die Wirbel an Kristalldefekte im ferromagnetischen Film gebunden sind.

Im dritten Experiment werden Dichtewellen in einem Magnonen Gas, durch den Einfluss einer zeitlichen und räumlichen Inhomogenität des externen Magnetischen Feldes, angeregt. Es wird hauptsächlich der Einfluss verschiedener experimenteller Parameter auf die Dispersionsrelation dieser Wellen untersucht. Dabei wird er-

sichtlich, dass das Erscheinen eines Bose-Einstein Kondensats, oberhalb einer kritischen Pumpleistung, einen bemerkenswerten Einfluss auf die Dispersionsrelation hat.

Die Beschleunigung eines, räumlich stark beschränkten, Kondensats durch eine Inhomogenität im externen magnetischen Feld ist Gegenstand der Untersuchungen im letzten Experiment. Es wird, basierend auf der Dispersionsrelation der Magnonen, ein Modell vorgeschlagen, welches alle experimentellen Befunde erklären kann.

Abstract

The present work is devoted to intrinsic properties and induced dynamics of a magnon Bose-Einstein condensate (mBEC). The condensate is created via intense parametric pumping which injects additional magnons into the thermal magnon gas. Subsequent thermalization of these additional magnons leads to a new thermal equilibrium and ultimately to the emergence of a Bose Einstein condensate (BEC). A thin yttrium iron garnet (YIG) film epitaxially grown on a gadolinium gallium garnet (GGG) substrate is used as a medium for magnons, due to its extraordinary long magnon lifetime. Brillouin light scattering (BLS) spectroscopy and magento-optical, time-resolved magnetometry are used to determine the lateral and temporal distribution of magnons.

The first kind of experiments presented in this work provides unambiguous experimental confirmation, that the strong over-occupation at the magnon ground state can be identified with a BEC. For this purpose a novel stroboscopic technique, based on time resolved magneto-optical magnetometry, providing unprecedented frequency resolution of below $200Hz$ was applied to study the condensate. The experiment has revealed a high degree of coherence of the condensate with a linewidth below $2MHz$ at the level of several GHz, corroborating the existence of mBEC. This experiment is necessary since all measurements, on such a system, reported so far utilized BLS which has a relatively poor energy resolution. Therefore it was not possible to determine whether the peak at the ground state originates from the lowest energy state or from energy states close to the ground state.

The second experiment examines the impact of the double degeneracy of the magnon ground state, in a thin ferromagnetic (FM) film, on the lateral distribution of the condensate. The observation of a non uniform lateral condensate distribution is another proof for the coherence of the two condensate components and a phase locking between them. The emergence of stationary quantized vortices in the ground state strongly suggests a superfluid nature of the magnon gas. A phenomenological model reveals that the vortices are pinned to crystalline defects in the YIG-film.

In the third experiment density waves are excited in a magnon gas by means of an inhomogeneity in the external magnetic field. The impact of several experimental parameters on the dispersion relation of these waves is the main subject of investigation here. It will be shown that the emergence of a BEC above a certain pumping power has a striking impact on the dispersion.

The acceleration of a strongly confined Bose-Einstein condensed magnon gas through an external field inhomogeneity will be demonstrated in the last experiment. A proposed model based on the magnon dispersion relation is capable of explaining all observed effects.

Contents

1 Introduction

Spin waves as the elementary excitations of a ferromagnet have been introduced by Bloch in 1930 [1] in order to describe the progression of the magnetization of a magnetic material as a function of temperature, nowadays known as the Bloch $T^{3/2}$-law. It has been found that spin waves have a characteristic frequency in the GHz range, hence they are easy to excited and detect by means of microwave techniques. Due to these properties spin waves have extensively been studied since the 1960's [2, 3, 4]. Theoretical models describing interactions of spin waves with microwave radiation have been reported shorly thereafter [5, 6, 7, 8]. However the examination of spin waves by means of microwave techniques was restricted to the observation of spin waves with very small wave vector. With the advent of magneto-optical detection of spin waves, it became possible to observe spin waves with larger wave vectors as well, in addition information about the spatial distribution, temporal evolution and wave vector becam accessible [9, 10, 11].

A microscopic theory of spin waves that accounts for the quantum-mechanical nature of spins has been developed and Holstein and Primakoff [12]. Their considerations gave rise to the concept of magnon as the elementary excitation of a ferromagnet. Magnons are spin flips that are distributed over many lattice sites. They can in many ways be treated as particles and belong therefore to the class of quasi-particles. Kinetic theories that deal with interactions between magnons have been developed by Dyson [13] and Oguchi [14]. Since excitation of one magnon reduces the total spin of the system by one, the system of magnons in a ferromagnet can be treated as a gas of particles with spin one.

In 1925 Bose [15]and Einstein [16] developed the quantum-statistical theory which describes the distribution of particles with integer spin among the accessible energy states resulting in the Bose-Einstein distribution. Einstein realized that this distribution function implies a phase transition which occurs when the density of the gas is strongly increased. This phase transition is known as Bose-Einstein condensation (BEC). The first observation of a BEC in dilute atomic vapors was done by Anderson *et.al.*[17] and Davis *et.al.*[18] in 1995. However effects like superconductivity [19] and superfluidity in liquid helium [20] of whom it is known that they are closely related to BEC have been observed long before the first realization of BEC in atomic vapors.

It has been predicted by Kalafati, Safonov and Melkov that a system of magnons

can as well undergo a phase transition into the Bose condensed state [21, 22, 23]. In 2006 Demokritov *et.al.*confirmed this prediction by measuring the distribution function of magnons after a large amount of magnons with a specific energy has been injected into the system [24]. Subsequent investigations strengthened their claim and revealed unique properties of this new state of the magnonic gas[25, 26, 27, 28, 29]. Theoretical models of this new state where established shortly thereafter [30, 31, 32, 33].

The present work is organized as follows.

Chapter 2 is devoted to general concepts of magnetism and magnetic ordering, as well as to elementary excitations of the latter. Together with the interactions of magnons with each other and with the enviorment, this chapter provides a basic understanding of the processes that appear in a gas of magnons.

The fundamental concepts of Bose-Einstein condensation are the subject of chapter 3. This chapter gives also a overview of Bose-Einstein condensation in various physical systems and a scetch of the mechanisms that lead to Bose-Einstein condensation in a magnon gas.

Chapter 4 presents the experimental techniques that where used and results that have been obtained, in the investigation of intrinsic features and the properties of dynamic excitations, in a Bose-Einstein condensed magnon gas.

2 Spin-Waves and Magnons

In this section a brief outline of the elementary magnetic excitations in a magnetic material, called spin waves, will be given. It starts off with a section about atomic magnetism, the very origin of magnetism in materials, which will be treated in the subsequent section. After this very general introductory part a closer look at the concept of spin waves will be made, followed by the spin wave dispersion relation in unbound media and in the special geometry of a thin film. The thin film geometry is of particular interest as all measurements in this work where done on thin ferromagnetic (FM) films. This part is followed by a survey of several methods that can be used to excite spin waves in a FM. All this is done in a semi classical treatment where the magnetic moment is treated as a classical vector.

The quantum mechanical treatment is in focus of the subsequent parts of this section. The concept of magnons, the quanta of spin waves, will be introduced and it will be shown, that spin waves can in many aspects be treated as a gas of particles. The interaction of these particles with each other and with their environment, especially the crystalline lattice and electromagnetic (em) radiation, is the topic of the last parts of this section.

2.1 Origin of magnetism and magnetic ordering

2.1.1 Atomic Magnetism

There are several sources for the magnetic moment of an atom. All of them are based on a quantum mechanical model thereof. The full quantum mechanical treatment is of course the one that gives the deepest insight into the underlying physics. However this treatment is very time and space consuming, hence a semi classical approach will be outlined in this section as it gives sufficiently good insight without being too elaborate.

The dominant contribution to the magnetic moment of an atom arises from its electron shell. In general the magnetic moment of an electron that is bound to a nucleus is given by

$$\vec{\mu} = \mu_B \frac{g}{\hbar} \vec{J} \tag{2.1}$$

with the Bohr magneton $\mu_B = \frac{e\hbar}{2m_e}$, the electron mass m_e and charge e, the g-factor g, the reduced Planck's constant $\hbar$ and the total angular momentum $\vec{J} = \vec{L} + \vec{S}$. Where the vector $|\vec{L}| = \sqrt{l(l+1)}\hbar$, with the azimuthal quantum number l, represents the orbital momentum and $|\vec{S}| = \sqrt{s(s+1)}\hbar$, with the spin quantum number s, the spin of the particle. The spin quantum number can only attain the value $s = \frac{1}{2}$ whereas the orbital angular momentum can have several values, depending on the principal quantum number of the electron $l = 0 \ldots (n-1)$. The absolute value of the total momentum is given by $|\vec{J}| = \sqrt{j(j+1)}\hbar$ with the quantum number of the total angular momentum $j = |l \pm s|$.

In the presence of an external magnetic field real space attains a preferred direction which is given by the direction of the external magnetic field. It is well known from quantum mechanics, that two components of a momentum operator are indeterminate while one, parallel to a preferred direction, is quantized. In this case only a momentum parallel to the external magnetic field can be determined through

$$\mu_z = \mu_B \frac{g}{\hbar} m_j \tag{2.2}$$

with the magnetic quantum number $m_j = -j \ldots 0 \ldots . \ldots j$. These formulas display the magnetic moment of an electron, that is characterized by the quantum numbers n, l, s, j, m_j. The whole magnetic moment of an atom is given as a superposition of the momenta from all its electrons. An atom with a non-zero magnetic moment is called **paramagnetic**.

It is apparent, that μ_z can either be positive or negative, hence a superposition of the magnetic moments of all electrons can in some cases lead to a complete annihilation of them. As a consequence atoms exist, that have no permanent magnetic moment at all. These atoms are called **diamagnetic**. Nevertheless diamagnetic atoms have a certain respond to a magnetic field. In the presence of a magnetic field a magnetic moment is induced in the atom, whose direction is opposite to the external field. This behavior of diamagnets can be explained with Lenz's law which states that

A change in magnetic flux induces an electric field such that a current which is caused by this electric field generates a magnetic field which counteracts its cause.

This way an external magnetic field causes changes in the movement of electrons in the atom which in turn generate a magnetic field that is oriented antiparallel to the external one. All atoms exhibit such an effect, however the induced magnetic moment is usually much smaller than the smallest magnetic moment arising from spin and orbital momentum thus it can usually be neglected in paramagnetic atoms.

It is also worth noticing that the nucleus of an atom has also a magnetic moment in general. However its value is at least three orders of magnitude smaller than the

permanent moment of the electron shell and still much smaller than the induced moment in a diamagnet and can therefore be neglected.[34]

2.1.2 Magnetic ordering in materials

The general respond of a material, that contains a large amount of atoms, on a external magnetic field can be written in the form

$$\vec{B_{in}} = \vec{B_{ext}} + \chi \vec{B_{ext}} = \vec{B_{ext}} + \vec{M} \tag{2.3}$$

Here $\vec{B_{in}}$ is the internal magnetic field, $\vec{B_{ext}}$ the external magnetic field and the tensor χ called magnetic susceptibility is a material parameter. Since χ is a tensor, the magnetization $\vec{M}$ and the external field $\vec{B_{ext}}$ must not necessarily be parallel to each other. Nevertheless in many materials and geometries they are parallel and χ can be regarded as a scalar.

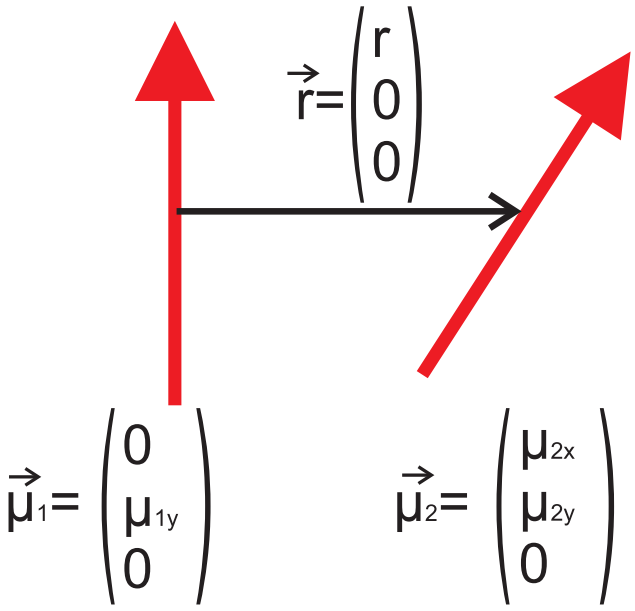

Figure 2.1: Two magnetic dipols $\vec{\mu}_1$ and $\vec{\mu}_2$ with different orientations that are separated by the vector $\vec{r}$.

In a material that consists of diamagnetic atoms the external magnetic field is weakened inside the material due to the antiparallel alignment of the induced magnetic moments with respect to the external field, hence $\chi < 0$. The behavior of materials that consist of paramagnetic atoms is much more complicated. It depends on the interactions between the magnetic moments in the material. In most cases

χ is greater zero, hence an external magnetic field is enhanced inside such a material, but there are also cases in which materials that consist of paramagnetic atoms behave as if they where made of diamagnetic atoms. These phenomena are in the focus of the next paragraphs.

Inside a paramagnetic material the magnetic moments of different atoms interact with each other through their magnetic field. The magnetic field of a magnetic moment $\vec{\mu}$ at the position $\vec{r}$ is given by

$$\vec{B}_d(\vec{r}) = \frac{\mu_0}{4\pi r^5}[3\vec{r}(\vec{r}\cdot\vec{r}) - \vec{\mu}r^2] \tag{2.4}$$

with the vacuum permeability μ_0. A second magnetic moment that is placed in a magnetic field in turn experiences a torque $\vec{\tau} = \vec{\mu} \times \vec{B}$. By putting the two formulas together one gets the torque that is exerted on a dipole through the magnetic field of another dipole. The relation, in the geometry shown in figure 2.1, is given by

$$\vec{\tau}_{DD} = -\frac{\mu_0}{2\pi r^3}\mu_{1y} \cdot \mu_{2x}\hat{e_z}. \tag{2.5}$$

As long as the two magnetic moments are not parallel to each other there is a torque which tries to minimize the non-parallel component. In order to judge whether the parallel or antiparallel configuration is preferred one can calculate the potential energy

$$E_{DD} = -\frac{\mu_0}{4\pi r^3}\mu_{1y}\mu_{2y} \tag{2.6}$$

This energy is minimized when μ_{1y} and μ_{2y} have opposite signs hence when the magnetic moments are antiparallel. As a consequence the dipole-dipole interaction between magnetic moments leads to a antiparallel alignment.

Materials with an antiparallel alignment of their magnetic moments are called **antiferromagnets** when all moments have the same strength. In this case there is no magnetization present in the absence of a magnetic field because the individual moments cancel each other out. When an antiferromagnet is placed into a magnetic field the material behaves like a diamagnet, as long as the field is not strong enough to overcome the antiparallel alignment. When the external field however becomes strong enough, all magnetic moments align parallel to the external field and the magnetization makes a jump towards positive values.

A material can also consist of different atoms with different magnetic moments. Nearest neighbors will again align antiparallel to each other, however, due to different

values of the magnetic moments there will remain a magnetization even without external magnetic field applied. These Materials are called **ferrimagnets**.

One can estimate the energy difference between parallel and antiparallel alignment. Atomic magnetic moments have the order of magnitude of the Bohr magneton μ_B [35]. And the distance between neighboring moments amounts approximately $1nm$. Hence the energy difference has order of magnitude

$$E = -\frac{2\mu_0\mu_B^2}{4\pi r^3} \approx 100\mu eV \tag{2.7}$$

This energy is equivalent to a temperature of $T = E/k_B \approx 1.2K$ with the Boltzmann constant $k_B = 8.617 \cdot 10^{-5} eV/K$. As a consequence thermal fluctuations at a temperature above $1.5K$ will destroy any ordering that is caused by dipolar interactions. Hence according to this theory most materials, made of paramagnetic atoms, at a temperature above $1.2.K$ should exhibit purely paramagnetic behavior without any influence from ordering.

On the other hand it is known, that most materials, which consist of paramagnetic atoms, exhibit a magnetic ordering well above $1.2K$. The magnetic ordering is, in this case, evoked through a second interaction that acts between magnetic dipoles: The so called exchange interaction. It is based on the Coulomb interaction between charged electrons and the symmetrization postulate for identical particles, but finally leads to magnetic ordering. When electron orbitals of adjacent atoms overlap, the potential energy of the electrons, due to Coulomb interaction between them, depends on their mutual spin orientation. This fact arises directly from the symmetrization postulate. For fermionic particles like electrons the postulate states that their total wave-function $\Psi(r_1, s_1, r_2, s_2) = \Phi(r_1, r_2)\sigma(s_1, s_2)$ must be anti-symmetric with respect to particle exchange. Hence if the spins are aligned parallel ($s_1 = s_2$) σ is symmetric hence Φ must be anti-symmetric and vice versa when they are aligned antiparallel. Consequently the potential energy $E = \hat{H}\Psi$ will have different values for the two orientations [36]. Since the exchange interaction arises only when electron orbitals overlap, the range of this interaction is very small and can be considered as acting only between nearest neighbors.

Strictly speaking the exchange interaction results in an energy difference between parallel and antiparallel alignment of adjacent magnetic moments which can be either positive or negative. If it is positive the parallel alignment is favorable in the other case when it is negative the antiparallel alignment is favorable. Calculation of the value of the exchange energy is rather complex. Its value depends on the overlap of electron orbitals which contribute to this interaction. However it turns out that in many cases this energy is high enough to maintain a magnetic ordering up to higher temperatures. The temperature at which an antiferromagnetic or ferrimagnetic

material looses its magnetic ordering is called Neel Temperature T_N. For negative values of the exchange energy the resulting magnetic ordering is the same that has been discussed for the dipolar interaction with the difference that ordering caused by exchange interaction remains up to higher temperatures.

In materials with positive exchange energy, another type of ordering arises. These materials are called **ferromagnets**. Due to the parallel alignment of their magnetic moments FM's have a large net magnetization without external field as long as their temperature is below the Curie temperature T_C.

2.2 Spin Waves

From a thermodynamical point of view a material makes the transition into a magnetically ordered state in order to minimize its free energy. A thermodynamic system will always try to reduce its free energy which is given by

$$F = E - TS. \tag{2.8}$$

The free Energy is a function of the inner Energy E and the Entropy S times temperature T. It is apparent that there are two competing influences on the free energy. In a microscopic system the energy of a system has to be minimized in order to get a stable state. In macroscopic systems, which consist of many particles, the situation is different. At zero temperature the condition to attain a stable or equilibrium state are identical for microscopic and macroscopic systems. At finite temperatures they differ from each other by the fact that in a macroscopic system the state with lowest inner energy is usually also the one with highest ordering and therefore lowest entropy. Nevertheless there exist a lot of cases where the loss of entropy is compensated by a much higher loss of inner energy such that the free energy can be minimized in an ordered state. Apparently this is the case in magnetically ordered materials well below the Curie or Neel temperature.

From this consideration it is apparent that the absolutely ordered state is not the one with lowest free energy, although it is, in most cases, the one with the lowest inner energy. Hence it can be favorable that a few magnetic moments of the ordered magnetic material are flipped increasing entropy by ΔS and potential energy by ΔE. However when $T\Delta S > \Delta E$ the free energy is reduced leading to a new stable state.

A flipped magnetic moment would however never stay localized. Adjacent magnetic moments will be influenced by it through exchange interaction and even distant moments would feel the flip through dipolar interaction. The resulting excitation is a magnetization wave. Since in many FM materials the magnetization is caused solely by the electron spin the term **spin wave** is much more common.

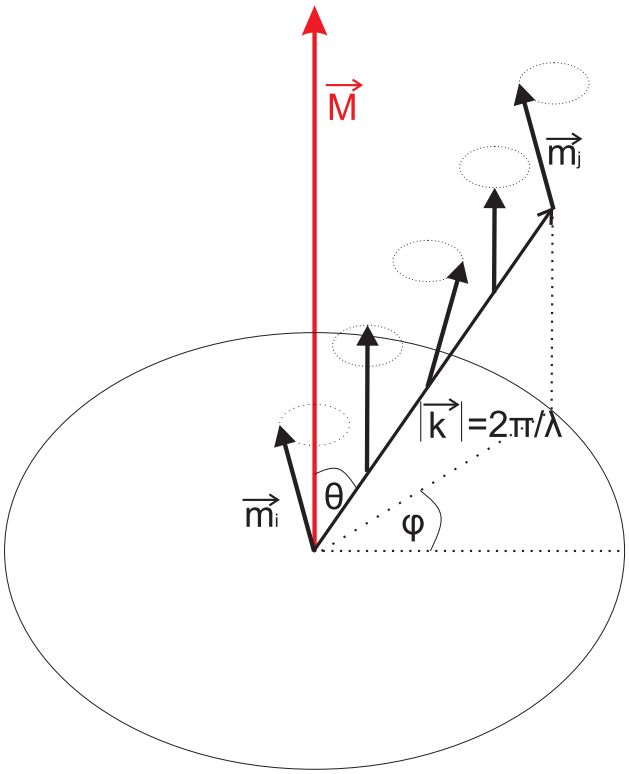

Figure 2.2: Nonuniform magnetization precession in a unbound FM. The moments in the FM precess with the same frequency at different phases. Moments at m_i and m_j precess with the same phases hence the wave vector $\vec{k}$ which connects them has a length of $|\vec{k}| = 2\pi/\lambda$ with the wavelength of the spin wave λ. In general λ is a function of θ. Due to the rotational symmetry of the system there is no dependence on ϕ.

In a spin wave spins are deflected from their equilibrium position by a certain angle and precess around the equilibrium position with a certain frequency f. If all moments precess in phase the excitation is called ferromagnetic resonance (FMR). Additionally there are also spin waves in which the moments do not precess in phase. Instead neighboring moments precess at different phases. The distance at which the next moment with the same precession phase is located is called the wavelength λ of the spin wave. In general it depends on the angle θ between the vector which connects the two moments and the external magnetic field (see figure 2.2).

The dependence of the angular frequency $\omega = 2\pi f$ on the wave vector $\vec{k}$ is called dispersion relation of spin waves. In an unbounded isotropic FM magnetized to saturation by an external field B_0 the dispersion relation can be written

$$\omega^2 = (\omega_H + \omega_M \lambda k^2)(\omega_H + \omega_M D k^2 + \omega_M \sin^2(\theta)) \tag{2.9}$$

with $\omega_H = \gamma B_0$, $\omega_M = \gamma \mu_0 M_S$, where M_S is the saturation magnetization, and the exchange constant D [37].

This dispersion relation can be derived from the equation of motion of a macroscopic magnetization in a magnetic field. Neglecting losses due to interactions between the magnetic system and the crystalline lattice the equation of motion can be written as

$$\frac{\partial \vec{M}}{\partial t} = -\gamma \vec{M} \times \vec{B} - \frac{\zeta}{M_S} \vec{M} \times (\vec{M} \times \vec{B}) \tag{2.10}$$

The form was proposed by Landau and Lifshitz in 1935. It does not deal with individual elementary magnetic moments or spins, but divides a FM material into cells which contain several elementary magnetic moments such that the vector $\vec{M}$ is given by $\vec{M} = \frac{\sum_i \vec{m}_i}{V}$ where V is the volume of the cell and the sum goes over all magnetic moments in the cell. The first term in this equation describes a torque that is exerted on the magnetization due to a field $\vec{B}$ whereas the second term describes the relaxation into its equilibrium position due to damping described by the phenomenological constant ζ. In a real system different interactions exert torques on the magnetic moment. This fact is accounted for by the introduction of an effective magnetic field $\vec{B}_{eff}$ whose components represent the contributions from different effects

$$\vec{B}_{eff} = \vec{B}_0 + \vec{B}_{ex} + \vec{B}_M + \vec{B}_{an} \tag{2.11}$$

$\vec{B_0}$ is the externally applied magnetic field, $\vec{B_{ex}}$ is the field that arises from exchange interaction, $\vec{B_M}$ is the field that arises from the magnetization[1] and $\vec{B_{an}}$ is the field that is caused by the crystalline anisotropy of the FM.

This approach has the advantage of being rather simple in concept and in mathematics but gives wrong results when one considers length scales that are of the order of the distance between elementary magnetic moments. This problem can be overcome by a microscopic theory which will be presented later.

In the derivation of equation 2.9 the magnetization and the effective field are split into two components

$$\begin{aligned} \vec{M} &= \vec{M_0} + \vec{m} \exp(i(\omega t + \vec{k}\vec{r})) \\ \vec{B} &= \vec{B_{eff}} + \vec{b_{eff}} \exp(i(\omega t + \vec{k}\vec{r})) \end{aligned} \tag{2.12}$$

[1] This field causes the dipole-dipole interaction.

$\vec{M_0}$ is the static part of magnetization and $\vec{m}$ the dynamic part that precesses with angular frequency ω. The same applies for the field $\vec{B_0}$ which is the static part of the effective field and $\vec{b_{eff}}$ its dynamic part that originates from the movement of spins hence it has the same time dependence.

In the linear approximation it is assumed that $|\vec{m}| << |\vec{M_0}|$, $|\vec{b_{eff}}| << |\vec{B_{eff}}|$ and that the FM is magnetized to saturation, hence $|\vec{M_0}| = |\vec{M_S}|$ and $\vec{B_{eff}}$ and $\vec{M_0}$ point in the same direction. Consequently after substituting ansatz 2.12 into the equation of motion 2.10 all higher order terms in $\vec{m}$ and $\vec{b_{eff}}$ can be neglected and one arrives at the equation

$$i\omega\vec{m} + \omega_H\vec{m} \times \vec{z_0} + \frac{\omega_M}{\mu_0}\vec{z_0} \times \vec{b_{eff}} = 0 \tag{2.13}$$

z_0 is the unity vector in the direction of $\vec{M_0}$ and $\vec{B_{eff}}$. In order to evaluate this formula it is necessary to obtain an expression for the dynamic component of the effective field. The external field is static in these considerations. Hence the dynamic component can only arise from $\vec{B_M}$ and $\vec{B_{ex}}$. The dynamic component of $\vec{B_M}$ can be found by substituting ansatz 2.12 into the magnetostatic Maxwell equations $\vec{\nabla} \times \vec{b} = \vec{\nabla}\vec{b} = 0$. This results in

$$\vec{b_M} = -\frac{\mu_0}{k^2}\vec{k}(\vec{m}\vec{k}). \tag{2.14}$$

The dynamic component of the field originating from exchange interactions is given by [37]

$$\vec{b_{ex}} = -Dk^2\vec{m} \tag{2.15}$$

Substituting 2.14 and 2.15 into 2.13 and setting the determinant, of the system of linear equations for the components of $\vec{m}$, to zero one finally arrives at the dispersion law 2.9. [38]

2.2.1 Spin- Wave dispersion relation in thin Films

In reality a FM medium is never extended to infinity, instead it has finite dimensions. The sample geometry gives rise to demagnetizing fields additionally boundary conditions, at the boundary between material and vacuum, for the magnetic field have to be taken into account. These effects alter the spin wave dispersion relation in a finite FM sample with respect to the case of an unbound one. However the changes are significant only for $k \ll 2\pi/l$, where l is a characteristic dimension of the sample.

This is derived from the fact that for spin waves with larger wave vectors the sample appears as being infinite.

In most experiments, regarding the observation of spin waves in a FM, the geometry is a thin film[2]. The phrase "thin film" means that one dimension of the sample is much smaller than the other two which are usually regarded as being infinite. In this case the thickness of the film is the characteristic length scale of the sample.

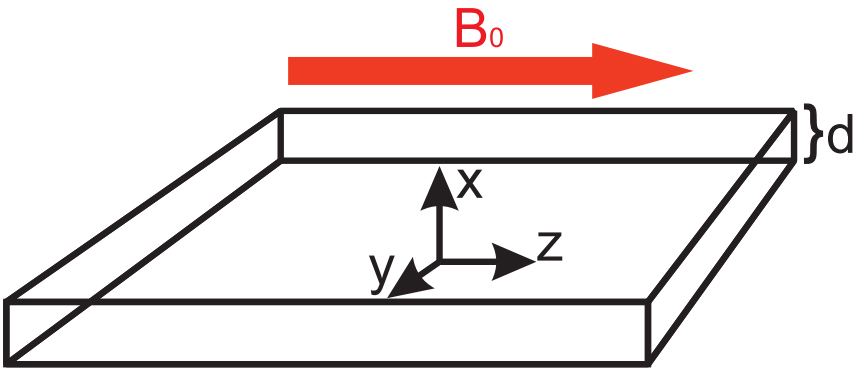

Figure 2.3: Geometry of a thin film.

The demagnetizing field of a FM with arbitrary shape can be written as

$$\vec{H}_{dem} = \overleftrightarrow{N}\, \vec{M} \tag{2.16}$$

The demagnetization tensor $\overleftrightarrow{N}$ is determined by the geometry. It is symmetric and diagonal for an ellipsoid of evolution when the axes of the coordinate system coincide with the axes of the ellipsoid. Calculation of demagnetization tensors is generally a difficult task. Fortunately the calculation turns out to be easy in the case of a thin film magnetized in plane, with the small dimension oriented along the x-axis of a Cartesian coordinate system. In this case the tensor has the form

$$\overleftrightarrow{N} = \begin{pmatrix} 4\pi & 0 & 0 \\ 0 & 0 & 0 \\ 0 & 0 & 0 \end{pmatrix} \tag{2.17}$$

It is apparent that a demagnetizing field occurs only in the case when the magnetization is aligned parallel to the x-axis. When the magnetization points along the z- or y-axis however no demagnetizing field occurs. The effects of boundary conditions

[2]Sometimes called slab.

on the dispersion relation of spin waves in a thin FM film has been evaluated by Damon and Eshbach in 1961 [39]. In their considerations exchange interactions where neglected and only dipolar interactions between spins where taken into account. The dispersion relation obtained under these circumstances cannot be written in explicit form anymore but becomes implicit. It is found that the connection between wave vector components k_y, k_z and angular frequency $\omega = 2\pi f$ of a spin wave can be found by solving the equation

$$(1+\eta^2) + 2\sqrt{1+\eta^2}\sqrt{-\frac{1+\eta^2+\kappa}{1+\kappa}}(1+\kappa)\cot\left[|k_y|d\sqrt{-\frac{1+\eta^2+\kappa}{1+\kappa}}\right] + (1+\kappa)^2\left(\frac{1+\eta^2+\kappa}{1+\kappa}\right) - \nu^2 = 0 \tag{2.18}$$

Whereas the value of k_x for a given pair k_y, k_z can be obtained by solving

$$(1+\eta^2) - 2|\sqrt{1+\eta^2}|\frac{k_x k_z}{k_y k_t^2}\cot(k_x d) - \left[\frac{k_x k_z}{k_y k_t^2}\right]^2 - \left(\frac{k}{k_t}\right)^4\left(1+\frac{k_t^2}{k^2\omega_H}\right) = 0 \tag{2.19}$$

with

$$\begin{aligned} \eta &= \frac{k_z}{k_y} \\ \kappa &= \frac{\omega_H\omega_M}{\omega_H^2+\omega} \\ \nu &= \frac{\omega\omega_M}{\omega_H^2+\omega} \\ k_t^2 &= k_x^2 + k_y^2 \\ k^2 &= k_x^2 + k_y^2 + k_z^2 \end{aligned} \tag{2.20}$$

For $(1+\kappa) < 0$ all wave vector components, including k_x, are imaginary leading to a oscillatory behavior of dynamic magnetization inside the sample in all spatial dimensions. These modes are called "volume modes". In contrast for $(1+\kappa) > 0$, k_x becomes imaginary which results in an exponential decay of dynamic magnetization with distance from the surface therefore these modes are called "surface modes".

The cotangent function is a periodic function whose values range from $-\infty$ to ∞ an infinite set of solutions exists for a given η and k_y. Each solution corresponds to a different spin wave mode characterized by different profiles of dynamic magnetization along the x direction. In the case of surface waves the argument in the cotangent function becomes imaginary and it can be replaced by a cotangent hyperbolic function. The cotangent hyperbolic function is monotonous function, hence

for each value of k_y and k_z only one solution exists consequently there is only one spin wave mode. The value of the imaginary k_x depends on the value of η. For $\eta > \sqrt{\frac{\omega_M}{\omega_H}}$ it becomes infinite, leading to a uniform distribution of dynamic magnetization across the sample. For smaller values of η, k_x decreases, leading to a confinement of the dynamic magnetization at one surface.

In the simplest case $k_y = 0 \Rightarrow \eta \to \infty$ equation 2.18 reduces to

$$2\cot\left(|k_z|d\sqrt{-\frac{1}{1+\kappa}}\right) = \frac{\kappa}{\sqrt{-(1+\kappa)}} \tag{2.21}$$

Although the theory of Damon and Eshbach, in its original form, accounts only for dipolar interactions between spins, exchange interactions can be included very easily. From the considerations in section 2.2 it turns out, that it is sufficient to introduce a new effective magnetic field

$$B_{eff} = B_0 + \mu_0 M_S D k^2 \tag{2.22}$$

The additional term in the effective field becomes important only for large wave numbers. Since in this limit the dispersion relation in the confined medium should coincide with that of an unbound medium this substitution can also be introduced in Damon Eshbach theory as long as D is not too large as to affect the dispersion relation at $k \ll 2\pi/d$, which is given in most materials. The substitution ensures that for large wave numbers $\omega \propto k^2$.

At this point it should be mentioned that there exists also a spin wave theory that contains both exchange and dipolar interactions and leads to an explicit form of the dispersion relation. This theory have been developed by Slavin and Kalininkos [40, 41] using normal mode theory. Although this theory is well suited to calculate the dispersion relation of volume modes with small k_x, it cannot render surface waves and gives wrong results for large k_x. Moreover k_x is in this theory solely determined by the mode number, whereas in Damon Eshbach theory k_x depends on the mode number as well as on the value of k_y and k_z.

2.2.2 Excitation of Spin Waves

Spin waves are present in all materials with magnetic ordering at temperatures above absolute zero. They are excited by means of thermal excitation and lead to a reduction of the free energy of the magnetically ordered material. Apart from these "thermal" spin waves, additional spin waves can be excited in such a material through various mechanisms. This section concentrates on excitation of spin waves with the

aid of alternating magnetic fields originating from em radiation with microwave frequencies.

The simplest way to excite spin waves is by means of direct excitation of magnetization precession through a spin wave antenna. A spin wave antenna is a piece of a conductor with a width of typically $10 - 50\mu m$ in close proximity to a FM. An alternating current that is send through this antenna creates an alternating magnetic field which in turn causes spins to precess with the same frequency. A necessary condition is that the excitation frequency is sufficiently high, namely higher than the frequency gap in the spin wave spectrum given by the Zeeman energy. Due to exchange and dipolar interactions the precession of magnetization spreads laterally, leading to a spin wave. Mathematically the driving field appears as a part of the effective dynamic part $\vec{b}_{eff}$ in equation 2.13.

However this process has several serious limitations. First of all the so produced spin waves cannot have a wave number that is greater than $k_w = \frac{2\pi}{w}$ where w denotes the width of the antenna. This can be understood intuitively, since all magnetic moments that are excited directly by the field of the antenna precess in phase, hence the area in which spins are excited directly specifies a wave number. As a consequence the antenna width specifies a wave number range. On the other hand the same argument leads to the fact that the angle between antenna and external field specifies the angle between the wave vector of the excited spin wave and the external magnetic field.

Spin waves that are created with this technique have the same frequency as the exciting alternating current. However there exist also processes in which the excited spin waves precess with half of this frequency. These processes are nonlinear and are the subject of the following sections.

Perpendicular Pumping

Another possible excitation mechanism is the so called parametric pumping process. Instead of exciting one specific spin wave mode, several modes with the same frequency but different wave vector and propagation direction are excited. A distinction is made between parallel pumping, perpendicular pumping and the general case of oblique pumping which contains parallel as well as perpendicular pumping processes.

The perpendicular pumping process is based on nonlinear coupling between different spin wave modes. If we assume a magnetization of the form

$$\vec{M} = M_0\hat{e}_z + \vec{m}_(\vec{r}, t) \tag{2.23}$$

and choose the Fourier transformed representation for the ac component of the magnetization

$$\vec{m}(\vec{r},t) = \sum_{\vec{k}} \vec{m}_{\vec{k}}(t) \exp(-i\vec{k}\vec{r}) \tag{2.24}$$

with the components of $\vec{m}_{\vec{k}}(t)$ now being complex $\vec{m}_{\vec{k}}(t) = \vec{m}^*_{-\vec{k}}(t)$ and substitute this ansatz into the Landau-Lifshitz equation of motion 2.10 together with the effective field $\vec{H}_{eff} = \vec{H}_0 + \vec{h} + \vec{h}_M + \vec{H}_{ex}$, where H_0 contains the static external and demagnetizing field, h represents the alternating component of the external field, h_M is the alternating demagnetizing field and H_{ex} the effective field of the exchange interaction, neglecting losses one arrives at two differential equations

$$-i\frac{da_0}{dt} = \omega_0 a_0 - \gamma(h_x + ih_y) + \Omega_{n0} \tag{2.25}$$

$$-i\frac{da_k}{dt} = (A_k + \gamma h_z)a_k + B_k a^*_{-k} + \Omega_{nk} \tag{2.26}$$

with

$$a_k = \frac{1}{M_0}(m_{\vec{k}x} + im_{\vec{k}y)} \tag{2.27}$$

$$a^*_{-k} = \frac{1}{M_0}(m^*_{-\vec{k}x} + im^*_{-\vec{k}y)} \tag{2.28}$$

$$A_k = \omega_H + Dk^2 + \frac{1}{2}\omega_M \sin^2(\theta_k) \tag{2.29}$$

$$|B_k| = \frac{1}{2}\omega_M \sin^2(\theta_k) \tag{2.30}$$

The terms Ω_{n0} and Ω_{nk} contain higher order mixed terms in a_k, a^*_k including a_0. Therefore they are responsible for the interactions of different modes with each another. For later comparison it should be mentioned at this point, that the k and $-k$ terms can be decoupled by a transformation similar to the third Holstein-Primakoff transformation. Perpendicular pumping means that the alternating part of the external field has no component in z-direction, hence $h_z = 0$. This leads to

$$\begin{aligned} \frac{dc_k}{dt} &= i\omega_k c_k \\ \frac{dc^*_{-k}}{dt} &= -i\omega_k c^*_{-k} \end{aligned} \tag{2.31}$$

with the new variables

$$
\begin{aligned}
a_k &= u_k c_k + v_k c_{ik}^* \\
a_{-k}^* &= v_k^* c_k + u_k c_{ik}^* \\
u_k &= \frac{1}{\sqrt{2}} \sqrt{\frac{A_k}{\omega_k} + 1} \\
v_k &= -\frac{1}{\sqrt{2}} \sqrt{\frac{A_k}{\omega_k} - 1} \\
\phi_k &= \arctan\left(\frac{k_y}{k_x}\right)
\end{aligned}
\tag{2.32}
$$

In a parametric pumping process the uniform mode a_0 is strongly excited[3] now coupling to other spin wave modes due to Ω_{n0} and Ω_{nk} leads to energy transfer from the uniform mode to other spin wave modes. At a certain transfer rate the losses due to dissipation are compensated and a spin wave mode will grow exponentially until another mechanism leads to saturation.

In order to determine the threshold for this process one can start by considering a system in which all modes are small compared to the uniform one. In this case terms up to second order in a_0 in Ω_{n0} and Ω_{nk} should be kept. Since Ω_{n0} contains only third and higher order terms in a_0 [5] the linearized form of equation 2.25 can be used. Supposing an circularly polarized alternating field oscillating with the frequency ω_P and allowing for spin wave losses via a substitution $\omega_0 \to \omega_o + i\omega_{r0}$ the amplitude of the uniform mode can be written in the following form

$$
a_0 = \frac{\gamma h}{\omega_0 - \omega_p + i\omega_{r0}} \exp(i\omega_P t) = a_0^0 \exp(i\omega_P t). \tag{2.33}
$$

However the term Ω_{nk} does contain second order terms in a_0 thus, neglecting all other terms it becomes

$$
\Omega_{nk} = \frac{\omega_M}{2} \frac{(k_x + ik_y)k_z}{k^2} a_0^* a_k - \frac{\omega_M}{8} \left(N_z a_k a_0 a_0^* - N_\perp a_0 a_0 a_{-k}^*\right) \tag{2.34}
$$

where N_z and $N_\perp$ are the components of the demagnetizing tensor parallel, respectively perpendicular to the z-direction. With the same assumptions and turning to variables c_k, c_{-k}^* one gets from equation 2.26

$$
\frac{dc_k}{dt} = i(\omega_k + T_k|a_0|^2)c_k + i(\rho_k a_0 + \xi_k a_0^2)c_{-k}^* \tag{2.35}
$$

[3] In most cases non-resonant.

and the adjoint equation.

With

$$\begin{aligned}
\rho_k &= -\frac{\omega_M}{4\omega_k}(\omega_k + \omega_H + Dk^2)\sin(2\theta)\exp(i\phi_k) \\
\xi_k &= \frac{\omega_k + A_k}{4\omega_k}\left(\omega_M \cos^2(\theta_k) - \omega_M \frac{N_\perp}{4\pi} + Dk^2\right) \\
T_k &= \frac{\omega_M}{4\omega_k}\left[2A_k\left(\cos^2(\theta_k) - \frac{1}{2}\sin^2(\theta_k) + \frac{N_z - N_\perp}{4\pi}\right) + \frac{\omega_M}{2}\sin^4(\theta_k)\right]
\end{aligned} \tag{2.36}$$

Comparing equation 2.35 with equation 2.31 it is apparent that the frequency of each mode is shifted by $T_k|a_0|^2$. This is the so called nonlinear frequency shift. Additionally a coupling between spin waves with wave vectors $\vec{k}$ and $-\vec{k}$ arises. It is well known, that a time dependent coupling between two oscillators can lead to an energy transfer between the source that causes the coupling and the coupled oscillators. In our case the coupling is caused by the heavily excited uniform mode, hence an energy transfer from the uniform mode to modes with $\vec{k}$ and $-\vec{k}$ will occur [42].

This process is most efficient in the case

$$\omega_P = \omega_1 + \omega_2 \tag{2.37}$$

where ω_1 and ω_2 are the oscillation frequencies of the coupled oscillators and ω_P the frequency of the alternating magnetic field. In the present case an additional condition has to be fulfilled, namely that the wave vectors of the excited spin waves must have the same value but different sign in order to ensure momentum conservation. This results in $\omega_1 = \omega_2 = \frac{\omega_P}{2}$. As a consequence the term $\xi_k a_0^2$ in equation 2.35 can be neglected. Usually at amplitudes a_0 up to threshold for parametric pumping, the nonlinear frequency shift is small and can therefore be neglected. Hence equation 2.35 reduces to

$$\frac{dc_k}{dt} = i\omega_k c_k + i\rho_k a_0 c_{-k}^* \tag{2.38}$$

and the adjoint equation. Solutions for these equations can be found with a form

$$c_k = c_{k0}^0 \exp(\upsilon t)\exp\left(i\frac{\omega_P}{2}t\right) \tag{2.39}$$

and adjoint. Where υ is a real quantity and much smaller than ω_P. This means that with the approximations made here the amplitude of the parametrically excited

modes will increase exponentially with time. Note that no dissipation has been taken into account for the derivation of this formula. Apparently the ultimate condition for instability is that υ becomes grater than zero. Whilst taking dissipation into account by the substitution $\omega_0 \to \omega_0 + i\omega_{rk}$ we can insert equation 2.39 into equation 2.38 and get two homogeneous algebraic equations for c^0_{k0} and c^{0*}_{-k0}. By setting the determinant of the system to zero and switching back to variables a we arrive at the equation

$$(\upsilon + \omega_{rk})^2 = (a^0_0|\rho_k|)^2. \tag{2.40}$$

At threshold $\upsilon = 0$, hence in order to get the threshold amplitude of the uniform precession mode the expression for a^0_0 has to be minimized with respect to k and θ_k while taking into account the dispersion relation of spin waves, hence

$$a^0_{0\mathrm{thr}} = \min\left(\frac{\omega_r k}{|\rho_k|}\right) = \min\left(\frac{\omega_{rk}\omega_P}{\omega_M(\omega_k + \omega_H + Dk^2)\sin(2\theta_k)}\right) \tag{2.41}$$

If θ_k would be independent of k the expression would be minimized for $k = 0$ and $k \to \infty$ at $\theta = 45°$. At intermediate k, the expression would be minimized for $\theta > 45°$. Since θ_k does depend on k it turns out that in a unbound medium θ_k is still equal 45° at $k = 0$ and $k \to \infty$ but has to become smaller than 45° at intermediate wave numbers in order to minimize 2.41. In thin films the situation is much more complicated due to different thickness modes and backward volume waves. The threshold behavior in such systems has been examined by Wiese *et.al.*[43].

In order to determine the threshold for perpendicular pumping in the external alternating field the expression for a^0_0 from equation 2.33 has to be substituted into equation 2.40 resulting in the expression

$$h_{\mathrm{thr}} = \min\left(\frac{2\omega_{rk}\omega_P\sqrt{\omega^2_{r0} + (\omega_P - \omega_0)^2}}{\gamma\omega_M \sin(2\theta_k)(\omega_P/2 + \omega_H + Dk^2)}\right) \tag{2.42}$$

Parallel pumping

Another very effective possibility to excite spin waves is called parallel pumping. It relies on the fact that the magnetization along the direction of the steady external field in a FM, magnetized to saturation, is reduced through the presence of spin waves, which was as we remember the original idea behind the concept of spin waves. Imagine a magnetization vector that precesses around an equilibrium position that coincides with the z-direction of a Cartesian coordinate system.

$$\vec{M} = \begin{pmatrix} M_x \\ M_y \\ M_z \end{pmatrix} = \begin{pmatrix} \hat{M}_x \cos(\omega t) \\ \hat{M}_y \sin(\omega t) \\ M_z \end{pmatrix} \tag{2.43}$$

If we take into account that the total length of the magnetization vector cannot be changed, hence $|\vec{M}| = M_0 = \text{const}$ its is easy to realize that the z-component of magnetization becomes smaller in the presence of spin waves. The z-component of the magnetization vector is given by

$$\begin{aligned} M_z &= \sqrt{M_0^2 - (M_x^2 + M_y^2)} \approx M_0^2 - \frac{1}{2M_0}(M_x^2 + M_y^2) + \cdots \\ &= M_0 - \frac{1}{4M_0}\left[(\hat{M}_x^2 - \hat{M}_y^2)cos(2\omega t) + \hat{M}_x^2 + \hat{M}_y^2\right]. \end{aligned} \tag{2.44}$$

It is easy to see, that $M_z \approx M_0$ provided $M_x, M_y \ll M_0$. When M_x and M_y become greater, higher order terms of the expansion 2.44 have to be taken into account. It is also worth noticing that when for some reason $M_x \neq M_y$ the value of M_z will oscillate with a frequency that is double the precession frequency of the spin around its equilibrium position. The non-equality of M_{x0} and M_{y0} is called ellipticity.

Ellipticity in a FM is mainly caused by two different mechanisms. Ellipticity can arise due to crystalline anisotropy that is present in most FM materials or from the shape anisotropy. In a sample where demagnetization factors transverse to the external magnetic field are not equal ellipticity arises since the component of $\vec{m}$ in the direction of larger demagnetizing factor will be smaller than in the other. Apparently a thin film magnetized in plane has a large ellipticity due to this effect hence its contribution is absolutely dominant.

The amplitude of the component of M_z oscillating with 2ω is according to equation 2.44 given by

$$m_{z2} = \frac{\hat{M}_x^2}{4M_0}\epsilon \tag{2.45}$$

with $\epsilon = 1 - \frac{\hat{M}_y^2}{\hat{M}_x^2}$. Thus each magnetization precession in the $x - y$ plane causes also an oscillation in z- direction with the double precession frequency. At elevated temperatures spin waves are present due to thermal fluctuations. When an alternating field is applied parallel to the z- direction it will couple to these spin waves and increase the precession angle. At a certain point the energy transfer from the external field compensates the losses due to dissipation and the instability arises.

In order to calculate the threshold of the external alternating field for the instability, h_z is not set to zero in the derivation of equation 2.31. As a consequence, an additional term appears in the differential equations for c_k and c^*_{-k}

$$\begin{aligned} \frac{dc_k}{dt} &= i\omega_k c_k + i\gamma h_z \frac{B_k}{\omega_k} c^*_{-k} \\ \frac{dc^*_{-k}}{dt} &= -i\omega_k c^*_{-k} - i\gamma h_z \frac{B^*_k}{\omega_k} c_k \end{aligned} \tag{2.46}$$

It is apparent that that coupling between wave vectors $\vec{k}$ and $-\vec{k}$ results directly from a component of alternating external field parallel to the equilibrium position. The quantity B_k that is caused by the dipolar interaction is related to the ellipticity through

$$\epsilon = \frac{2|B_k|}{A_k + B_k}. \tag{2.47}$$

From equation 2.30 it can be seen that ellipticity is greatest for $\theta_k = 90°$. The threshold field can be determined by substituting an external field of the from $h_z = h_{0z}\cos(\omega_P t)$ into equations 2.46 which leads to

$$h_{z\,\mathrm{thr}} = \min\left(\frac{\omega_P \omega_{rk}}{\gamma\omega_M \sin^2(\theta_k)}\right) \tag{2.48}$$

As expected the threshold is first reached for spin waves with highest ellipticity.

Saturation of spin wave amplitudes under parametric excitation

In the preceding section only lowest order nonlinear terms has been taken into account. As a consequence the spin wave amplitude grows exponentially. Although dissipation has been taken into account, via the substitution $\omega_0 \to \omega_0 + i\omega_{rk}$, there seems to be no mechanism that limits the exponential grow of spin wave amplitudes in this approximation.

The most obvious saturation cause is that the dynamic magnetization component can not exceed the value of the saturation magnetization. However saturation processes take place much earlier based on at least three different mechanisms: A reaction of the parametric spin waves on pumping, a phase mechanism and the nonlinear damping. The first mechanism can, for parallel pumping, be regarded as leading to a decrease of the quality factor Q of the resonator that creates the pumping field. For perpendicular pumping the consequence is different. In this sce-

nario the energy transfer to parametric spin waves can be treated as an additional source of damping that becomes infinite above threshold for parametric instability. Consequently the amplitude of the uniform precession mode saturates, just when h reaches the threshold value, at $a_{0\,\mathrm{thr}}^{0}$ given by equation 2.41. This effect finally leads to a reduction of the imaginary part of the nonlinear susceptibility above threshold, hence to a reduced absorption of pumping power. As a consequence a steady state is reached where the gain from the pumping field and the losses due to dissipation are equal. A more detailed treatment of this process can be found in the last section of [5].

The phase mechanism in turn is caused by nonlinear processes that fulfill the condition

$$\omega_{\vec{k}} + \omega_{-\vec{k}} = \omega_{\vec{k}'} + \omega_{-\vec{k}'} \tag{2.49}$$

thus two spin wave quanta, whose properties will be treated in the next section, with opposite wave vector, that were created directly by the parametric pumping process, scatter and create two new spin wave quanta with still opposite but different wave vector with respect to the original ones. For parametric magnons the sum of phases of spin waves with $\vec{k}$ and $\vec{k}'$ is constant. Although the above mentioned process preserves this relation, the sum will be different for the new magnon pair. If one takes into account third order terms in equation 2.26 one can see, that the coupling between pumping field and parametric spin waves is most efficient when the sum is equal $\frac{\pi}{2}$. Hence any scattering of the kind 2.49 will lead to a reduced coupling. As this mechanism depends strongly spin wave amplitude, it is responsible for saturation [37, 44]. It turns out that this mechanism is dominant in the saturation of parametric excitation for parallel pumping yet it provides only a small contribution to the saturation at perpendicular pumping.

The nonlinear damping finally is caused by interaction between three spin wave quanta of which at least one is a parametric one. This effect increases the damping ω_{rk} hence contributes to the saturation.

2.3 Quantum mechanical treatment of Spin-Waves: Magnons

Although the methods used in the last sections gave a lot of insight in the physics of spin waves they are not able to explain all observed effects. First of all, the magnetic medium is assumed to be continuous and not consisting of discrete magnetic moments. This assumption is a good approximation for FM conductors, where the free electrons contribute to a magnetization that is almost continuous. However it is

a bad approximation for FM insulators where the magnetic moments are attached to atoms on lattice sites that are fixed in position. It also does not consider quantum mechanics which demand that that the projection of the spin on the axis of an external magnetic field can only take on quantized values. This concept finally leads to quasi particles called magnons which are the elementary excitations of a FM. For the sake of simplicity the medium considered in the following sections is assumed to be unbound.

In quantum mechanics it is convenient to start with a Hamilton operator that describes the energy of the system in terms of natural variables,

$$\begin{aligned}\mathcal{H} = &\underbrace{-2\sum_{i\neq j} J(\vec{r}_{i,j})\vec{S}_i\vec{S}_j}_{exchange} \underbrace{- 2\mu H \sum_i S_{iz}}_{Zeeman} \\ &\underbrace{+1/2\sum_{i\neq j}\left(\frac{\hbar^2\gamma^2}{r_{i,j}^5}\right)[r_{i,j}^2\vec{S}_i\vec{S}_j - 3(\vec{r}_{i,j}\vec{S}_i)(\vec{r}_{i,j}\vec{S}_j)]}_{dipolar}\end{aligned} \tag{2.50}$$

and the state of the system

$$\left|\vec{S}_1 S_{1z}, ..., \vec{S}_N S_{Nz}\right\rangle. \tag{2.51}$$

The state 2.51 here is given by the spin projection S_{iz} and the total spin $\vec{S}_i$ at each lattice site i in a crystal with N lattice sites. In our case the Hamiltonian contains the Zeeman energy of a spin in an external field, the dipolar- and the exchange interaction between spins.

In order to obtain the dispersion relation $\omega(k)$ The Hamiltonian 2.50 has to be transformed into the form $\mathcal{H} = \sum_k \hbar\omega(k) c_k^\dagger c_k$ by choosing appropriate basis states. This has been done by Holstein and Primakoff [12]. A rigorous treatment would require a lot of space and give not much physical insight as most steps are pure algebra. Hence in the following, only the most important steps in the diagonalization of the Hamiltonian 2.50 will be shown.

In a first step the operators $\vec{S}_i$ and S_{iz} for the total spin and the spin projection are replaced by spin deviation creation and annihilation operators a and $a^\dagger$. The state of the system is changed to the number of deviations of each spin from the equilibrium position $|n_1...n_z\rangle$ with $n_i = S - S_{iz}$ where S denotes the length of each vector $\vec{S}_i$[4]. As the spin is quantized in the equilibrium position, the spin deviation can only occur in discrete steps. The transformation can be written

[4]The length of the vector $\vec{S}_i$ is assumed to be equal at each lattice site.

$$
\begin{aligned}
S_i^+ &= \sqrt{2S}\sqrt{1-\frac{a_i^\dagger a_i}{2S}}a_i \\
S_i^- &= \sqrt{2S}a_i^\dagger\sqrt{1-\frac{a_i^\dagger a_i}{2S}} \\
S_{iz} &= S - a_i^\dagger a_i \\
S_i^\pm &= s_{ix} \pm i s_{iy} \\
\vec{S}_i \cdot \vec{S}_i &= S(S+1)
\end{aligned}
\tag{2.52}
$$

In order to get analytical expressions for $a_i^\dagger$ and a_i, the term $\sqrt{1-\frac{a_i^\dagger a_i}{2S}}$ has to be expanded

$$
\begin{aligned}
S_i^+ &= \sqrt{2S}\left(a_i - \frac{a_i^\dagger a_i a_i}{4S} + \dots\right) \\
S_i^- &= \sqrt{2S}\left(a_i^\dagger - \frac{a_i^\dagger a_i^\dagger a_i}{4S} + \dots\right).
\end{aligned}
\tag{2.53}
$$

At low magnon densities, when the reduction of magnetization due to precessing spins is small compared to the magnetization without precessing spins, hence

$$
\frac{\left\langle a_i^\dagger a_i \right\rangle}{S} = \frac{M_0 - M_{mag}}{M_0} \ll 1 \tag{2.54}
$$

the expansion 2.53 can be stopped after the first term and one gets

$$
\begin{aligned}
S_i^+ &= \sqrt{2S}a_i \\
S_i^- &= \sqrt{2S}a_i^\dagger
\end{aligned}
\tag{2.55}
$$

The quadratic term of the new Hamiltonian takes over the form

$$
\mathcal{H} = \sum_{i \neq j} f(\vec{r}_{i,j}) a_i^\dagger a_j. \tag{2.56}
$$

Higher order terms can be neglected at temperatures well below the magnetic ordering temperature. A term that does not contain $a_i^\dagger$ or a_j can be set to zero

without changing the physics as it produces merely an energy offset. The factor $a_i^\dagger a_j$ in equation 2.56 flips the ith spin up and the jth spin down, leading to a total spin deviation of one since each electron carries spin 1/2. It is apparent that this kind of excitation cannot be elemental. We know from the previous section that a spin deviation never stays localized du to interactions among the spins but spreads in a wave like manner.

In order to isolate elementary excitations of a spin system a Fourier transformation is utilized. First of all it is a mathematical necessity but it also has a deep physical meaning. By using the Fourier transform one makes the step from localized flipped spins to collective excitations where each spin flip is smeared out over virtually all lattice sites in the material. The creation and annihilation operators become

$$\begin{aligned} b_k &= N^{-1/2} \sum_j \exp(i\vec{k}\vec{r_j}) a_j \\ b_k^\dagger &= N^{-1/2} \sum_j \exp(-i\vec{k}\vec{r_j}) a_j^\dagger \end{aligned} \tag{2.57}$$

with $\vec{r_i} = \sum_{i=1}^{3} \alpha_i \vec{A_i}$ where $\vec{A_i}$ are the three vectors defining the unit cell of the magnetic material in real space. The Hamiltonian now takes the form

$$\mathcal{H} = \sum_k A_k b_k^\dagger b_k + \frac{1}{2} \sum_k (B_k b_k b_{-k} + B_k^* b_{-k}^\dagger b_k^\dagger) + \dots \tag{2.58}$$

with

$$\begin{aligned} A_k &= \sum_{i \neq j} 2SJ(\vec{r}_{i,j})[1 - \exp(i\vec{k}\vec{r}_{i,j})] + \hbar\omega_H + \frac{1}{2}\hbar\omega_M \sin^2(\theta) \\ B_k &= \frac{1}{2}\hbar\omega_M \sin^2(\theta) \exp(-i2\phi) \end{aligned} \tag{2.59}$$

Where $J(\vec{r}_{i,j})$ denotes the exchange integral between lattice sites i and j. When $A_k >> B_k$ the second term in the Hamiltonian can be neglected and A_k gives the dispersion relation. When dipolar interactions are neglected, B_k and the last term in A_k becomes zero and no further steps have to be done, since Hamiltonian 2.58 is already diagonal in that case. However when dipolar interactions are considered $A_k >> B_k$ is not fulfilled in general and one last transformation has to be made that is known as the Bogolyubov transformation [7]

$$\begin{aligned} c_k &= u_k b_k + v_k b_{-k}^\dagger \\ c_k^\dagger &= u_k b_k^\dagger + v_k^* b_{-k}^\dagger \end{aligned} \tag{2.60}$$

with

$$u_k = \cosh\left(\frac{\operatorname{arctanh}\left(\frac{|B_k|}{A}\right)}{2}\right)$$
$$v_k = \exp\left(i2\phi_k\right)\sinh\left(\frac{\operatorname{arctanh}\left(\frac{|B_k|}{A}\right)}{2}\right) \tag{2.61}$$

Now the Hamiltonian has the desired form

$$\mathcal{H} = \sum_k \hbar\omega c_k^\dagger c_k + \ldots \tag{2.62}$$

with $\hbar\omega^2 = A_k^2 - |B_k|^2$. The operator $\omega c_k^\dagger$ is called magnon creation operator and c_k is called magnon annihilation operator.

It is apparent that when $B_k = 0$ we can reassemble the result of the second Holstein-Primakoff transformation. However if $B \neq 0$ the result differs. Of special interest is dependence of c_k and $c_k^\dagger$ on B_k as it gives us information about the spin of a magnon. With $B_k \to 0$ we get $u_k \to 1$ and $v_k \to 0$ hence a magnon that is exchange dominated has spin one since b_k and $b_k^\dagger$ are the Fourier transform of a spin lowering respectively rising operator. But if $|B_k| \neq 0$ the operators c_k and $c_k^\dagger$ will also contain contributions from a spin rising respectively lowering operator. Consequently the spin of magnons which are dominated by dipolar interactions becomes smaller than one. Nevertheless u_k is always greater than $|v_k|$ hence c_k always decreases the total spin of the system and $c_k^\dagger$ increases it. In the case of YIG in a external magnetic field $B_0 \approx 130mT$ the spin of a magnon with $k \vec{=} 0$ has a value of 0.8 which is likewise the smallest value of the magnon spin.

In general the summation in A_k goes over all $\vec{r}_{i,j}$. A first simplification one can make is to assume that the exchange integral becomes very small for spins that are far away from each other, such that only nearest neighbors have to be taken into account in the summation. Another simplification is that the exchange integral is the same for all nearest neighbors. With these assumptions A_k takes the form

$$A_k = 2SJZ(1-\gamma) + \hbar\omega_H + \frac{1}{2}\hbar\omega_M \sin^2(\theta)$$
$$\gamma = \frac{1}{Z}\sum_{\vec{\delta}} \exp(-\vec{k}\vec{\delta}) \tag{2.63}$$

where $\vec{\delta}$ denotes the vector from one lattice site to its nearest neighbors. The dispersion relation can now be written as

$$\hbar\omega^2 = [2SJZ(1-\gamma) + \hbar\omega_H][2SJZ(1-\gamma) + \hbar\omega_H + \hbar\omega_M \sin^2(\theta)] \tag{2.64}$$

In a primitive cubic crystal system nearest neighbors are oriented along the $\pm x$, $\pm y$ and $\pm z$ axes at a distance a and one gets

$$\begin{aligned}\gamma =& \frac{1}{6}[\exp(ik_x a) + \exp(-ik_x a) + \exp(ik_y a) + \exp(-ik_y a) + \exp(ik_z a) + \exp(-ik_z a)] \\ =& \frac{1}{3}[\cos(k_x a) + \cos(k_y a) + \cos(k_z a)]\end{aligned} \tag{2.65}$$

In the limit where the wavelength of the spin wave is much larger than the lattice constant $ka << 1$ one gets $\gamma \approx 1 - \frac{a^2k^2}{2}$ and with $D = \frac{SJZa^2}{\hbar\omega_M}$ we arrive at a dispersion relation that is identical with the result that has been obtained with classical theory (equation 2.9). Consequently the quantum mechanical dispersion relation differs from the classical ones only in the regime where the condition $ka << 1$ is not fulfilled hence for very short spin waves [7].

2.3.1 Properties of Magnons

The quantum mechanical treatment gave us a lot of insight into the physics of spin waves. It has been shown that spin waves can be treated as quasi particles that can be created or annihilated. These quasi particles are called **magnons**. Since excitation of one magnon reduces the total spin of the system by one, magnons can be regarded as being Bosons.

A magnon is characterized by energy

$$E = \hbar\omega \tag{2.66}$$

and momentum

$$\vec{p} = \hbar\vec{k}. \tag{2.67}$$

Given by the dispersion relation 2.64. Du to a spin close to one the distribution of magnons among all accessible energies can be determined by Bose-Einstein statistics which will be introduced in a forthcoming section. Due to these properties magnons are called quasi-particles which move with a velocity of $\vec{v} = \frac{d\omega}{d\vec{k}}$ and posses a mass off

$m_i = \frac{d^2\omega}{dk_i^2}$. Due to the anisotropy of the dispersion relation caused by the symmetry breaking of a magnetic field, the velocity and mass of a magnon depends on the direction of its movement with respect to the external magnetic field. In contrast to real particles a magnon has no defined spatial extend, instead a magnon has to be treated as the elementary excitation of a FM material, meaning that it is not possible to excite a fraction of a magnon. In that sense a magnon is rather comparable to a phonon which is the elementary excitation of an em field.

2.3.2 Magnon relaxation theory

In the preceding sections it has been assumed that magnon densities are very small, hence interactions among magnons[5] are negligible. This approach is valid if one considers thermally excited magnons in a FM material well below the temperature of magnetic ordering, as in this case $M(T) \approx M(0)$. However interactions among magnons become important at elevated temperatures where $M(T) \ll M(0)$. At this juncture approximation 2.55 is not valid anymore. Furthermore higher order terms in the Hamiltonian 2.62 have to be taken into account in order to describe the temporal evolution of the system in a proper way. The same applies when additional magnons are injected, e.g. by a parametric pumping process.

Beyond that interactions between magnons and the environment[6] and interactions with the em field[7] have been previously neglected although in some cases they were introduced via a phenomenological relaxation frequency[8].

In the following all these interactions will be treated in more detail.

Magnon-Magnon interactions

Bloch [1] as well as Holstein and Primakoff [12] did not consider magnon-magnon interactions in their original papers as they concentrated on thermal magnons in a FM well below the temperature for magnetic ordering. Interactions among magnons were first considered by Dyson [13] in a very rigorous treatment. However this paper is of high mathematical complexity and not easy to understand in terms of physical interpretation. Another attempt has been made by Oguchi [14] in terms of an expansion of the Holstein-Primakoff theory. In both derivations dipolar interactions where neglected. When dipolar interactions are neglected, all terms in the Hamiltonian 2.62 conserve the total number of magnons hence only terms with equal number

[5] Magnon-magnon interactions.
[6] Mainly the crystalline lattice (magnon-phonon interactions).
[7] Magnon-photon interactions.
[8] Imaginary part of the precession frequency.

of creation and annihilation operators appear. If however dipolar interactions are included additional terms appear that do not conserve the total magnon number.

The Hamiltonian 2.62 up to fourth order has the form:

$$\mathcal{H} = H_2 + \underbrace{H_3 + H_4}_{H_P}. \tag{2.68}$$

The first term H_2 contains quadratic terms in c_k and $c_k^\dagger$ given by 2.62, H_3 terms of third order and H_4 terms of fourth order in the same variables. These terms can be treated as a perturbation of the second order Hamiltonian 2.62. Higher order terms can usually be neglected.

H_2 contains only one term proportional to $c_k^\dagger c_k$. Such an expression applied to an state gives the number of magnons with momentum k, hence this term determines the energy of magnons[9].

H_3 contains terms

$$\begin{aligned} H_3 = &\sum_{k_1,k_2,k_3} V_{k_1,k_2k_3} c_{k_1}^\dagger c_{k_2} c_{k_3} \delta(k_1 - k_2 - k_3) \\ &+ \sum_{k_1,k_2,k_3} V_{k_1k_2,k_3}^* c_{k_1} c_{k_2}^\dagger c_{k_3}^\dagger \delta(k_1 - k_2 - k_3) \end{aligned} \tag{2.69}$$

Recalling that $c_k^\dagger$ and c_k are creation and annihilation operator for magnons respectively, H_3 is easy to interpret. In the first term two magnons with wave vector k_2 and k_3 are annihilated and one magnon with wave vector k_1 is created. The Kronecker delta function ensures momentum conservation. This is the so called magnon confluence process in which two magnons merge into one. The second term describes a process where one magnon with wave vector k_1 is destroyed and two with wave vector k_2 and k_3 are created. This process is called the three magnon splitting process in which one magnon splits into two magnons. It is apparent that this term is caused by dipolar interactions. In equation 2.69 only momentum conservation has been taken into account however energy conservation must also be accounted for. Energy conservation is ensured through Fermi's golden rule [45] that states

$$w_{i\to f} = |\langle f|H_P|i\rangle|^2 \delta(\epsilon_i - \epsilon_f). \tag{2.70}$$

In words: The transition rate from an initial state $|i\rangle$ into a final state $\langle f|$ is given by the matrix element $|\langle f|H_P|i\rangle|^2$ times the delta function $\delta(\epsilon_i - \epsilon_f)$. Hence due

[9] The Eigen states of a Hamiltonian describe the energy of the system.

to the delta function a transition from one state into another can only be executed when both have the same energy.

A serious restriction for all processes that change the energy and momentum of a magnon is based on the fact that final magnon states have to fit into the dispersion relation. Due to this restriction three magnon processes are, in many cases, forbidden. Additionally these processes are caused exclusively by dipolar interactions, hence when exchange interactions dominate they are negligible.

All these restrictions are generally much easier to account for in the case of four magnon processes. That is why in a magnon system the fourth order Hamiltonian H_4 has still a large influence on magnon-magnon interactions although it incorporates more particles than the third order Hamiltonian H_3. In many cases H_4 even dominates interactions among magnons. It contains terms

$$\begin{aligned} H_4 = & \sum_{k_1,k_2,k_3,k_4} V_{k_1,k_2k_3k_4}\, c^\dagger_{k_1} c_{k_2} c_{k_3} c_{k_4}\, \delta(k_1 - k_2 - k_3 - k_4) \\ & + \sum_{k_1,k_2,k_3,k_4} V^*_{k_1k_2k_3,k_3}\, c_{k_1} c^\dagger_{k_2} c^\dagger_{k_3} c^\dagger_{k_4}\, \delta(k_1 - k_2 - k_3 - k_4) \\ & + \sum_{k_1,k_2,k_3,k_4} V_{k_1k_2,k_3k_3}\, c_{k_1} c_{k_2} c^\dagger_{k_3} c^\dagger_{k_4}\, \delta(k_1 + k_2 - k_3 - k_4) \\ & + \sum_{k_1,k_2,k_3,k_4} V^*_{k_1k_2,k_3k_3}\, c^\dagger_{k_1} c^\dagger_{k_2} c_{k_3} c_{k_4}\, \delta(k_1 + k_2 - k_3 - k_4) \end{aligned} \tag{2.71}$$

The first two terms do not conserve the total magnon number hence they can only be caused by dipolar interactions. They describe processes where one magnon splits into three magnons and vice versa. The last two terms describe processes in which two magnons are annihilated and two are created, leading to a new energy and momentum distribution without changing the number of magnons. These processes are caused by exchange interactions and are, in most cases, dominant.

It is apparent, from the above considerations that there are several processes that can lead to a redistribution of energy in a magnon system if for example one magnon energy is strongly over occupied due to external excitation processes [7].

Magnon-Phonon interactions

Up to now the magnon system has been treated as being isolated from its environment. However this is an apparently bad approximation. Interactions between the magnon system and its environment have been taken into account in the classical treatment through the inclusion of a relaxation frequency ω_{rk} leading to energy dissipation. In these considerations no attention has been drawn to the mechanisms

that lead to this energy dissipation. It was simply a necessity in order to describe experiments in a proper way.

The system that is in closest proximity to the spin system in this case is the crystalline lattice. The elementary excitations of a crystalline lattice are called phonons. Phonons are the quasi particles of the displacement waves in a periodically structured lattice [35]. Displacement waves are coupled to spin waves mainly through two mechanisms.

The first mechanism relies simply on the fact that the strength of dipolar and exchange interactions depends on the distance between spins. Hence in the presence of a displacement wave the distance between lattice sites will change periodically, leading to a coupling between spin waves and displacement waves.

The second mechanism is based on spin-orbit coupling [34] of the atoms on the lattice sites. The spacing between atoms in a crystalline lattice is determined through a balance between attracting and repelling forces caused mainly by electric interactions between adjacent atoms. These forces depend on the mutual alignment of electron orbitals. Asymmetric electron orbitals are caused by the orbital momentum of electrons in an atom. Spin orbit coupling forces the orbital momentum to precess when a spin wave is present. Along with a precession of the angular momentum, the asymmetric electron orbital will follow the precession of the orbital momentum leading to a change in the mutual orientation of neighboring orbitals. This leads to a change in their spacing and finally results in a displacement wave. The process also works the other way.

The detailed treatment of this processes in terms of including such interactions into the Hamiltonian 2.50 and subsequent transformation in terms of magnon and phonon creation and annihilation operators is extremely formidable. While the first mechanism is already inherently present in that Hamiltonian an additional term has to be introduced in order to account for the second one. Abrahams and Kittel proposed a way to introduce magneto-elastic relaxations into this model by using a phenomenological expression for the magneto-elastic energy [46]. More details about this theory can be found in [47].

According to this theory additional terms appear in the Hamiltonian 2.68 that describe interactions between magnons and phonons. In each of these individual processes momentum and energy conservation has to be taken into account. One possible magnon-phonon interaction is the direct conversion of a magnon into a phonon or vice versa, however this process is only allowed in the regions in phase space where the dispersion relations of both quasi-particles cross.

A process that is much more likely is the conversion of one magnon into a magnon, with changed energy and momentum, and a phonon. The inverse process is of course also possible. Both processes conserve the magnon number but lead to an

energy transfer from the magnon system to the crystalline lattice and are therefore responsible for dissipation.

It turns out that at large wave vectors the first is dominant while the latter is dominant at small wave vectors. This is due to the condition that the group velocity of involved magnons in the first process has to be greater than the velocity of the involved phonons, making it probable only for magnons with large wave vector.

The energy of magnons with small wave vector is dissipated directly into the crystalline lattice mainly due to the so called Kasuya-LeCraw process [7] in which a magnon with small wave vector and energy interacts with a phonon from the optical branch creating a magnon with larger wave vector and energy. Obviously this process leads to an energy transfer from the phonon system to the magnon system. In subsequent processes however the magnon can loose energy due to the above mentioned process as it has a sufficiently high wave vector now. One could also imagine processes in which a magnon with small wave vector gains a larger wave vector due to magnon-magnon interactions and looses energy to the lattice through a subsequent magnon phonon process.

However it turns out that all the effects described above still give only a small contribution to the dissipation of magnons with small wave vector. Indirect processes that involve magnetic impurities in the chemical composition of the crystal, which are exchange coupled to the other spins in the crystal and posses an orbital momentum, give the largest contribution in this case. The involved mechanisms are the valence exchange mechanism, the slowly relaxing impurity and the rapidly relaxing impurity. The most important of which is the slowly relaxing impurity. These processes exhibit pronounced temperature dependence. Details can be found in [37, 7].

In FM metals the interaction of magnons with conduction electrons dominates magnon dissipation. Since this work deals exclusively with FM insulators, this kind of interactions will not be treated here. The interested reader is referred to [37, 7].

2.3.3 Magneto-Optical Effects and Interaction of Magnons with Light

The last mayor interaction between the magnon system and its environment that has not been addressed so far is the interaction between magnons and the quanta of the em field, namely photons. We start with a classical treatment.

Since interactions between a magnetic system and light change the polarization state of the latter it is convenient to define the different polarization states. It turns out that the magnetic field of the em wave can be neglected in the following considerations as it is by a factor, of the speed of light, smaller than the electric. In

fact the first proposal for an interaction between magnons and photons was based on a direct magnetic-dipole interaction, however it was realized soon that this kind of interaction is much too weak as to cause the observed effects. Hence in the following the treatment of a em wave will be restricted to the description of its electric field. The electric field of a plane em wave with angular frequency ω in vacuum propagating in the positive z-direction of a Cartesian coordinate system is given by

$$\vec{E}(\vec{r},t) = \vec{E}_0 \exp[i(\omega t - k_z z)] \tag{2.72}$$

The form of $\vec{E}_0$ determines the polarization state. For linear polarization, parallel to the x-axis

$$\vec{E}_0^{\text{lin},x} = E_0 \hat{e}_x \tag{2.73}$$

for linear polarization parallel to the y-axis

$$\vec{E}_0^{\text{lin},y} = E_0 \hat{e}_y \tag{2.74}$$

The basis states of linear polarization are defined by the unit vectors for the x and y direction. Hence one can write for arbitrary orientations of the linear polarization

$$\vec{E}_0^{\text{lin}} = E_0[\sin(\sigma)\hat{e}_x + \cos(\sigma)\hat{e}_y] \tag{2.75}$$

with σ being the angle between y- axis and $\vec{E}_0^{\text{lin}}$. E_0 is the amplitude of the electric field.

For left hand circular polarized light

$$\vec{E}_0^{\text{circ } l} = E_0 \underbrace{(\hat{e}_x - i\hat{e}_y)}_{\hat{e}_-} \tag{2.76}$$

An em wave can also exhibit a circular polarization in which the vector of the electric field rotates around the wave vector k with angular frequency ω. One has to distinguish left- and right-hand polarized light. For right hand circular polarized light

$$\vec{E}_0^{\text{circ } r} = E_0 \underbrace{(\hat{e}_x + i\hat{e}_y)}_{\hat{e}_+} \tag{2.77}$$

where $\hat{e}_-$ and $\hat{e}_+$ are the unit vectors for left and right hand polarized light. It is apparent from equations 2.76 and 2.77 that the unit vectors for circular polarized light can be obtained from a linear combination of the unit vectors of linear polarization. The other way around can also be realized via

$$\begin{aligned} \hat{e}_x &= \frac{1}{2}(\hat{e}_+ + \hat{e}_-) \\ \hat{e}_y &= \frac{1}{2i}(\hat{e}_+ - \hat{e}_-) \end{aligned} \tag{2.78}$$

Hence linear polarized light can be represented as a superposition of a right and a left hand circular polarized light. On the other hand a right hand polarized wave can be represented as a superposition of two linear polarized waves with polarization vectors perpendicular to each other and a phase difference by $\frac{\pi}{2}$ since

$$\begin{aligned} \vec{E}^{\text{circ } r}(t) &= E_0(\hat{e}_x \exp(i\omega t) + \hat{e}_y \exp(i\omega t + \frac{\pi}{2})) \\ &= E_0(\hat{e}_x + \exp(\frac{\pi}{2})\hat{e}_y) \exp(i\omega t) = E_0 \underbrace{(\hat{e}_x + i\hat{e}_y)}_{\hat{e}_+} \exp(i\omega t) \end{aligned} \tag{2.79}$$

The last major polarization state is the elliptical polarization which is a generalization of circularly polarized light. It can also be constructed from a superposition of two linear polarized waves with a phase shift with respect to each other. However in this case the amplitudes of the two linear waves have different values and the phase shift must not amount $\pi/2$.

$$\vec{E}^{\text{ell}}(t) = E_x \hat{e}_x \exp(i\omega t) + E_y \hat{e}_y \exp(i\omega t + \phi) \tag{2.80}$$

The difference between E_x and E_y determines the ellipticity whereas the value of ϕ determines the orientation of the major axis with respect to $\hat{e}_x$ as well as the ellipticity. The microscopic origin of interactions between magnetic moments and light is based on the fact that the electric field of a linear polarized incoming em wave with polarization perpendicular to the magnetization forces a bound electron to oscillate around its equilibrium position. This oscillating electron in turn creates a new em wave with linear polarization and polarization axis mainly parallel to the

oscillation direction of the electron. However, in the presence of a magnetic moment, the electron will not oscillate parallel to the external field but under a certain angle which leads to a tilted major polarization axis of the emitted light with respect to the incoming. This phenomenon is known as magnetic circular birefringence. With the same arguments incident circular polarized light will become elliptically polarized. This effect is called magnetic linear birefringence and is quadratic in magnetization [48].

Other magneto-optical effects arise when the oscillation of the electron is damped. The easiest damping mechanism one can think of is based on the fact that an oscillating electron exerts a force on the nucleus to which it is bound leading to oscillations of the latter, leading to the creation of phonons. As the mass of the nucleus is at least three orders of magnitude larger than the mass of the electron this interaction is rather weak. Stronger absorption mechanisms in insulating crystals arise from other processes that can be found in [49]. One effect that arises from absorption is called magnetic circular dichroism it is based on different absorption coefficients acting upon the incoming light for left- and right-hand circular polarized components of the wave. This effect occurs when the polarization of the incoming light is perpendicular to the magnetization. As a result linear polarized light becomes elliptically polarized. A similar effect is observed when the polarization plane is parallel to the magnetization leading to magnetic linear dichroism with the result that circularly polarized light becomes elliptically polarized [50].

The equation of motion for an electron with charge e and mass m_e in a potential $V(x, y, z)$, subjected to a velocity dependent damping, in the presence of a magnetization $\vec{M}$ driven by an electric field $\vec{E}$, is given by

$$m_e\ddot{\vec{r}} + \vec{b}\dot{\vec{r}} + \vec{o}\vec{r} + e\mu_0\dot{\vec{r}} \times \vec{M} = -e\vec{E} \tag{2.81}$$

with a damping coefficient $\vec{b}$ that depends on the direction of oscillation and $\vec{o} \approx \vec{\nabla}V$. As we are looking for small oscillations of the electron around an equilibrium position only the first Taylor expansion of the binding potential at the equilibrium position is taken into account.

Without loss of generality we can assume, that the incoming em wave is linear polarized, all results can be easily rewritten for the case of circular polarized light. With $\vec{E} = \vec{E}_0 \exp(i\omega t)$ solutions of the form $\vec{r} = \vec{r}_0 \exp(i\omega t)$ can be found. Substituting these two expressions into equation 2.81 and using the definition of a dipolar electric moment $\vec{p} = -e\vec{r}_0$ we find that the electric dipolar moment, that oscillates with angular frequency ω is a linear function of the incident electric field.

$$\overleftrightarrow{Q}\ \vec{p} = \vec{E}_0 \tag{2.82}$$

with

$$\overleftrightarrow{Q} = \begin{pmatrix} \frac{\omega_{0x}^2 - \omega^2 + i\omega g_x}{e^2} & \frac{i\mu_0\omega}{em_e} M_z & -\frac{i\mu_0\omega}{em_e} M_y \\ -\frac{i\mu_0\omega}{em_e} M_z & \frac{\omega_{0y}^2 - \omega^2 + i\omega g_y}{e^2} & \frac{i\mu_0\omega}{em_e} M_x \\ \frac{i\mu_0\omega}{em_e} M_y & \frac{i\mu_0\omega}{em_e} M_x & \frac{\omega_{0z}^2 - \omega^2 + i\omega g_z}{e^2} \end{pmatrix} \tag{2.83}$$

where $\vec{\omega}_0^2 = \frac{1}{m}\vec{\sigma}$ and $\vec{g} = \frac{1}{m}\vec{b}$. As the geometry will be defined later by the principal axes of the crystalline structure of the considered material all components of $\vec{M}$ have to be taken into account. We see, that magnetization occurs only in the off diagonal elements of $\overleftrightarrow{Q}$. So in the absence of magnetization $\vec{p}$ and $\vec{E}_0$ are parallel to each other. However in the presence of a magnetization this is not the case anymore. The oscillating dipole in turn emits light by itself. If the magnetization is static the emitted light will have the same frequency as before but a different polarization state. Most of the emitted radiation has $\vec{k} \perp \vec{p}$ and is linear polarized $\vec{E}_0 || \vec{p}$.

In order to determine the dipolar electric moment that is induced through the electric field of a em wave, equation 2.82 has to be rewritten in the form

$$\vec{p} = \overleftrightarrow{\chi}_{el}\, \vec{E}_0 \tag{2.84}$$

the tensor $\overleftrightarrow{\chi}_{el} = \left(\overleftrightarrow{Q}\right)^{-1}$ is called electric susceptibility in analog to the magnetic susceptibility introduced in section 2.1.2. Due to the inversion of $\overleftrightarrow{Q}$ components of the electric susceptibility are rational functions of the magnetization up to fourth order. The diagonal elements nevertheless still contain terms that are independent of magnetization.

The potential energy of an electric dipole $\vec{p}$ in a electric field $\vec{E}$ is given by

$$U_{pot} = -\vec{p} \cdot \vec{E}. \tag{2.85}$$

In order to describe magneto optical interactions quantum mechanically, an additional term has to be added to the Hamiltonian 2.50 that accounts for this potential energy. The form for this term that has been suggested by Louden [51] has the form

$$H_{MO} = \sum_{\alpha,\beta} \sum_{\vec{R}} E_1^{\alpha}(\vec{R}) E_2^{\beta}(\vec{R}) \chi^{\alpha\beta}(\vec{R}) \tag{2.86}$$

where $\vec{E}_1$ and $\vec{E}_2$ are the electric fields of the incident respectively scattered em wave. The summation goes over all combinations of Cartesian coordinates α and β

and over all lattice sites in the crystal denoted by $\vec{R}$. The tensor $\chi^{\alpha\beta}(\vec{R})$ contains only terms that depend on magnetization and has the same form as the electric susceptibility derived from classical theory but with the components of magnetization replaced by the corresponding operators. This Hamiltonian can be interpreted as the potential energy of an electric dipole in the electric field of the incident EM wave, where the dipole is created through the action of the emitted EM wave [51].

When we assume that the magneto optical coupling is rather weak the components of $\overleftrightarrow{\chi}_{el}$ can be expanded as powers of the magnetization. This has been done by Le Gall *et.al.*[52]

$$\frac{N}{V}\chi^{\alpha\beta}(\vec{R}) = \sum_{\mu} K_{\alpha\beta\mu}(\vec{R}) M^{\mu}_{\vec{R}} + \sum_{\mu,\nu} G_{\alpha\beta\mu\nu}(\vec{R}) M^{\mu}_{\vec{R}} M^{\nu}_{\vec{R}} \tag{2.87}$$

terms of higher order than quadratic are neglected. In crystalline systems many of the tensor components $\overleftrightarrow{K}$ and $\overleftrightarrow{G}$ are zero by symmetry [10]. In a crystal where the magnetic moments are located on a cubic lattice like in YIG, the tensor $\overleftrightarrow{\chi}$ reduces to

$$\frac{N}{V}\chi^{\alpha\beta}(\vec{R}) = \begin{pmatrix} G_{11}M_x^2 + G_{12}(M_y^2+M_z^2) & KM_z + G_{44}(M_xM_y + M_yM_x) & -KM_y + G_{44}(M_zM_x - M_xM_z) \\ -KM_z + G_{44}(M_xM_y - M_yM_x) & G_{11}M_y^2 + G_{12}(M_x^2+M_z^2) & KM_x + G_{44}(M_yM_z - M_zM_y) \\ KM_y + G_{44}(M_zM_x - M_xM_z) & -KM_x + G_{44}(M_yM_z - M_zM_y) & G_{11}M_z^2 + G_{12}(M_x^2+M_y^2) \end{pmatrix} \tag{2.88}$$

By using an analogy to the first and second Holstein Primakoff Transformation 2.52 and 2.57 new variables for the magnetization $b^{\dagger}_{\vec{k}}$ and $b_{\vec{k}}$ can be obtained. Their relation to the magnetization operators are given by [50]

$$\begin{aligned} M(\vec{R})^{\pm} &= M_x(\vec{R}) \pm iM_y(\vec{R}) \\ M^{+}(\vec{R}) &= \sqrt{\frac{2\hbar\gamma N M_0}{V}} \sum_{\vec{k}} b_{\vec{k}} \exp(i\vec{k}\vec{R}) \\ M^{-}(\vec{R}) &= \sqrt{\frac{2\hbar\gamma N M_0}{V}} \sum_{\vec{k}} b^{\dagger}_{\vec{k}} \exp(-i\vec{k}\vec{R}) \\ M^{z}(\vec{R}) &= M_0 - \sqrt{\frac{\hbar\gamma N}{V}} \sum_{\vec{k},\vec{k}'} b^{\dagger}_{\vec{k}} b_{\vec{k}'} \exp[-i(\vec{k}-\vec{k}')\vec{R}]. \end{aligned} \tag{2.89}$$

The usual approximation can be made, that the number of magnons does not change the total magnetization significantly, hence $M^z(\vec{R}) = M_0$. With these trans-

[10] See e.g. [53].

formations the magneto-optical Hamiltonian 2.86 can now be written in terms of magnon operators and takes the form

$$H_{MO} = \sqrt{\frac{\hbar\gamma N M_0}{2N}} E_1 E_2 \sum_{\vec{k},\vec{R}} [A^{(+)} b_{\vec{k}} \exp(i\vec{k}\vec{R}) + A^{(-)} b^{\dagger}_{\vec{k}} \exp(-i\vec{k}\vec{R}) \tag{2.90}$$

The form of $A^{(+)}$ and $A^{(-)}$ is determined by the direction of the magnetization relative to the crystalline axes. If M_0 is oriented along the [001] direction they are given by

$$\begin{aligned} A^{(-)} &= 2M_0 G_{44}(\hat{e}_1^z \hat{e}_2^+ + \hat{e}_1^+ \hat{e}_2^z) + iK(\hat{e}_1^z \hat{e}_2^+ - \hat{e}_1^+ \hat{e}_2^z) \\ A^{(+)} &= 2M_0 G_{44}(\hat{e}_1^z \hat{e}_2^- + \hat{e}_1^- \hat{e}_2^z) - iK(\hat{e}_1^z \hat{e}_2^- - \hat{e}_1^- \hat{e}_2^z) \end{aligned} \tag{2.91}$$

where $\hat{e}_1^z$, $\hat{e}_1^+$ are the unit vectors of polarization of the incident and $\hat{e}_2^z$, $\hat{e}_2^+$scattered light[11]. Therefore equation 2.91 determines the selection rules for the polarization of both waves. In the most important case, where the incident light is polarized linearly in the plane parallel to the magnetization and are scattered in the forward or backward direction, the polarization of the scattered light will still be linear and in the same plane, but rotated by 90° around the propagation direction.

In order to determine the amount of light that is scattered into a solid angle Ω with frequency ω_2 the differential cross section is needed. According to Wettling *et.al.*[50] for Stokes scattering it is given by

$$\frac{d^2h}{d\Omega d\omega_2} = \frac{\hbar\gamma M_0 \omega_1 \omega_2^3 \bar{n}_2}{2\pi c_0^4 \bar{n}_1} |A^{(-)}|^2 (n_M + 1)\delta(\omega_1 - \omega_2 - \omega_m) \tag{2.92}$$

Where c_0 is the speed of light in vacuum, n_M is the number of magnons with frequency ω_M with wave-vector $\vec{k}_M = \vec{k}_1 - \vec{k}_2$. It is apparent that this term is only non zero in the case $\omega_2 = \omega_1 - \omega_m$. However $\omega_M \ll \omega_1, \omega_2$ hence for the prefactor one can set $\omega_1 = \omega_2 = \omega_0$. Additionally the refractive index for the incident $\bar{n}_1$ and for the scattered $\bar{n}_2$ light will not differ significantly and can be treated as equal. Taking the above arguments into account the differential cross section reduces to

$$\frac{d^2h}{d\Omega}_S = \frac{\hbar\gamma M_0 \omega_0^4}{2\pi c_0^4} |A^{(-)}|^2 (n_M + 1) \tag{2.93}$$

in the same way one can obtain for the Anti Stokes process

[11] The z-axis is defined by the direction of M_0.

$$\frac{d^2h}{d\Omega}_{AS} = \frac{\hbar\gamma M_0\omega_0^4}{2\pi c_0^4}|A^{(+)}|^2 n_M \tag{2.94}$$

Recalling that at elevated temperatures and also under external magnon injection $n_M \gg 1$ it becomes clear that the intensity of Stokes and anti-Stokes processes differ only by the ratio between $|A^{(+)}|^2$ and $|A^{(-)}|^2$. For the above mentioned case however both values are equal and Stokes and Anti Stokes peaks should have identical intensity.

From table 2.1 one can find the relation between the above mentioned magneto-optical effects and the components of the expanded electric susceptibility 2.88. It is apparent that all magneto-optical effects up to second order contribute to the interaction between magnons and light.

A detailed analysis of the above established formalism that leads to realistic light scattering spectra of thin FM films can be found in [54, 55]

Magneto-Optical Effect	magnetic circular birefrigence (Faraday rotation)	magnetic linear birefrigence (Voigt effect)	magnetic circular dichroism (Faraday ellipticity)	magnetic linear dichroism
Orientation between $\vec{k}_1$ and $\vec{m}_0$	parallel	perpendicular	parallel	perpendicular
Underlying physical mechanism	different refractive indices for light with left- and right hand circular polarization	different refractive indices for linear polarized light parallel and perpendicular to the magnetization	different absorption coefficients for light with left- and right hand circular polarization	different absorption coefficients for linear polarized light parallel and perpendicular to the magnetization
Polarization state of scattered light with incident linear polarization	linear with tilted axis	no change if $\vec{E}\|\|\vec{M}_0$ or $\vec{E}\perp\vec{M}_0$ elliptical else	elliptical or circular	no change if $\vec{E}\|\|\vec{M}_0$ or $\vec{E}\perp\vec{M}_0$ linear with tilted axis else
Polarization state of scattered light with incident circular polarization	no change	elliptical or linear	no change	elliptical or linear
Relation to components of electrical suszeptibility [50]	Φ_{MCB} $= \frac{\pi}{\lambda_0}\mathcal{R}(n_r - n_l)$ $\frac{\pi M_0}{\lambda_0 \bar{n}_{re}} K^{im}$	Ψ_{MLB} $= \frac{2\pi}{\lambda_0}\mathcal{R}(n_{\|\|} - n_{\perp})$ $= \frac{2\pi M_0^2}{\lambda_0 \bar{n}_{re}} G_{44}^{re}$ for $\vec{M}_0\|\|[111]$	Φ_{MCB} $= \frac{4\pi}{\lambda_0}\mathcal{I}(n_r - n_l)$ $\frac{4\pi M_0}{\lambda_0 \bar{n}_{re}} K^{re}$	Ψ_{MLB} $= \frac{4\pi}{\lambda_0}\mathcal{I}(n_{\|\|} - n_{\perp})$ $= \frac{4\pi M_0^2}{\lambda_0 \bar{n}_{re}} G_{44}^{im}$ for $\vec{M}_0\|\|[111]$

Table 2.1: Survey of magneto-optical effects. λ_0: Wavelength of the unscattered light. $n_{r,l}$ refractive index for right and left hand circularly polarized light. $n_{||,bot}$ refractive index for linear polrized light with polarization axis parallel and perpendicular to the magnetization.

3 Bose Einstein condensation

3.1 Distribution functions of ideal gases

The concept of Bose-Einstein condensation (BEC) was discovered by Einstein during his investigations of the statistics of indistinguishable particles, namely atoms [16]. His investigation was based on a method which has been invented by Bose in order to derive Planck's law [56] on the basis of statistical considerations [15] instead of ad hoc assumptions. In order to provide the reader with a broader understanding of the mechanisms that lead to BEC some key aspects of the statistics of a ideal gas will be outlined in the following.

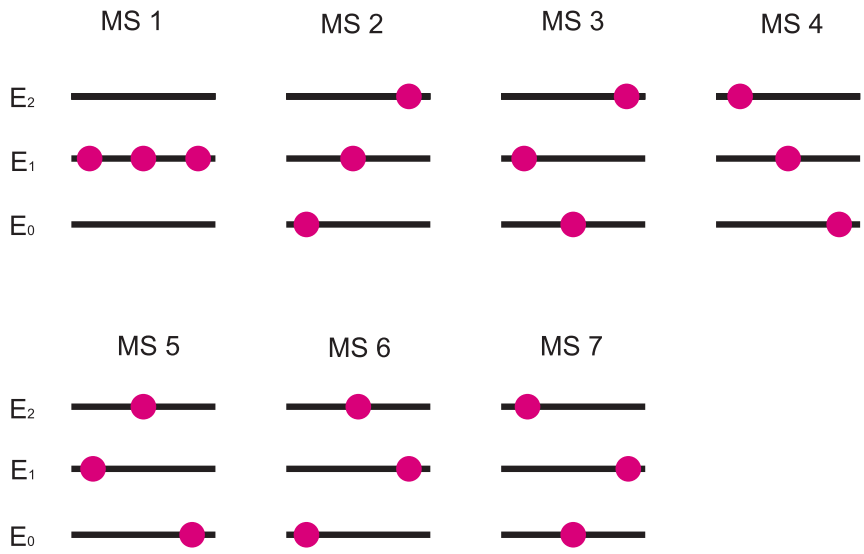

Figure 3.1: Possible microstates, for a three particle, three energy level system with $E_0 = 0$, $E_1 = \epsilon$ and $E_2 = 2\epsilon$, for the macrostate $E_{tot} = 3\epsilon$.

First of all let us introduce the concept of an ideal gas. An ideal gas is a congregation of a large amount[1] of identical particles[2] confined in a certain volume. Let

[1] Typically of order 10^{23}

[2] Note, that identical and indistinguishable are two different concepts. For example two balls may be absolutely identical in all physical measurements like mass, volume and color. Nevertheless

us, for the moment, assume that the number of particles is fixed, we will consider the impact of a non fixed particle number later.

The particles in the gas can exchange energy. However interactions between particles are so weak, that their contribution to the total energy of the ideal gas can be neglected. Hence the total energy of the gas can be written as a sum of single particle energies and no interaction energies have to be taken into account.

A fundamental concept in statistical physics is the concept of macro- and microstates. A macrostate is determined by a macroscopic variable that is measureable e.g. the total energy of the gas or the mean energy of each particle in the gas[3]. A microstate in turn describes the properties of each particle individually e.g. the energy of each particle. There is no way to measure the microstate of a gas that contains 10^{23} particles although it is principally possible. Nevertheless the microstate it is a very helpful concept. In figure 3.1 all possible microstates of a three level system ,that contains three particles and is characterized by the macrostate $E_{tot} = 3\epsilon$, are shown. All microstates represent the same macrostate and all of them are equally likely. However if we are interested in the information of how many particles are in which energy state, we can make the statement that the probability of finding one particle in each energy state is $P_{111} = \frac{6}{7}$ and the probability to find all three particles in the energy E_1 is $P_{010} = \frac{1}{7}$. Hence the first distribution is much more probable. In general a distribution which allows for the most microstates is also the most probable one. This argument becomes even stronger when one considers real thermodynamic systems with a very large number of states and particles. In this case there is always one particular distribution that has an overwhelmingly large number of microstates whereas all other distributions have a comparatively small number of microstates. Hence the probability to find the system in this particular distribution is approximately one. If we denote the number of particles in the energy state E_i with n_i, the total number of microstates of a specific particle distribution, for a system of distinguishable particles with no restrictions on the number of particles in each energy state, can be written as

$$R = \frac{(\sum_i n_i)!}{\prod_i n_i!} = \frac{N!}{\prod_i n_i!} \tag{3.1}$$

where the product goes over all energy states. In order to find the most probable distribution n_i, 3.1 has to be maximized. It is well known that this function exhibits only one maximum and no minimum, therefore it is sufficient to find the n_i's for

two such balls are always distinguishable as long as one keeps track of their trajectory in real space. Hence due to their trajectories they are distinguishable unless they do not occupy the position in space, which is impossible in classical physics.

[3]Which turns out to be proportional to the temperature of the gas.

which the variation of R with respect to n_i is equal zero. For convenience it is useful to search for the maximum of $ln(R)$ instead of R. Since the logarithm is a monotonous function of its argument the maximum will be at the same position. Equation 3.1 can then be written

$$ln(R) = \ln(N!) - \sum_i \ln(n_i!) \tag{3.2}$$

now we can make use of Stirling's approximation which states

$$\ln(x!) \approx x \ln(x) - x. \tag{3.3}$$

Stirling's approximation is very well suited for large x. However, it produces a relatively small error even for small x. With this approximation we can write

$$\ln(R) = N \ln(N) - N - \sum_i n_i \ln(n_i) - n_i. \tag{3.4}$$

In order to find the maximum for $\ln(R)$ with respect to n_i, we have to find out what happens to $\ln(R)$ if we vary n_i by a small amount dn_i. The total number of particles is fixed, hence

$$dN = \sum_i dn_i = 0. \tag{3.5}$$

It follows that

$$d\ln(R) = \sum_i \ln(n_i) dn_i. \tag{3.6}$$

In order to get the maximum of $\ln(R)$ we must demand that $d\ln(R) = 0$, with the constraints of particle conservation 3.5 and energy conservation

$$E = \sum_i \epsilon_i n_i = const. \Rightarrow dE = \sum_i \epsilon_i dn_i = 0 \tag{3.7}$$

with ϵ_i being the single particle energy in the i'th energy state. Using Lagrange multipliers α and β we get the condition

$$d\ln(R) = -\sum_i (\ln(n_i) - \alpha - \beta\epsilon_i) dn_i = 0. \tag{3.8}$$

This condition can be fulfilled for all n_i only if

$$\ln(n_i) - \alpha - \beta\epsilon_i = 0 \tag{3.9}$$

which can be rewritten into the more popular form

$$n_i = \exp(\alpha)\exp(\beta\epsilon_i) \tag{3.10}$$

The constant α is easily eliminated by using the relation

$$\begin{aligned} \sum_i n_i = \sum_i \exp(\alpha)\exp(\beta\epsilon_i) = N \\ \rightarrow \exp(\alpha) = \frac{N}{\sum_i \exp(\beta\epsilon_i)} = \frac{N}{Z} \end{aligned} \tag{3.11}$$

where we have introduced the partition function Z.

The elimination of β is much more complex and leads to an important link between thermodynamics and statistical mechanics. By using several thermodynamic relations and Boltzmann's formula for the entropy $S = k\log(T_{max})$ one finds

$$\beta = -\frac{1}{k_B T} \tag{3.12}$$

Hence the final form of the most probable distribution function of classical particles is given by

$$n_i = \frac{N}{Z}\exp\left(-\frac{\epsilon_i}{k_B T}\right) \tag{3.13}$$

In a system, in which the particle number is not conserved[4] or in which energy can be exchanged with the environment equation 3.13 has to be generalized, nevertheless the principle form will remain the same. The interested reader is referred to e.g.[57]. This kind of distribution was derived by Maxwell and Boltzmann in 1860 and is

[4] E.g. due to chemical reactions in which two atoms react an build one molecule.

therefore called Maxwell Boltzmann distribution. It is very successful in describing the properties of atomic gases that contain a large number of individual particles.

In the year 1900 Paul Drude made an attempt to derive the properties of electrically conducting materials on the basis of a microscopic kinetic theory. He treated the free electrons in the conductor as a gas of particles in the presence of a lattice, which is made out of ions that are localized on lattice sites [58]. In his considerations he implicitly used the Maxwell Boltzmann distribution function to determine the velocities of the electrons in the gas.

It turns out that Drude's theory describes some features of a conductor qualitatively correct. One of the results of the theory is the linear relationship between applied electric field and the current density which is a verification of Ohm's law, which has been obtained experimentally. Nevertheless the Drude's theory fails in the description of many other effects e.g. in the correct description of the conductivity when an ac electric field is applied. It does not describe the temperature dependence of conductivity correctly, it does not account for the different temperature dependencies of conductors and semi conductors and it vastly overestimates the electron heat capacity. These discrepancies are mainly caused by the incorrect assumption that electrons are classical particles whose trajectories can in principle be followed, making them distinguishable. At the advent of quantum mechanics it became clear, that the position and velocity of a particle cannot be determined with absolute precision. The product of uncertainties, in position and velocity, of a particle cannot be arbitrarily small. This phenomenon has been discovered by Werner Heisenberg and is called uncertainty principle. The principle is formulated in a very general way, such that all observables whose quantum mechanical operators does not commute cannot be determined simultaneously with absolute precision. This includes uncertainty in the measurement of all components of an angular momentum as well as the uncertainty in the measurement of energy and time. For position and impulse of a particle the relation can be written as

$$\Delta x \Delta p \geq h \tag{3.14}$$

with Planck's constant h. Hence the full characteristics of an object can not be described in these terms, however they can be described by a wave function that satisfies the Schrödinger equation. The wavelength of a particle can be calculated by an equation derived by Louis de Broglie

$$\lambda = \frac{h}{mv} \tag{3.15}$$

The de Broglie wavelength determines a length scale that is attached to every moving object. As long as two objects are at a distance that is much larger than their wavelength one can follow their paths and they can be considered as being distinguishable hence they can be treated as ordinary particles. However when the distance between two identical objects becomes on the order of their de Broglie wavelength, their wave functions overlap and the particles are indistinguishable. Electrons in a conductor with their very small mass have deBroglie wavelength that is comparable to their mutual distance in the conductor, hence the consequences of indistinguishability have to be taken into account.

The indistinguishability has a huge impact on the collective dynamics of these objects. A many body system of objects cans be described by a many body wave function that defines the state of the system. If the indices of two objects are mathematically exchanged, all physical properties should remain the same. This is only fulfilled when the, many body, wave function is an Eigen state of the operator that exchanges the indices of two particles (called permutation operator). The permutation operator has exactly two different eigenvalues, namely $\lambda = \pm 1$. Accordingly two types of objects exist in nature. The particles whose eigenvalue is one are called Bosons and the ones with eigenvalue minus one called Fermions. The spin statistics theorem [59] states, that Bosons have integer spin, while Fermions have half-integer spin.

It can easily be shown, that a many body wave function with $\lambda = -1$ does not allow that two particles are in the same quantum state [5]. It turns out, that the indistinguishability has to be taken into account if one wants to determine the distribution function for fermions and bosons. Additional quantum numbers, like spin, momentum or angular momentum lead to a degeneracy of each energy state. Particles within one such degenerate state are not distinguishable due to the above mentioned effect.

[5] See e.g. [60] chapter 8.

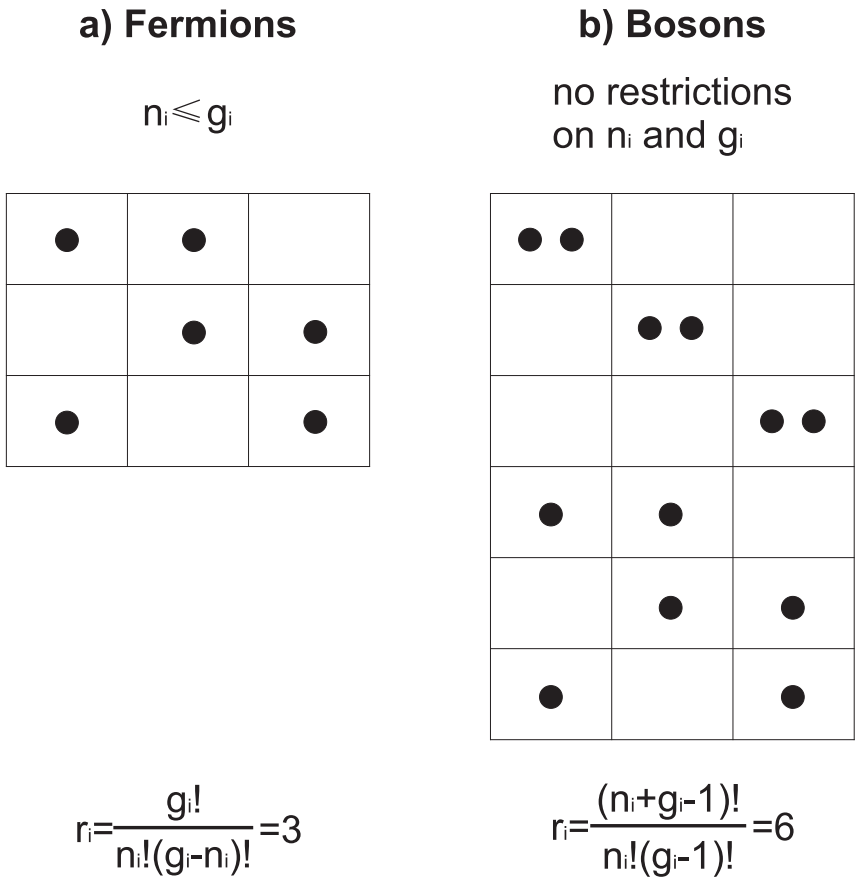

Figure 3.2: Different possibility of arrangements of $n_i = 2$ particles in a $g_i = 3$ fold degenerate energy state for a)Bosons and b) Fermions.

If we consider e.g. two fermions in a three fold degenerate state there are three possible arrangements as can be seen from figure 3.2a. In general when n_i fermions have to be distributed over the g_i degenerate states at energy ϵ_i. The number of possible combinations is

$$r_i = \frac{g_i!}{n_i!(g_i - n_i)!}. \tag{3.16}$$

Since the particles in the different energy states are distinguishable the total number of combinations in a system containing several energy states is a product of the number of combinations in each of them

$$R = \prod_i \frac{g_i!}{n_i!(g_i - n_i)!}. \tag{3.17}$$

The distribution function can be obtained in exactly the same way as for the Maxwell-Boltzman distribution. By using again Stirling's approximation the variation of $\ln(R)$ with n_i is given by

$$d(\ln(R) \approx \sum_i \ln\left(\frac{g_i - n_i}{n_i}\right) dn_i \tag{3.18}$$

By takeing into account the conditions for particle 3.5 and energy 3.7 conservation one arrives at

$$\ln\left(\frac{g_i - n_i}{n_i}\right) + \alpha + \beta\epsilon = 0 \tag{3.19}$$

in order to maximize R. This can be rewritten into the more popular form

$$n_i = \frac{g_i}{\exp\left(\frac{\epsilon_i - \mu}{k_B T} + 1\right)}. \tag{3.20}$$

The distribution 3.20 was first derived by Enrico Fermi [61] and independently by Paul Dirac [62]. It is named Fermi-Dirac distribution after its inventors. Thermal equilibrium is an important and stable state of a many body system. A system that has reached thermal equilibrium will stay in that state, until it is perturbed by an external source. The state of thermal equilibrium is characterized by a minimum in the free energy 2.8. The parameter μ is called chemical potential and can be identified with the derivative of the free energy with respect to the particle number[6]. Hence in a system with no particle conservation the chemical potential will be equal to zero in thermal equilibrium since the free energy will be minimized with respect to the particle number.

In order to derive the distribution function for Bosons one has to count the number of combinations in a g_i fold degenerate energy state with n_i particles when several particles are allowed to occupy one degenerate state. One example with two particle and three states can be seen in figure 3.2b. The number of combinations is given by

$$r_i = \frac{(n_i + g_i - 1)!}{n_i!(g_i - 1)!}. \tag{3.21}$$

The distribution function can be derived in exactly the same way as for fermions. This kind of distribution function was first derived by Satyendranath Bose [15] for

[6] See e.g. [57].

a gas of photons at thermal equilibrium with radiating and absorbing atoms. For photons no particle number conservation has to be taken into account, as photons can be created and annihilated by the atoms. Consequently in his considerations α was equal to zero. Einstein [16] applied Bose's theory to a gas of atoms or molecules in which the particle number is constant and arrived at the distribution function

$$n_i = \frac{1}{\exp\left(\frac{\epsilon_i - \mu}{k_B T}\right) - 1}. \tag{3.22}$$

This distribution function is called Bose-Einstein distribution.

3.2 Thermodynamics of Magnons

The thermal equilibrium of a system, which is at equilibrium with a thermal bath, is defined as the state with lowest free energy 2.8. We have introduced the concept of magnons as the quasi particles of magnetic excitations. With the aid of this concept together with the distribution function 3.22 that has been derived in the previous section, the state of a ferromagnetic (FM) material in thermal equilibrium can now be described in terms of quantum statistics. The energy of each magnon is determined through its wave vector $\vec{k}$, hence 3.22 can be written

$$n_{\vec{k}}(E_{\vec{k}}) = \frac{1}{\exp\left(\frac{E_{\vec{k}} - \mu}{k_B T}\right) - 1}. \tag{3.23}$$

We have seen in section the sections 2.2.2 and 2.3.2 that the number of magnons is not conserved, instead they can be created and destroyed, hence $\mu = 0$. Additionally, it has been shown in section 2.3, that every magnon has spin one which is connected with a magnetic moment $g\mu_B$[7]. Based on these considerations it is now possible to calculate the temperature dependent magnetization of a FM via

$$M(T)V = M(0)V - g\mu_B \sum_{\vec{k}} n_{\vec{k}} = M(0)V - \gamma\hbar \sum_{\vec{k}} \frac{1}{\exp\left(\frac{E_{\vec{k}} - \mu}{k_B T}\right) - 1} \tag{3.24}$$

where $M(0)$ is the magnetization of the FM at $T = 0K$ and V its volume. The summation goes over all components of $\vec{k}$ across the first Brillouin zone. This summation can be replaced by an integral if the spacing between different points in

[7] See section 2.1.1.

k-space is sufficiently small. Then assuming a cubic lattice with lattice constant a the sum can be written as $\sum_{\vec{k}} = \frac{V}{(2\pi)^3}\int_{-2\pi/a}^{2\pi/a} d^3k$, which leads to

$$\begin{aligned} M(0) - M(T) &= \frac{g\mu_B}{(2\pi)^3}\int_{-2\pi/a}^{2\pi/a} \frac{d^3k}{\exp\left(\frac{\hbar\omega_{\vec{k}}}{k_BT}\right)-1} \\ &= \frac{g\mu_B}{\sqrt{2}}\left(\frac{k_BT}{2\pi\hbar\omega_M\lambda}\right)^{3/2} \mathrm{Li}_{3/2}\left[\exp\left(\frac{\hbar\omega}{k_BT}\right)\right] \\ &\approx \frac{g\mu_B}{\sqrt{2}}\left(\frac{k_BT}{2\pi\hbar\omega_M\lambda}\right)^{3/2} \mathrm{Li}_{3/2}[1] \propto T^{3/2} \end{aligned} \tag{3.25}$$

where we have used the dispersion relation for spin waves without dipolar interactions $\omega = \omega_H + \gamma D k^2$. This approximation can be made as most magnons in the system are dominated by exchange interactions thus the error one makes here is negligible. Equation 3.25 renders the famous $T^{3/2}$ law obtained by Bloch [1] in 1930. The $T^{3/2}$ law has been confirmed by numerous experiments, hence it is justified to treat magnons as Bosons also from an experimental point of view.

3.3 Theory of Bose Einstein Condensation

The idea of BEC dates back to Einstein's original paper about the statistics of atoms [16]. He noticed that when the number of particles and the temperature are fixed the volume can not be made arbitrarily small without violating the distribution function. In the following the problem will be treated in more detail. In order to calculate the total number of particles in a real system, where the spacing between adjacent energy levels is very small, it is convenient to replace the sum over all energy states by an integral over the density of states

$$N = \sum_i \frac{g_i}{\exp\left(\frac{E_i-\mu}{k_BT}\right)-1} \approx \int_{E_0}^{\infty} \frac{\rho(E)}{\exp\left(\frac{E-\mu}{k_BT}\right)-1} dE. \tag{3.26}$$

In order to determine the density of states $\rho(E)$ of the considered system one can choose the same way as Bose [15] and Einstein [16] did. Consider a system of particles with no inner degrees of freedom. Each particle can be characterized by its location and its impulse. The impulse of a particle is determined by its energy via

$$\begin{aligned} E &= E_0 + R(p_x^2 + p_y^2 + p_z^2) \\ \rightarrow p_x^2 + p_y^2 + p_z^2 &= \frac{E - E_0}{R} \end{aligned} \tag{3.27}$$

where R is a proportionality factor. Note that equation 3.27 renders the magnon dispersion relation in a infinite medium without dipolar interactions if we set $E_0 = \hbar\gamma B_0$ and $R = \frac{\omega_M \lambda}{\hbar}$ respectively the dispersion of a free particle when we set $E_0 = 0$ and $R = \frac{1}{2m}$.

The total phase space occupied by all particles in the system is given by

$$\Phi = \int dxdydydp_x dp_y dp_z = \frac{4V\pi}{3}\left(\frac{E - E_0}{R}\right)^{3/2} \tag{3.28}$$

where we have to use the formula for the volume of a sphere and where we have assumed, that the gas is confined in a volume $V = x \cdot y \cdot z$. To determine the change in phase space upon a small variation of the energy it is necessary to calculate the derivative of equation 3.28 with respect to the energy

$$\frac{d\Phi}{dE} = \frac{2\pi V}{R^{3/2}}\sqrt{E - E_0} \tag{3.29}$$

Now physics comes into play. According to equation 3.14 the product of the uncertainties in location and impulse is always greater than h, hence particles that occupy a "cell" of volume h^3 in phase space are indistinguishable. In order to determine the number of cells in a phase space element it has to be divided by the volume of one cell and we arrive at

$$\rho(E) = \frac{V}{4\pi^2}(R\hbar^2)^{-3/2}\sqrt{E - E_0} \tag{3.30}$$

with this expression for the density of states, the total number of particles can be written as

$$N = \frac{V}{4\pi^2}(R\hbar^2)^{-3/2}\int_{E_0}^{\infty} \frac{\sqrt{E - E_0}}{\exp\left(\frac{E-\mu}{k_B T}\right) - 1} dE. \tag{3.31}$$

By utilizing the substitution $y = \frac{E - E_0}{k_B T}$ hence $dE = k_B T dy$ and $w = \frac{E_0 - \mu}{k_B T}$ this transforms into

$$N = \frac{V}{4\pi^2}\left(\frac{k_B T}{\hbar^2 R}\right)^{3/2}\int_0^{\infty} \frac{\sqrt{y}dy}{\exp(y + w) - 1} = \frac{V}{4\pi^2}\left(\frac{k_B T}{\hbar^2 R}\right)^{3/2} J(w) \tag{3.32}$$

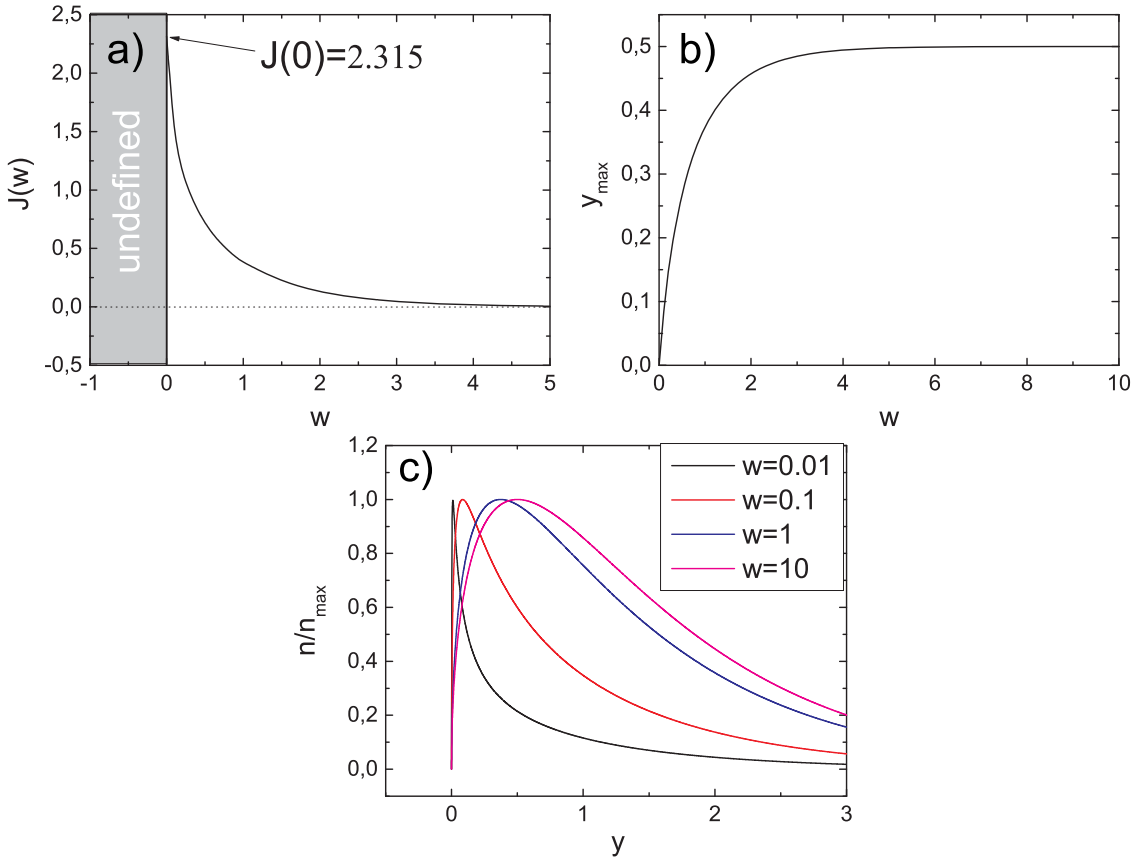

Figure 3.3: a) Plot of the function $J(w)$ as defined in the text. b) Value of the normalized energy y with maximum occupation as a function of w. c) Plot of the normalized particle density n as a function of the normalized energy y, at various values of w.

A plot of the function $J(w)$ is shown in figure 3.3a. It is apparent, that $J(w)$ is a limited function. At large w ($\mu \ll E_0$) it approaches zero asymptotically, whereas it reaches a maximum value, of $J(0) = 2.315$, at $w = 0$ ($\mu = E_0$). An important consequence of this circumstance becomes clear when we rewrite equation 3.32 into the form

$$\frac{n}{T^{3/2}} = \tilde{J}(w) \tag{3.33}$$

with $\tilde{J}(w) = \frac{1}{4\pi^2}\left(\frac{k_B}{\hbar^2 R}\right)^{3/2} J(w)$ and $n = \frac{N}{V}$. Since all other parameters are constant, $\tilde{J}(w)$ depends only on the value of w. When we consider a gas of particles at constant temperature and start to increase the particle density[8], the value of $\tilde{J}$

[8]By increasing the particle number in a fixed volume or by reducing the volume with a fixed particle

has to increase as well. As a consequence the chemical potential μ increases because all other parameters that determine w are fixed. However this only works until the chemical potential reaches the value of E_0 in which case $\tilde{J}$ attains its maximum value. The question now is what happens when the particle density is further increased? In order to find an answer to this question a first step is to determine the energy at which most particles gather. This can be done by calculating the derivative of the occupation function

$$N_y = \frac{V}{4\pi^2}\left(\frac{k_B T}{\hbar^2 R}\right)^{3/2} \frac{\sqrt{y}}{\exp(y+w)-1} \tag{3.34}$$

with respect to the normalized energy y, setting the derivative to zero and solving for y. At the end of this procedure one gets the energy with maximum occupation y_{max} as a function of w in the form

$$y_{max} = \frac{1}{2} + \mathcal{W}\left(-\frac{1}{2}\exp\left[-\frac{1}{2} - w\right]\right) \tag{3.35}$$

where $\mathcal{W}(x)$ is the Lambert $\mathcal{W}$ function. The normalized energy with the highest occupation as a function of the parameter w is plotted in figure 3.3b. It is apparent, that at large values of w, hence when the chemical potential is much smaller than the energy of the ground state, y_{max} tends to $\frac{1}{2}$, however at small values of w, when the chemical potential approaches the energy of the ground state, however the maximum occupation tends to the ground state. This can also be seen in figure 3.3c which is a plot of the occupation function at various values of w. When w is large, the distribution is rather broad with a maximum at $y = \frac{1}{2}$ whereas at small values of w the maximum shifts towards the ground state and the occupation becomes narrower. At very small values of w the distribution gets sharply peaked close to the ground state. Nevertheless the occupation at $y = 0$ stays always zero. Why is that?

It is because the density of states is zero at $E = E_0$ although there has to be at least one energy state. This is an error that has been introduced when the summation over all energy states has been replaced by an integral in equation 3.26. In general this error can be neglected, as the ground state usually makes only a small contribution to the total particle number. This changes when the chemical potential comes close to the energy of the ground state. In this case the occupation of the ground state can not be neglected anymore. The error can be omitted by putting all particles that do not fit into the distribution function due to the restriction 3.33 into the ground state. At very large particle densities and low temperature it can even occur that a majority of all particles occupies the ground state. Particles

number.

in the ground state form the BEC. The same situation can be achieved when the temperature is reduced at constant particle density. The ultimate condition for a BEC is given by

$$\frac{n}{T^{3/2}} > \frac{k_B^{3/2}}{4\pi^2\hbar^3} R^{-3/2} J(0) = 1.107 \cdot 10^{66} R^{-3/2} J(0) \tag{3.36}$$

For a gas of Nitrogen atoms ($m = 14u$) $R = \frac{1}{2m} = 1.075 \cdot 10^{25} kg^{-1}$ and under normal pressure ($p \approx 100Pa$) at room temperature ($T \approx 273K$) we get a particle density of $n_{N_2} \approx 2.7 \cdot 10^{22} m^{-3}$. If we cut out a certain volume of the gas and want to condense it, the critical temperature can be determined through 3.36 and has a value of $T_{BEC,N_2} \approx 52\mu K$. The problem is that before this temperature is reached the nitrogen gas makes a transition into a solid state and hence can not be treated as an ideal gas anymore. Nevertheless it is possible to achieve the conditions for BEC by decreasing the temperature and pressure, keeping the gas in a metastable state.

A different approach has been chosen in [24] in order to get obtain a condensation of magnons. As interactions between magnons are very weak[9] and their density can be increased by e.g. parametric pumping it is much easier to increase the magnon density instead of cooling the sample. In order to determine the necessary increase in density it is necessary to calculate the magnon density at thermal equilibrium

$$\begin{aligned} n_{th} = n(\mu = 0) &= \frac{k_B^{3/2}}{4\pi^2\hbar^3} \left(\frac{T}{R}\right)^{3/2} J\left(\frac{E_0}{k_B T}\right) \\ &= 1.107 \cdot 10^{66} \left(\frac{T}{R}\right)^{3/2} J\left(\frac{E_0}{k_B T}\right) \end{aligned} \tag{3.37}$$

The factor R for magnons in YIG is given by $R_{mag} = \frac{\lambda \omega_M}{\hbar} = 2.876 \cdot 10^{29} kg^{-1}$. The density that is necessary for BEC can be calculated from equation 3.36 taking into account, that $E_0 = \hbar\gamma B_0$ the additional magnon density that has to be created by parametric pumping is given by

$$\begin{aligned} \Delta n = n_{BEC} - n_{th} &= \frac{k_B^{3/2}}{4\pi^2\hbar^3} \left(\frac{T}{R}\right)^{3/2} \left[J(0) - J\left(\frac{E_0}{k_B T}\right)\right] \\ &= 7.17 \cdot 10^{21} T^{3/2} \left[J(0) - J\left(1.344 \frac{B_0}{T}\right)\right] \end{aligned} \tag{3.38}$$

[9] Magnons never bond together and can always be treated as a gas even at very high densities.

Under realistic experimental parameters ($T \approx 300K$, $B_0 \approx 100mT$) the amount of additional, necessary for magnon Bose Einstein condensation (mBEC), amounts $\Delta N \approx 5.5 \cdot 10^{24} m^{-1}$. Neumann *et.al.*have determined the absolute increase in magnon density in YIG subjected to parametric pumping. They found a value of $\Delta n_P = 1.310^{25} m^{-1}$ [63]. Hence it is possible to inject a sufficient amount of magnons ti reach the critical density that is necessary for mBEC. However these additional magnons are injected at a single well defined energy. Therefore the system is brought out of thermal equilibrium. Hence the injected magnons have to thermalize in order to describe them in terms of statistical mechanics. This issue will be addressed in a forthcoming section.

3.3.1 Properties of Bose Einstein Condensates

BEC has been observed in a variety of physical systems. The first observation of an effect, that is nowadays known to be related to BEC, was done by Heike Kamerlingh Onnes. He was the first one who was able to liquefied helium which makes it possible to reach very low temperatures. During his study of the electrical transport properties of Mercury, he noticed that below a certain temperature the resistivity drops to zero and a current can be maintained without any applied voltage [64]. This discovery has been made in the year 1911. At that time no one thought about relating this effect to a BEC, especially because quantum mechanics have not been developed. In a microscopic theory of superconductivity developed by Bardeen *et.al.*[65] it has been shown that when there is a attractive force between electrons in a conductor[10], no matter how weak, electrons will construct pairs known as Cooper pairs. This pairs then "condense" into an energy state that lies above the original Fermi level.

Another system that exhibits BEC appears to be the liquefied Helium itself. Keesom, a former PhD student of Onnes found that the heat capacity of Helium as a function of temperatur makes an unsteady jump at a certain temperature, known as the lambda point [20]. This unsteadiness in the heat capacity was related to superfluidity[11] by Kapitza [66]. Landau developed a two fluid model of superfluid Helium [67] where below the lambda point the Helium splits into two parts, one "normal" part and a "condensed" part.

The two aforementioned systems however can not be regarded as a "pure" BEC as they are by no means ideal gases. Nevertheless these systems exhibit features which are associated with BEC. The first "pure" BEC has been created by Anderson *et.al.*in 1995, in a dilute atomic vapor of Rubidium-87 atoms [17] and in the same year by Davis *et.al.*in a gas of sodium atoms [18]. These systems are much closer

[10] In this case mediated through phonons.

[11] A superfluid is a fluid with no viscosity hence it experiences no friction when flowing.

to an ideal gas than liquid Helium or electrons in a superconductor. Despite the differences of atomic condensates, liquid helium and electrons in a superconductors, these systems share a lot of common features in the condensed state. One of the most intriguing features is the appearance of quantized vortices. A vortex in any of these systems can not have arbitrary angular momentum, instead each vortex has a specific angular momentum that is determined by the properties of the system. Quantized vortices have been observed in liquid Helium [68], in Type II superconductors [19] as well as in trapped atomic gases [69]. Because quantized vortices are a consequence of superfluidity, they give a strong hint for the latter. Additionally superfluidity has also been observed directly in liquid Helium, through frictionless flow [66, 70], and in superconductors, by the existence of a persistent current with no applied voltage. In the case of atomic condensates no independent verification of superfluidity has been reported so far. This is attributed to the fact, that atomic condensates have to be kept in an magneto-optical trap in order to maintain the extremely low temperatures[12] which are necessary for condensation.

Another intriguing property of all three systems is the coherence of all particles within the condensate. This means that one does not have to consider the individual phases of all particle wave functions in the condensate. Instead all particle wave functions can be described by the same phase and consequently by one wave function leading to the concept of a macroscopic matter wave. The existence of quantized vortices is already a manifestation of this feature; however most people associate coherence rather with interference effects like they occur e.g. in optics. Indeed interference has been observed in vessels filled with liquid Helium that are connected via small pinholes [71] and in weakly coupled superconductors [19, 72]. In atomic condensates interference has been demonstrated by a direct collision of two seperated condensates. As a result interference fringes with high and low density can be observed [73].

Apart from systems that consist of real matter particles, BEC has also been observed in various quasi particle gases.

In fact superconductors can be seen as the first quasi particle systems in which a BEC like phase transition has been observed. This assertion is based on the fact that electrons are not able to condense due to their fermionic nature; however Cooper pairs, which are a sort of quasi particles that exhibit a bosonic nature, are allowed to condense into a single energy state. Another very interesting system of quasi particles, in which BEC has been observed, are exciton-polaritons in semiconductor cavities excited by intense EM radiation [74, 75]. Exciton polaritons are quasi-particles that describe bound electron hole pairs in e.g. a semiconductor.

[12] Usually in the nano Kelvin regime.

It is apparent that the concept of BEC is very general and can be applied to various physical systems.

3.3.2 Theoretical description of Real Bose Einstein condensates

The theoretical description of weakly interacting Bose-Einstein condensed gases has been developed over many years. In order to describe the superconducting state Ginsburg and Landau introduced the concept of a order parameter Ψ in the context of a thermodynamic theory. After formulation of the BCS theory [65] this order parameter could be interpreted as the square root of the Cooper pair density times a complex phase $\Psi = \sqrt{(}n)e^{i\phi} \Rightarrow |\Psi|^2 = n$. As to describe vortices in superfluid condensates Gross and Pitaevskii used a nonlinear Schrödinger equation to determine the time evolution of the order parameter [76]. The general form of the Schrödinger equation is given by

$$i\hbar\frac{\partial}{\partial t}\Psi(\vec{r},t) = \left[-\frac{\hbar^2}{2m}\vec{\nabla}^2 + V(\vec{r},t)\right]\Psi. \tag{3.39}$$

It contains contributions from kinetic and potential energy. In an ideal non-interacting Bose gas, the potential $V(\vec{r},t)$ is caused only by external sources. However such a system does not exist in reality and interactions between particles in the condensate have to be accounted for. This can be attained by separating the potential into an internal and an external one

$$V(\vec{r},t) = \underbrace{\int \Psi(\vec{r}',t)V(\vec{r}'-\vec{r})\Psi(\vec{r},t)d\vec{r}'}_{V_{int}(\vec{r},t)} + V_{ex}(\vec{r},t) \tag{3.40}$$

the inter-particle potential $V(\vec{r}'-\vec{r})$ tends to zero for large distances, hence if we assume an potential that depends only on the distance between the particles and not on their mutual orientation (s-wave scattering potential) and that the condensate density does not change significantly on the range of the inter-particle potential, the internal potential can be written as

$$V_{int}(\vec{r},t) = |\Psi(\vec{r},t)|^2 \int V_{eff}(\vec{r})d\vec{r}. \tag{3.41}$$

This leads to the famous Gross-Pitaevskii equation

$$i\hbar\frac{\partial}{\partial t}\Psi(\vec{r},t) = \left[-\frac{\hbar^2}{2m}\vec{\nabla}^2 + V_{ex}(\vec{r},t) + g|\Psi(\vec{r},t)|^2\right]\Psi \tag{3.42}$$

with $g = \int V_{eff}(\vec{r})d\vec{r}$. In other systems additional terms might be added in order to account e.g. for different inter-particle potentials acting among condensed particles and between condensed and non-condensed ones. Other terms can also account for the creation and annihilation of particles in systems where the particle number is not conserved. These equations are generally referred to as Ginsburg Landau models as they rely on the concept of a macroscopic order parameter. The theoretical description of superconductors is very different from that of other BEC systems, as it incorporates the formation of Cooper pairs. Additionally there is large variety of effects, connected with electric and magnetic fields, due to the electric charge of the particles[13] [19].

Under several aspects the description of superfluid liquid Helium is much easier than that of superconductors. However this system can by no means be regarded as a system of non- or even weakly-interacting particles. Therefore hydrodynamic relations have to be considered in order to describe this system correctly. For further information the interested reader is referred to e.g. [77, 78, 79, 80].

3.4 Bose Einstein Condensation of Magnons

In 1981 Lavrinenko *et.al.*observed em radiation from the magnon ground state, when magnons with higher energies where injected into the system via parametric pumping [81]. The existence of radiation from the ground state suggests that its occupation exceeds the equilibrium value by far. In the same paper Lavrinenko *et.al.*proposed a mechanism that is responsible for the redistribution of magnons from the pumped state into the ground state. This mechanism relies on direct scattering from the pumped state into the ground state, compensating losses and leading, at sufficiently strong pumping, to a instability of the ground state, therefore they named the effect "kinetic instability". In 1989 Snoke showed theoretically, that thermal equilibrium in a Bose gas can be reached within a few characteristic scattering times when the system has been brought out of equilibrium [82]. The system he considered, where excitons in a semiconductor. Kalafati *et.al.*applied this concept to a magnonic systems and gave an alternative explanation for the observation of Lavrinenko *et.al.*based on successive thermalization of the pumped magnons leading to a new equilibrium state with increased chemical potential and ultimately[14] to a BEC that forms at the ground state [21, 83, 22, 23]. At that time it was not possible to determine which of the two proposed mechanisms actually occurs.

In 2006 Demokritov *et.al.*presented measurements that gave strong evidence that the latter mechanism is responsible for the accumulation of magnons in the ground

[13] E.g. the Meissner effect.
[14] At sufficiently high pumping powers.

state. By using Brillouin light scattering[15] they where able to map the magnon density as a function of space, frequency, time and wave vector in a thin YIG film whilst injecting magnons into an energy state that is close to FMR by parametric pumping. These measurements revealed that the injected magnons do not reach the ground state directly but successively giving evidence for a thermalization process [24, 84, 85, 29, 86, 28]. Shortly thereafter the coherence of the magnon BEC (**mBEC**) has been demonstrated through decay characteristics [27, 26] and through intense monochromatic microwave emission from the ground state [86]. There have also been attempts to describe the properties of the condensate theoretically with the aid of a phenomenological Ginsburg-Landau model [33] and a Hamiltonian description [30].

The formation of mBEC can be well understood qualitatively in terms of magnon relaxation theory. In section 2.3.2 the most important scattering processes in a magnon system have been introduced. The rate of these processes can, theoretically, be determined by the transition rate given by Fermi's golden rule 2.70. It has been argued that the four magnon scattering process is the dominant process in many cases, albeit the transition rate of a four magnon process depends strongly on the magnon density due to its nonlinearity.

It has also been pointed out in section 2.3.2 that the number of magnons is not fixed. Instead magnons can be destroyed due to interactions with the crystalline lattice and due to magnon-magnon interactions. However the dependence on magnon densities for these relaxation processes is not as strong as for the four magnon scattering.

Hence at high magnon densities one can imagine a situation in which the scattering rate among magnons exceeds scattering rates that lead to a reduction of the magnon number. Hence for a sufficiently short time the magnon system can indeed be treated as being isolated from the environment. This is the regime of quasi-equilibrium, meaning that the magnon system itself can be in thermal equilibrium[16] although it is not in thermal equilibrium with the environment[17].

In general in such a quasi equilibrium state the magnon temperature as well as the chemical potential of the magnon system (see3.23) will differ from the corresponding values of the phonon gas which also obeys Bose Einstein statistics.

This scenario has been realized by Dzyapko *et.al.*[84]. Once a short pumping pulse injected a large amount of magnons with certain energy into the system, it was allowed to evolve freely without any external perturbation. After a certain time the distribution of magnons, which had initially a strong over-occupation at the

[15] See section 4.3.1.
[16] The magnon distribution can be described by the Bose-Einstein statistics.
[17] In this case phonons.

energy state, in which magnons have been injected, could again be described by the Bose-Einstein statistics. In the experiment the thermalization time depended strongly on the amount of injected magnons as it is expected from four magnon scattering processes. However for a certain time span the chemical potential of this new distribution was grater than zero because the dissipation of magnons was much slower than interactions among them.

The situation can be compared to water in a thermos bottle. The water in the thermos can be seen in analogy to the magnon system at high density and the air around the thermos in analogy to the phonon system. In absolute thermal equilibrium the temperatures of the water and the surrounding air are the same. If now an ice cube is thrown into the water the energy distribution of the water molecules is not thermal anymore as there are too many molecules with low energy. However, after a certain time, the ice cube melts due to scattering processes between low energy molecules and high energy molecules, hence the molecules in the ice cube gain energy from the liquid which results in a thermalization. After a certain time the energy distribution in the bottle is thermal again but the water has a lower temperature than before. However as the water inside the thermos is only weakly coupled to its environment the temperature of the water will differ from the temperature of the latter. In this situation the water can be seen as being in a quasi equilibrium. It takes a long time to reestablish total thermal equilibrium due to the poor coupling of the two systems.

In fact atomic condensates are also by no means in a thermal equilibrium but in a quasi equilibrium. At the densities and pressures present in the atomic clouds, in which BEC has been observed, the stable equilibrium state would be a solid. However the experimentalists take advantage of the fact, that when single atoms bond in order to build a solid excess energy emerges. This energy has to be transferred to another particle to ensure energy conservation. Hence the elementary processes that lead to the conversion from the gaseous to the solid state are three particle processes. These processes are sufficiently rare in real experiments to allow for thermalization after each cooling step before the whole atom cloud reaches the solid state. Nevertheless atoms leave the gas at a constant rate during the whole process [87]. So its particle number is strictly speaking **not conserved** but like in a magnonic system this fact is negligible as long as the characteristic inter-particle scattering time is much shorter than the characteristic time a particle needs to leave the system.

4 Study of the mBEC ground state

The experimental part of this thesis is divided into two major parts. The experiments of the first part deal with the properties of a unperturbed mBEC, whereas the second part concentrates on the properties of dynamic excitations in a mBEC.

The first experiment of the first part aims at the determination of the distribution function close to the ground state. All experiments that deal with mBEC so far have been carried out with the experimental technique of Brillouin light scattering (BLS) [24, 85, 84, 25, 28]. Only one experiment involved the detection of microwaves emitted from the condensate however this technique had to incorporate a magnon confluence process, hence the observed properties can be influenced by this process [86]. The problem with BLS is its relatively poor resolution regarding the frequency of magnons. However a good frequency resolution is crucial in order to determine whether the signal from the ground state originates from magnons in one energy state or from several energy states close to the ground state. The answer to this question is crucial for a definite proof that BEC really occurred, as in this case only the ground state should have an extraordinary large occupation.

The second experiment of the first part investigates the coherence properties of the mBEC. Coherence is a important property of Bose-Einstein condensed systems and has been observed in all of these systems that has been found so far, including superconductors [19, 72], liquid Helium below the lambda point [71], atomic condensates [73] and exciton polarition condensates [74]. The coherence of mBEC has also been under investigation [26, 27, 31]. This experiment builds up on the previous one an demonstrates the existence of a spatially non uniform ground state due to an interference between the condensates localized in the two degenerate ground states of the thin film dispersion relation. Additionally this finding shows that there is a fixed phase difference between the two condensates.

4.1 Creation of mBEC

In contrast to atomic condensates the experimental setup for Bose-Einstein condensation (BEC) in a magnonic system is rather simple. It is sufficient to inject a large amount of magnons into a ferromagnet with suitable characteristics. No cooling is needed when the amount of additional magnons is high enough to satisfy relation

3.36 at room temperature.

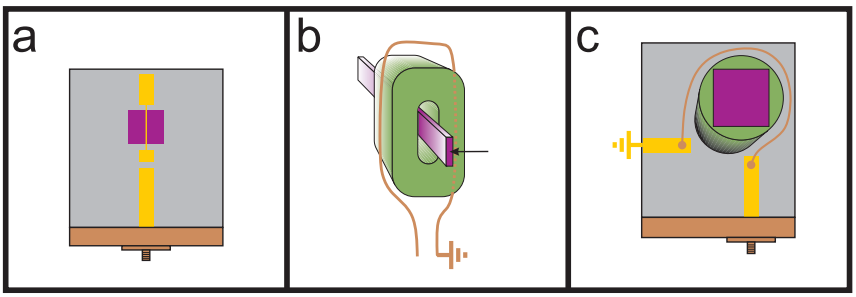

Figure 4.1: Three different geometries that can be used in order to inject additional magnons necessary to achieve mBEC. a) A microstrip is fed with a microwave current. The microstrip is capacitively coupled to a resonator via a air gap. Du to reflections at the ends of the resonator a standing wave with a large amplitude is created. Additionally the resonator can also be provided with a narrow region in order to spatially confine the microwave current leading to even higher amplitudes of the microwave field. The magnetic part of the microwave field excites magnons in a FM film placed on top of the resonator. b) A conducting wire is fed with a microwave current at one side and grounded on the other. Due to the close vicinity to a dielectric resonator with suitable shape, eigen oscillations of the microwave field inside the dielectric can be excited. A high dielectric constant of the resonator material causes a reflection of the microwaves at the material-air boundary. When a appropriate mode is excited a strong oscillating magnetic field is produced inside the resonator. This magnetic field is used to inject magnons into a FM placed inside the hole. c) A microstrip is fed with a microwave current. The microstrip is cut into two pieces and replaced by a conducting wire in between. The conducting wire is wrapped around a cylindrical dielectric resonator. The microwave field around the wire excites self oscillations of the same frequency inside the dielectric resonator like in **b**. A part of the microwave field in the resonator leaks into the surrounding space and is used to excite magnons in a FM film placed on top of it.

All experiments done so far in the field of mBEC used Yttrium Iron Garnet (YIG) thin films epitaxially grown on Gadolinium Gallium Garnet(GGG) [88, 89]. Due to its Curie Temperature of $T_C = 560K$ it is well suited for applications at room temperature. In addition it is prominent for its extraordinary high magnon-phonon relaxation time of $\tau_{mag-phon} \approx 0.5\mu s$ and strong nonlinearity leading to a small magnon-magnon relaxation time. At this point it should be mentioned, that YIG is not a true ferromagnet (FM). In fact it is a ferrimagnet with 20 sublattices. However all sublattices are strongly exchange coupled to one another, making modes in which some of the sublattices precess out of phase occur only at rather high precession

frequencies. Thus, in the region of interest ranging up to frequencies of $10GHz$, YIG can be regarded as a FM [90].

Magnons can be pumped by means of a microstrip [24], a wire [91] or a dielectric resonator. The resonator acts as an amplifier for the microwaves that are supplied by a microwave generator. Due to reflection and superposition of microwaves inside the resonator high amplitudes of the magnetic and electric fields can be reached so as to allow for parametric excitation of magnons [1]. The various excitation schemes are drawn schematically in figure 4.1. It is important to keep in mind, that the amount of injected magnons varies vastly among the different excitation schemes, even when the same pumping power is applied.

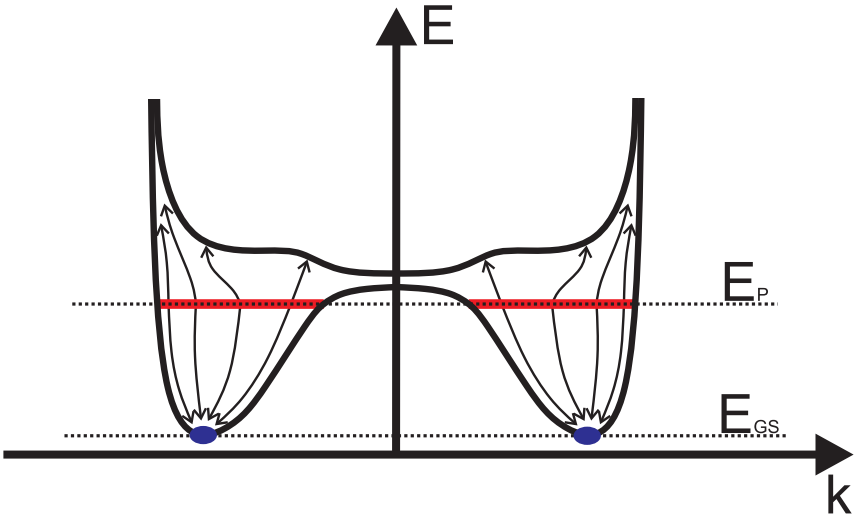

Figure 4.2: Schematic of the processes that finally lead to mBEC. The black lines indicated the upper and lower boundary of the spin wave dispersion relation in a thin film. A large amount of magnon states with various wave vectors exist in between these boundaries. Primary magnons with energy E_P are injected via parametric pumping. At sufficiently high pumping powers they populate all magnon states that are accessible at that energy. Scattering processes between magnons cause a energy and momentum change of primary magnons leading to a redistribution into all possible magnon states.

The basic steps that lead to mBEC are shown in figure 4.2. The microwave field of the resonator injects magnons at the energy E_P which is determined by the frequency of the microwave field f_P via

$$E_P = h\frac{f_P}{2} \tag{4.1}$$

[1] See section 2.2.2.

with Planck's constant h. These magnons are called primary magnons. Because of the additional magnons the system can no longer be regarded as being in thermal equilibrium since the occupation at E_P vastly exceeds the amount of magnons that should be present at this energy according to the Bose-Einstein distribution.

It has been pointed out in section 2.3.2 that magnons are able to interact with each other, leading to an exchange of energy and momentum. Under suitable conditions this kind of stochastic processes will lead to a redistribution of primary magnons over all possible magnon states ending up in a distribution that can again be described by Bose-Einstein statistics. However the parameters, temperature and chemical potential, of the new distribution will differ from the previous values.

However at the same time magnons leave the system at a constant rate due to interactions with phonons. This is the main reason why a material with very high magnon-phonon interaction times is needed. Because only in the case when the magnon-magnon relaxation time is much shorter than the magnon-phonon relaxation time a new thermal equilibrium can be reached before the additional magnons leave the system. In the other case the magnon distribution would simply never be able to reach a state in which it is describable by Bose-Einstein statistics with new parameters, instead the overpopulation close to E_P would spread into some adjacent energy states and become smaller until the former state is reached again and the magnon distribution can again be described by Bose-Einstein statistics with the same parameters as before [85].

Thanks to the extraordinary large magnon-phonon relaxation time in YIG it is possible to reach a quasi-equilibrium state with non-zero chemical potential [84]. When the pumping power exceeds a certain threshold which is mainly determined by the geometry of the excitation scheme, the value of the chemical potential of the new distribution function becomes as large as the lowest energy state. According to section 3.3 this results in $y = 0$ and marks the threshold for mBEC [24, 26]. However, in contrast to all other known BEC systems, the magnon dispersion relation in thin films exhibits two degenerate energy minima at opposite momenta. Hence in such a system two condensates are created. The consequences of this fact are the subject of investigation in section 4.3.

Although the basic principle of mBEC is well understood the particular scattering processes, that lead to the redistribution of magnons, are still under theoretical investigation. However it is clear that four magnon processes play a major role, as they do not suffer from energy and momentum conservation restrictions like the three magnon process and they conserve the magnon number. An additional feature that is in favor of this process lies in the fact that the four magnon scattering time depends strongly on magnon density. As a consequence the magnon-magnon relaxation time becomes smaller the more magnons are injected into the system.[92]

4.2 Determination of the absolute line-width of a mBEC

4.2.1 Concept

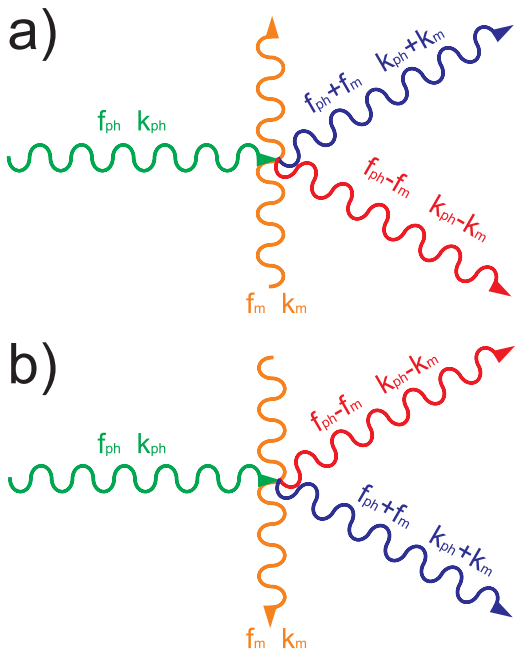

Figure 4.3: Schematic drawing of light scattering on magnons with wave vector a)k and b)$-k$ with stokes and anti-stokes processes

The experiment is based on the interactions between photons and magnons as described in section 2.3.3. When a photon interacts with a magnon its frequency gets slightly shifted, depending on weather it is a stokes or anti-stokes process, to the red or to the blue. In the first case a magnon is created in the latter it is annihilated. To ensure impulse conservation the impulse of the magnon has to be carried away by the photon when a magnon is annihilated or it has to be provided by it in the case where a magnon is created. This leads to a diffraction of the inelastically scattered light into an angle determined by the momentum of the magnon.

When photons pass a FM that has a large occupation of magnons at a particular energy E_m and momentum $\pm\vec{p}_m$, a part of them will be diffracted into angles $\theta_{1,2} = \pm \arcsin\left(\frac{p_m}{p_{ph}}\right)$ due to the above mentioned reasons. The light that has been scattered into the angle θ_1 contains blue shifted photons which result from interactions with magnons with momentum $\vec{p}_m$ and red shifted photons that has been scattered on magnons with momentum $-\vec{p}_m$ and vice versa for θ_2. Hence each beam contains two different frequency components originating from scattering on magnons at $\vec{p}_m$ and $-\vec{p}_m$. In addition in both beams a number of elastically scattered photons with unchanged frequency can be found. Elastically scattered photons originate from diffraction on defects on the surface of the FM and also from impurities and lattice distortions within it. The three frequencies are shown in figure 4.4a. The coexistence of photons with three slightly different frequencies within one light beam leads to the effect of beat caused by interference which results in an amplitude modulation of the light. However if there is no fixed phase relation between magnons with momentum $\vec{p}_m$ and $-\vec{p}_m$ the positions of maxima and minima from interference of individual photons will not

coincide. As a consequence the modulations will be averaged out in a long term measurement and no beat can be observed in the transmitted light anymore. But if the phase difference is fixed the maxima and minima will coincide leading to an observable amplitude modulation. Assuming that the intensities from stokes- and anti-stokes processes are equal, the resulting amplitude of the light at a particular position in space can be written as

$$E = A[\sin(2\pi(f_{ph} - f_m)t) + \sin(2\pi(f_{ph} - f_m)t)] + B\sin(2\pi f_{ph}t) \tag{4.2}$$

with the frequency of the magnon $f_m = \frac{E_m}{h}$. The function is plotted in figure 4.4b. The power that can be detected by a photomultiplier is proportional to the squared amplitude and is shown in figure 4.4c. The frequencies components that are present in the squared signal and their amplitudes are summarized in table 4.1.

0	f_m	$2f_m$	$2(f_{ph} - f_m)$	$2f_{ph} - f_m$	$2f_{ph}$	$2f_{ph} + f_m$	$2(f_{ph} + f_m)$
$2A^2 + B^2$	$2AB$	A^2	$A^2/2$	AB	$A^2 + B^2/2$	AB	$A^2/2$

Table 4.1: Frequencies and amplitudes in the squared signal.

However all components that contain the original photon frequency f_{ph} can be neglected. The value of f_{ph} amounts several hundred Terahertz, amplitude modulation with such high frequencies are not observable by conventional detectors. On the other hand even frequencies that contain f_m have still to high to be observed by them.

Nevertheless these frequencies can be made observable with the aid of the stroboscopic principle. For this purpose the light is not send through the FM continuously, but in short pulses with a fixed repetition frequency. The duration of each pulse must be much smaller than $\frac{1}{2f_m}$. In this case the amplitude of the individual pulses will be modulated. The situation is illustrated in figure 4.4d. The resulting signal will now have a pronounced peak at the laser repetition frequency f_{lr} and at zero frequency DC[2]. Due to the modulation of individual pulses, however four additional peaks emerge in the spectrum between DC and f_{lr} at

$$\begin{aligned} f_{lr1} &= f_{lr} - (f_m - n \cdot f_{lr}) \\ f_{lr2} &= f_{lr} - 2(f_m - n \cdot f_{lr}) \\ f_{dc1} &= f_m - n \cdot f_{lr} \\ f_{dc2} &= 2(f_m - n \cdot f_{lr}) \end{aligned} \tag{4.3}$$

[2]The DC signal reflects the mean intensity that is received by the photomultiplier.

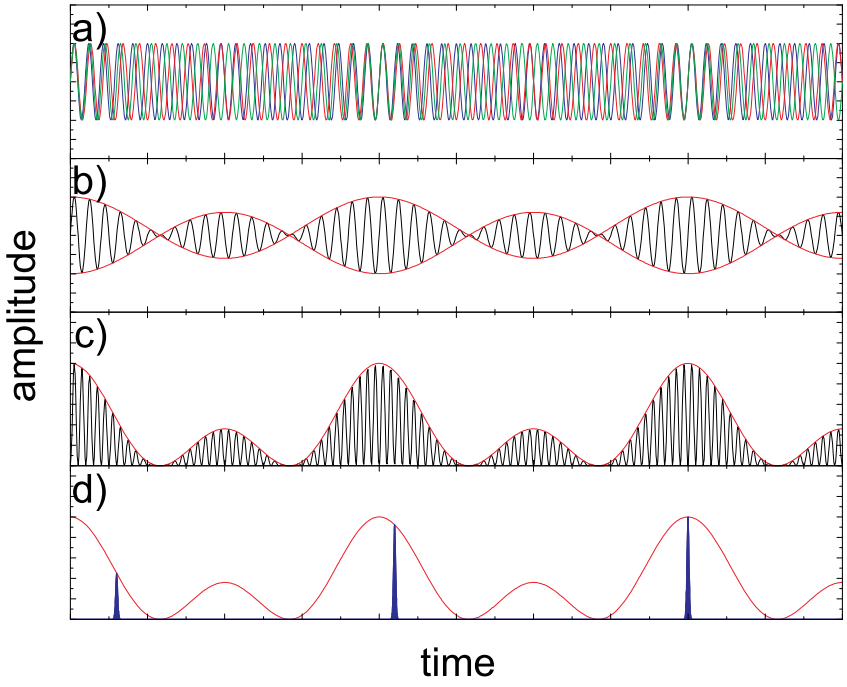

Figure 4.4: Schematic representation of the involved frequencies in the experiment. a) Amplitude of the electric field of a em wave consisting of three slightly different frequencies. Green: unshifted; Red: red shifted; Blue: blue shifted. b) Resulting amplitude of the em wave after interference c) Power received by a photomultiplier d) Principle of a stroboscopic measurement

Here f_{lr1} and f_{dc1} refer to the signal first harmonic, originating from amplitude modulations with the magnon frequency whereas f_{lr2} and f_{dc2} refer to the second harmonic originating from amplitude modulations with the double magnon frequency. The natural number n refers to the number of full periods $\frac{1}{f_m}$ between two light flashes. In the case of magnons with a single precession frequency these additional peaks would be absolutely sharp having a FWHM of zero. But if, for some reasons, the precession frequency is not well defined but has a certain width, the peaks f_{lr1} and f_{dc1} will be broadened by the same amount and the second harmonic signal by twice the amount. It is clear that with such a system it is not possible to determine the absolute magnon frequency since the number of full periods $\frac{1}{2f_m}$ is unknown. However this technique is a powerful tool to determine the linewidth of magnons at a particular frequency and to find small frequency shifts in their spectrum.

4.2.2 Experimental arrangement

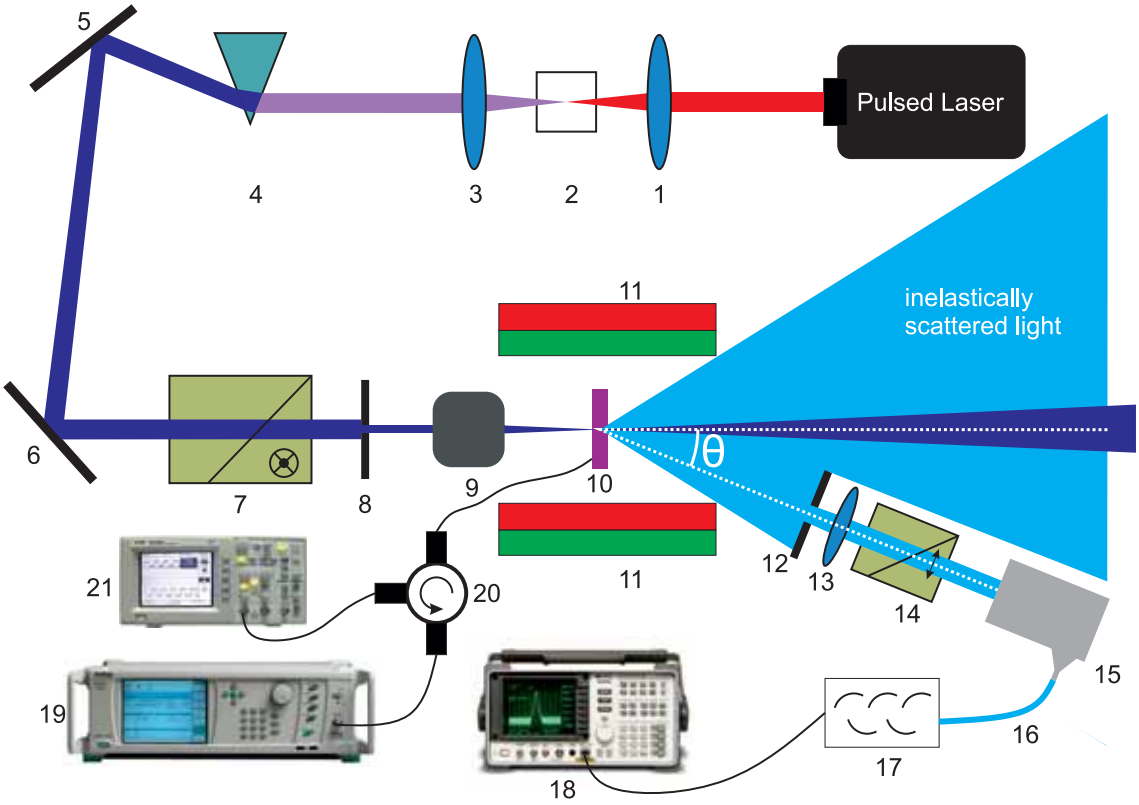

Figure 4.5: Experimental Setup for the determination of the absolute linewidth of a mBEC by means of the stroboscopic principle. 1. Lens 2. α-BBO crystal 3. Lens 4. Quartz prism 5,6. Mirror 7. Calcite polarizer 8. Pinhole 9. Camera objective 10. Device under Test 11. Permanent magnet 12. Pinhole 13. Lens 14. Calcite Polarizer 15. Fiber collimator 16. Optical multimode fiber 17. Photomultiplier 18. Spectrum analyzer 19. Microwave generator 20. Y-circulator 21. Digital Oscilloscope. Black lines are coaxial cables.

The setup for a measurement, with the concept developed in the previous section, is shown in figure 4.5. A pulsed laser produces light pulses with a duration below one hundred femtoseconds at a repetition rate of $f_{lr} \approx 80MHz$. The repetition rate is fixed within one series of measurements but can vary between different measurements. The laser wavelength is tunable between 700nm and 1080nm. To find the optimum laser wavelength two conditions have to be fulfilled. The sample should be transparent and magneto-optical effects should be as strong as possible at this wavelength. Measurements of the Faraday rotation on YIG samples have been carried out by Wettling *et.al.*[93]. It was found that a maximum of the Faraday rotation

occurs at a laser wavelength of approximately $430nm$. However our YIG samples are highly absorptive at this wavelength. As a compromise a wavelength of $\lambda_L = 490nm$ has been chosen. Unfortunately this wavelength is not within the tunability range of the pulsed laser. In order to reach it, the Laser is tuned to $980nm$ and the light first send through a $\alpha - BaB_2O_4$ (α-BBO) crystal which generates, due to its optical nonlinearity, higher harmonics of the incident light [94]. To achieve the high power density that is required to produce higher harmonics in the crystal the light from the laser is first focused onto it and collimated afterwards. However, only a few percent of the transmitted light gets converted. Since in this experiment we are interested only in the second harmonic of the laser light a prism is used to direct other wavelengths out of the beam path.

After conversion into the desired wavelength the laser light is send through a calcite polarizer in order to get a well defined polarization state. A pinhole is used to reduce the beam diameter before it gets focused onto the YIG sample with a camera objective in order to reduce the amount of elastically scattered light that reaches the detector. A camera objective is used, since it is corrected for spherical aberration and astigmatism, leading to small size of the focused laser spot. The sample design is similar to that from figure 4.1a with the only difference that the substrate of the microstrip has a hole where the resonator gets narrow, such that the narrow part of the resonator has no support and is held only by its connections to the wider parts of the resonator. With this design light can transmit the YIG sample close to the resonator and be analyzed afterwards. The microwave resonator is connected to a tunable microwave generator a Y-circulator is used to observe the reflected microwave power on the oscilloscope. External magnetic field can be swept by changing the distance between the two permanent magnets.

Once the light has passed the YIG sample it is collected by a lens, send through a second polarizer in order to discriminate between elastically and inelastically scattered light and coupled into an multimode optical fiber through a fiber collimator with an off axis parabolic mirror. The three components are placed on a rotatable optical rail, so that light scattered into different angles can be collected. The multimode fiber directs the collected light onto a photomultiplier where it is converted into electrical signals that are proportional to the squared amplitude of its electric field. The electric signal is send to a spectrum analyzer in order to examine its spectral components.

4.2.3 Results

This section is divided into two paragraphs. The first paragraph reports on measurements that have been made in order to determine the inherent frequency resolution of the setup described in the previous section. The second paragraph presents re-

sults that have been obtained with this setup on a YIG sample in which magnons are injected via parametric pumping above the threshold for mBEC.

Pre-Measurements

In order to evaluate the principle frequency resolution of the system ferromagnetic resonance (FMR) has been excited inside the sample. For this purpose the resonator is fed with microwaves at a particular frequency with moderate power and the external field is changed until a substantial change in the reflected microwave power can be observed. The change in the reflected microwave power originates from a strong absorption of microwaves when the FMR condition is fulfilled leading to a substantial change in the quality factor of the resonator and consequently to a change in the reflected power.

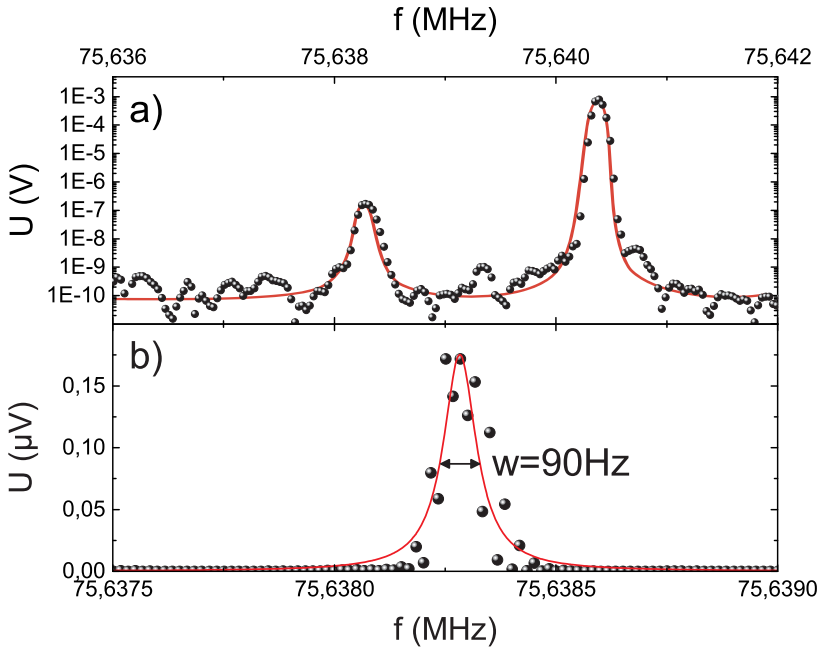

Figure 4.6: Spectrum of the electric signal from the photomultiplier close to the laser repetition frequency when FMR is excited in the FM. a) Relative magnitude of the spectral components in logarithmic scale. The tall peak represents the spectral component from the laser repetition frequency f_{lr}, the small peak originates from the amplitude modulation of the individual light pulses due to the interaction with magnons and is located at f_{r1}. The red line is a guide for the eye. b) Peak at f_{r1} in linear scale. The red line is a Lorentzian fit through the data points revealing a $w = 90Hz$ width of the peak.

At FMR the momentum of magnons is zero, hence the light is inelastically scattered in the forward direction $\theta = 0°$. To get rid of the light that passes the sample without being scattered at all the two polarizers where set to total distinction, such that most photons that did not interact with magnons do not reach the photomultiplier. Without microwaves a single peak in the spectrum at the output of the photomultiplier can be found at the laser repetition frequency because although the polarizers are set to total distinction they are not able to filter out all of the unscattered photons.

When microwaves are turned on two additional peaks appear. To interpret the spectrum that can be seen in figure 4.6a one should account for the fact that calcite polarizers have a distinction ratio of typically 100,000:1. Taking into account that most of photons traverse the sample, without being inelastically scattered, it is obvious that even with the two polarizers set to total distinction a large amount of them reaches the photomultiplier. As a consequence the first harmonic signal is dominant in the spectrum. It is well known that the width of FMR in frequency is determined only by the stability of the source of excitation. The microwave generator used in the present experiment has a accuracy in the μHz regime.

Nevertheless it can be seen from figure 4.6b that the FMR peak has width of $w = 90Hz$ which is much larger than the stability of the involved excitation source. Apparently the width of the peak is limited by the resolution bandwidth of the spectrum analyzer which determines the accuracy of the used experimental setup. For comparison the frequency resolution of the Brillouin light scattering (BLS) technique is limited to $50MHz$ [26] therefore an improvement by six orders of magnitude in frequency resolution has been achieved.

Measurements

A BEC is a state of matter in which a large quantity of particles occupies a single energy state, namely the ground state. However up to now there has been no experimental or theoretical work that defines what a single energy state in a magnonic system actually is.

Discrete energy levels occur only in confined systems. The distance between adjacent energy levels is determined by the spatial extents of the confined region. In a confined region a wave can only have certain wavelengths. Waves with other wavelengths are quickly destroyed due to interference when they are reflected at the borders of the region. In a region with open ends and length l these wavelengths are given by $\lambda_j = \frac{2l}{j}$ with the natural number j. Expressed in momentum of the corresponding quasi-particles this gives $p_j = \hbar\frac{\pi j}{d}$ leading to a discretization in momentum space. With use of the dispersion relation the spacing between adjacent energy states can be calculated.

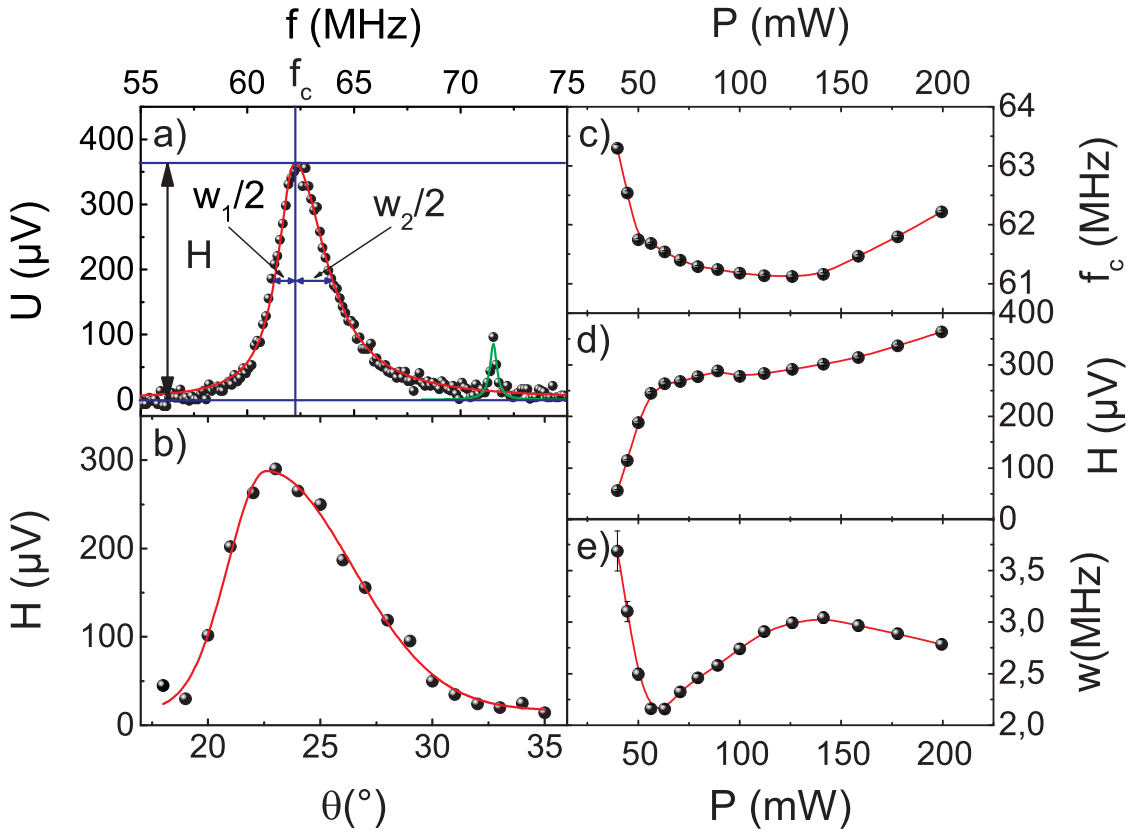

Figure 4.7: Characteristics of the spectral peak originating from an mBEC as a function of pumping power P and scattering angle θ. The condensate was created by injecting primary magnons with an energy of $E_P = 17.91\mu eV$ into a YIG film placed in a magnetic field with a strength of $B_0 = 149,3mT$. a) Part of the spectrum of the electric signals from the photomultiplier. The high and broad peak originates from magnons close to the ground state; the small and narrow peak originates from primary magnons. The red line is a bi-Lorentzian fit through the data points in the whole interval. The green line is a Lorentzian fit through the data points close to the small peak. Important parameters of the bi-Lorentzian fit are marked in the figure. b) Dependence of mBEC peak height H on angle θ at a pumping power of $P = 126mW$. The red line is a bi-Gaussian fit through the data points. c) Dependence of the mBEC-peak central frequency on pumping power. d) mBEC-peak height as a function of pumping power. e) Full width at half maximum of the mBEC-peak as a function of pumping power. In c),d) and e) the red line is a guide for the eye and θ is set to 23°.

From the above considerations it is found that the spacing between energy levels in a $5\mu m$ thick YIG-film around the ground state has a value of $70kHz$ when the condensate is confined in a region of $50\mu m$ in z-direction and a value of $17kHz$

with a confinement of $100\mu m$. A spatial width of the condensate between these two values has been reported by Dzyapko *et.al.*[91]. However it should be kept in mind, that there is hardly any confinement in y-direction hence in reality energy levels are even closer.

However all energy levels are subjected to several broadening mechanisms the most fundamental of which arises from Heisenberg's time energy uncertainty. The width of an energy level is determined by the mean life-time of particles in this state. Expressed in frequency via $E = hf$ the width is given by $\Delta f \geq (4\pi\Delta t)^{-1}$. The life-time of magnons in the ground state above the threshold for condensation has been determined by Demidov *et.al.*to a value of $\Delta t \approx 250ns$ leading to a frequency broadening of $\Delta f = 0.6MHz$. Hence individual energy levels can principally not be distinguished in this measurement. Nevertheless it is interesting to investigate whether the measured linewidth is indeed comparable to the value given by uncertainty principle and how this value changes with experimental parameters.

The signature of mBEC in the spectrum from the photomultiplier can be seen in figure 4.7a. The small narrow peak originates from parametric magnons whereas the large broad peak originates from magnons close to the ground state. While the parametric peak exhibits a symmetric Lorentzian shape, the peak from the ground state can be best fitted with a bi-Lorentz function given by

$$\begin{aligned} &\text{if } f < f_c \\ &\quad U(f) = H\frac{w_1^2}{4(f-f_c)^2 + w_1^2} \\ &\text{else} \\ &\quad U(f) = H\frac{w_2^2}{4(f-f_c)^2 + w_2^2} \end{aligned} \tag{4.4}$$

The meanings of the used parameters are illustrated in figure 4.7a. The total width of the peak is given by $w = \frac{w_1}{2} + \frac{w_2}{2}$.

Dependence of the ground state peak height as a function of the scattering angle θ has been determined at pumping powers from which it is known that mBEC occurs. The results are plotted in figure 4.7b. From the bi-Gaussian fit, that is defined analogous to the bi-Lorentz function 4.4, it is found that the maximum is located at $\theta_{max} = 22.6 \pm 0.16°$ which corresponds to a momentum of $p_m = 5.19 \pm 1.99 \cdot 10^{-28} Ns$[3] parallel to the external magnetic field. The value coincides very well with previous BLS-measurements of Demidov *et.al.*[28].

Once the optimum angle θ has been determined, pumping power is swept and characteristics of the ground state peak are recorded. Figure 4.7c shows the central

[3]This corresponds to a wave number of $k_M = (4.92 \pm 1.89) \cdot 10^6 m^{-1}$.

frequency of the peak as a function of pumping power. At small pumping powers a negative frequency shift can be seen. This is probably due to the nonlinear frequency shift that arises from the reduction of magnetization in the presence of magnons. Unfortunately a quantitative evaluation is not possible as the absolute magnon density cannot be determined in this experiment. However at large pumping powers a positive frequency shift is observed this might be attributed to interactions between magnons at high densities leading to change in the ground state energy of magnons.

The change of the peak height with pumping power can be seen in figure 4.7d. It basically reproduces the results from previous measurements on mBEC that have been reported in e.g. [85]. A strong increase starting from small pumping powers and a subsequent saturation of the magnon density due to nonlinear dissipation mechanisms is can be observed. Strong increase in peak height marks the threshold for mBEC subsequent saturation is probably due to the saturation of spin wave amplitudes under parametric excitation as described in section 2.2.2.

In Figure 4.7e the width of the ground state peak as a function of pumping power is plotted. Starting from $P = 40mW$ the width decreases with increasing pumping power until it reaches a minimum at $P_{min} = 60mW$ with a value of $w_{min} = 2.1MHz$. Further increase of the pumping power leads to a increase of the width until a maximum is reached at $P_{max} = 140mW$ with a value of $w_{max} = 3MHz$. Subsequent increase of pumping power leads to a furthermore reduction of the peak width.

Attributed to a lack of theoretical models that describe the behavior of a magnonic system beyond the threshold for mBEC there is no satisfying explanation for the observed peak widths. The decrease of peak width starting from small pumping powers is most probably due to the formation of an mBEC in which a large number of magnons occupies a single energy state. Due to the aforementioned reasons single energy levels can principally not be resolved. However the minimum width of $w_{min} = 2.1MHz$ is close to the limit given by the time energy uncertainty of $0.6MHz$. It should also be kept in mind that the mBEC is created at, for BEC, extraordinary high temperatures, namely room temperature. Thus energy states close to the lowest energy state will also be strongly occupied. Although it has be asserted in section 4.2.1 that coherence, which should be only given for magnons in the ground state, is a necessary condition for magnons to be observed with this experiment, it is imaginable that due to the overlap of energy states also magnons in states close to the ground state are coherent and can thus be observed. The observed values are in agreement with previous measurements of Dzyapko *et.al.*[86] on the width of the ground state peak with other methods.

A better quantity which determines whether BEC has taken place might be the drop-off width of the peak towards lower frequencies $\frac{w_1}{2}$. In the experiment values

of this quantity down to $\frac{w_1}{2} = 0.53MHz$ has been observed which is even lower than the estimated limit due to energy time uncertainty. Hence one can indeed state that in a magnon gas, in which magnons have been injected above the threshold for mBEC, the ground state is the energy state with the largest occupation. That is the necessary and sufficient criterion for BEC. Further measurements of the line width in a more confined geometry in which individual energy states are well separated can give a further proof of this conclusion. The instability of a mBEC at high magnon densities arising from a attractive interaction between magnons as proposed by Tupitsyn *et.al.*[30] is a good candidate to explain the peak broadening above P_{min}.

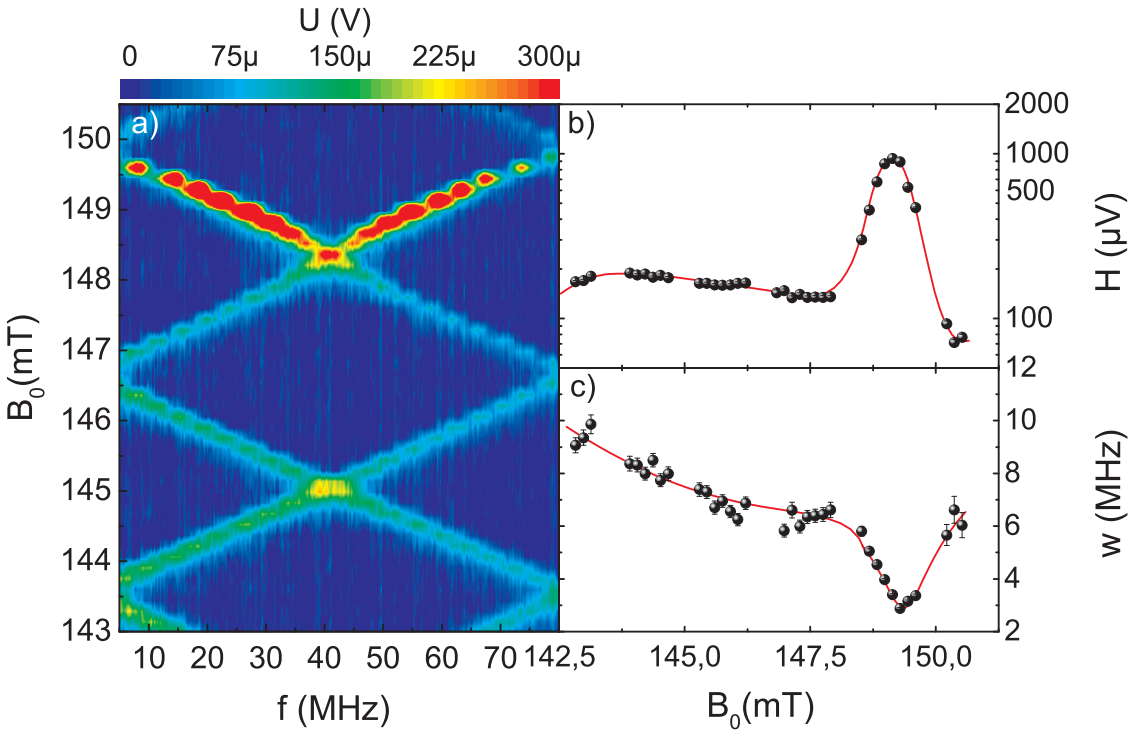

Figure 4.8: Evolution of the spectral peaks f_{rep1} and f_{dc1} with changing external magnetic field. The energy of injected magnons has a value of $E_p = 17.91\mu eV$, the pumping power has a value of $P = 100mW$. Scattered light is collected under an angle $\theta = 23°$. a) Contour plot of the spectrum between DC and f_{lr} as a function of the external magnetic field. The peaks move with a gyromagnetic ratio of $\gamma = 26 \pm 1 \frac{MHz}{mT}$. b) Width and c) height of the bi-Lorentzian fit to one of these peaks as a function of the external magnetic field.

The evolution of the spectrum, between DC and f_{lr} at a pumping power of $P = 100mW$ with otherwise identical parameters to the previous measurement, is shown in figure 4.8a. The external magnetic field determines the energy of all magnons in

the system according to equation 2.9 and 2.21. All other properties of the dispersion relation are determined by the shape of the sample and material parameters.

A change of magnetic field thus changes the energy of the magnon ground state whereas the energy of pumped magnons, which is determined through the shape of the resonator and the frequency of the microwave source, remains constant. This has a striking impact on the thermalization of magnons. In the extreme case where the ground state energy and the energy of pumped magnons coincide there is no need for a thermalization since a large number of magnons is injected directly into the ground state. However such an object cannot be called a BEC as it does not arise from thermodynamics.

In figure 4.8a one can nicely see the change in ground state frequency with increasing magnetic field. Since in YIG magnetic moments arise only due to unpaired spins in Fe-ions [90] the frequency of spin waves depends linearly on the external magnetic field with the electron gyromagnetic ratio of $\gamma_{el} = 28\frac{MHz}{mT}$. This value has been confirmed by numerous experimental works. However in this measurement a value of $26 \pm 1\frac{MHz}{mT}$ has been determined. A possible explanation for a slight deviation of the measured value from the standard one might be a hybridization between the lowest spin wave mode and a phonon mode which, at the magnetic fields considered here, cross each other close to the spin wave ground state. As a result the minimum of the hybridized mode is shifted in frequency and k-space. Since the phonon mode is not affected by the external magnetic field the frequency of this new ground state will have a different dependence on the external magnetic field than the non-hybridized one. This interpretation is also supported by measurements of the same dependence at higher magnetic fields where no phonon mode crosses the lowest magnon mode close to its minimum. In this case the change in frequency is given by the electron gyromagnetic ratio.

Peak height as a function of the external field is plotted in figure 4.8b. When the magnetic field is increased the energy difference between pumped magnons and the ground state ΔE becomes smaller. The dependence has a poorly pronounced maximum at approximately $B_{0,max1} \approx 143mT$ and a sharp maximum at $B_{0,max2} = 149mT$. The origin of the first maximum is not clear. It is known, that when ΔE becomes too large hardly any magnons reach the ground state and the peak height should drop to zero. However in a simple model one would expect that H increases monotonously until ΔE becomes zero and drop abruptly afterwards. Instead the peak height decreases moderately at fields above $B_{0,max1}$ before a sharp increase between $B_{0,inc} \approx 148mT$ and $B_{0,max2}$, followed by a sharp decrease of H. It seems natural to assume that the maximum height marks the point where ΔE becomes zero because magnons can only be pumped into existing states. However in this case the peak height should decrease more rapidly than it has been observed in the experiment, on the other hand the slow decrease might be due to a non resonant

excitation caused by higher order parametric processes that inject magnons at the pumping frequency. So it remains unclear whether this maximum marks the point $\Delta E = 0$ or not.

The peak width as a function of external magnetic field is illustrated in figure 4.8c. When ΔE becomes smaller, less scattering processes are necessary for the pumped magnons to reach the ground state. As a consequence more of them can gather at the ground state before they dissipate into phonons leading to a narrower peak. Starting from $B_0 = 142mT$ the width of the ground state peak decreases moderately until a value of the external field of $148mT$ is reached. From this point on the width decreases very quickly until it reaches a minimum at $B_{0,min} = 149mT$ with a value of $w = 2.88MHz$. This value is higher then the smallest one determined in the previous one. This is attributed to the value of the pumping power used in this experiment.

4.2.4 Conclusion

It has been demonstrated, that the magnon distribution exhibits a sharp peak at the ground state when additional magnons are pumped into a magnon gas beyond the threshold for mBEC. The smallest linewidth determined in this experiment has a FWHM of $2.1MHz$. The half width at half maximum towards smaller energies has a minimum value of $0.53MHz$ thus demonstrating that the ground state has the highest occupation among all energy states. This gives definite proof to the assertion that the magnon gas made the transition into a BEC. A positive frequency shift in the central frequency of the peak at high injection rates indicates that the interaction between magnons is attractive.

4.3 Non Uniform Ground State and Quantized Vortices

4.3.1 Experimental arrangement

The experimental technique used in this experiment is, as in the previous section, based on interactions between magnons and photons. The elementary processes are the same as illustrated in figure 4.3. However in this setup one is not dependent on the interference of phonons scattered by magnons with opposite wave vectors. Instead a Fabry Perot interferometer is used as a band pass filter, hence the frequency of each photon that reaches the interferometer can be determined directly without the need of interference with other photons.

The distance between mirrors in a FPI determines the central frequency of the band pass filter; hence by sweeping it, photons with different frequency shifts can be detected. With this technique it is possible to measure the amount of photons that have been inelastically scattered by magnons with various energies. By relating the number of counts of the photomultiplier to the distance between the mirrors a spectrum of the scattered light can be obtained. A spatial map can be obtained by moving the sample in the two lateral directions before accumulating the next spectrum. Relating the displacement of the sample to the recorded spectra gives the desired spatial density map of magnons with various frequencies. However, it should be kept in mind that not all magnons interact with photons with equal likelihood. This effect has to be considered whilst interpreting the recorded spectra. Since a high spatial resolution of the measurement is crucial, in order to observe the desired effect, special attention will be given to this issue.

Figure 4.9 shows a draft of the experimental setup. A CW-laser is used as a photon source. The most important demand for the laser light is a high degree of monochromaticity, as light scattering events on magnons are rather rare any sub-bands of the laser light would lead to increased noise in the measurements. A small beam divergence and high degree of coherence of the beam allows for diffraction limited focal spot size which is necessary for high spatial resolution. Stability of the output power of the laser is crucial for unambiguous interpretation of the recorded spectra. A diode pumped, solid state, single mode laser, operating at an output frequency of $\lambda_L = 532nm$ meets all these requirements.

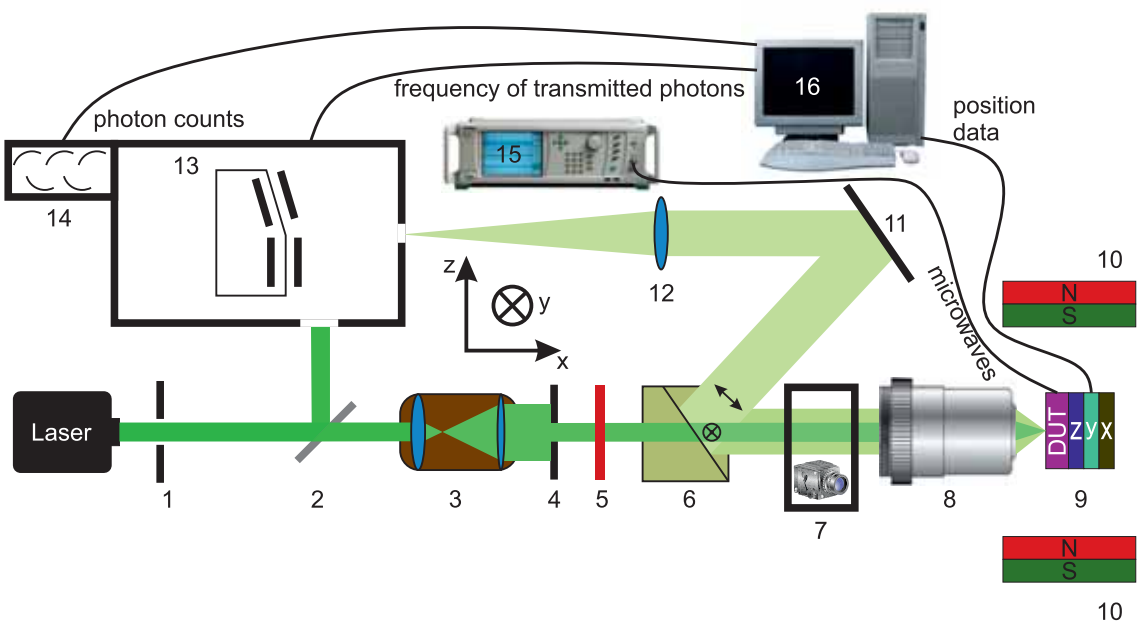

Figure 4.9: Experimental Setup for mapping of magnon densities with frequency and diffraction limited spatial resolution. 1. Pinhole 2. Beam splitter 3. Beam expander 4. Pinhole 5. Half wave plate 6. Calcite polarizer 7. Imaging system 8. Microscope objective 9. Device under test (DUT) together with x,y and z translation stage 10. Permanent magnet 11. Mirror 12. Lens 13. Scanning Tandem Fabry Perot Interferometer 14. Photomultiplier 15. Microwave generator 16. Computer. Black lines are electric cables.

The tandem Fabry Perot interferometer (TFPI) that has been used in the experiment needs a reference beam in order to actively adjust the spacing and the tilt angle between the mirrors in it as these quantities can be influenced by temperature variations, vibrations of the optical table and acoustic waves. For this purpose the laser beam is split into two parts by a beam splitter. One part of the light is subsequently used as the reference, while the other is used for measurements. A pinhole behind the laser prevents that light, which has been back scattered from the beam splitter, enters the output terminal of the laser, as in this case the laser might become unstable.

In a next step the light is send through a beam expander which, in the ideal case, expands the beam without changing any of its characteristics, and a pinhole in order to get a uniformly illuminated cross section of the beam with even smaller divergence.

A half wave plate and a calcite polarizer are used in order to adjust the laser beam power and to establish a well define polarization state of the incident light. The half wave plate tilts the major polarization axis of the partially polarized laser

light, such that only a part of it is transmitted into the forward direction through the polarizer while the remaining light is directed out of the beam path.

The well collimated laser beam with homogeneously illuminated cross section and well defined polarization state is directed onto the entrance aperture of a microscope objective, where it is focused onto the device under test (DUT). The schematic of the DUT investigated in this experiment is shown in figure 4.1a. The microscope objective allows the light to be focused into a almost diffraction limited spot due to correction for spherical aberration and astigmatism. The DUT is mounted on a translational stage, with piezo actuators, movable in the x, y and z-direction. Movements in z- and y-direction are responsible for two dimensional mapping of magnons, while the purpose of movement along the x-direction is to place the sample into the focal spot of the laser beam. Piezo actuators allow for a positioning accuracy of approximately ten nanometer. Hence the spatial resolution of the setup is not limited by the accuracy of the positioning system but by the diameter of the laser spot size which is, even in the diffraction limited case, always greater than half the wavelength of the laser light[4].

The scheme employed in the experiment makes use of the quasi-back scattering technique. In this scheme the light is focused onto a boundary layer between segments of the DUT with different dielectric constants at which it is reflected. The choice of the boundary layer determines to what kind of magnons the experiment is sensitive and what the spatial resolution will be.

When the FM film faces the laser beam and the light is focused onto the boundary layer between FM and air, highest spatial resolution can be obtained. However the volume in which photons and magnons can interact is restricted to a small region close to the material-air barrier. In a perfectly focused laser beam only the evanescent part of the light which penetrates into the FM can interact with magnons. This part of the light is subjected to an exponential decay of its intensity along a path perpendicular to the boundary layer. The penetration depth is determined by a propagation constant which is a material parameter with a certain dependence on the wavelength of the light. Hence magnon modes with a high density at the boundary layer produce stronger signals than those mainly located in the volume of the FM.

In the other case when light is focused onto the boundary between FM and substrate[5], the light traverses the whole sample[6] before it gets reflected. This way all magnon modes with various profiles across the thickness of the FM can be detected. However this increase in sensitivity can only be reached at the expense of spatial

[4] In this case the diameter of the focal spot is greater than $266nm$.
[5] E.g. the YIG/GGG interface.
[6] This is only possible when the sample is sufficiently transparent for light at the laser frequency.

resolution as the beam diameter changes whilst travelling through the FM film.

In order to achieve the highest spatial resolution, the beam is focused onto the FM air barrier. Owing to the fact that only the lowest lying magnon mode is of interest in this measurement which has a sufficiently high density at the boundaries of the YIG-film. Since the z- and y-directions of the translational stage are not absolutely perpendicular to the incident laser beam, the sample will be brought out of focus when moved along these directions for spatial mapping. To correct for this error an imaging system has been installed that allows observation of the focal spot, on the sample, during the measurement. When the sample is brought out of focus, an increase of the spot size is perceived by the camera and the sample is moved along the x-direction until the spot has the same size as before.

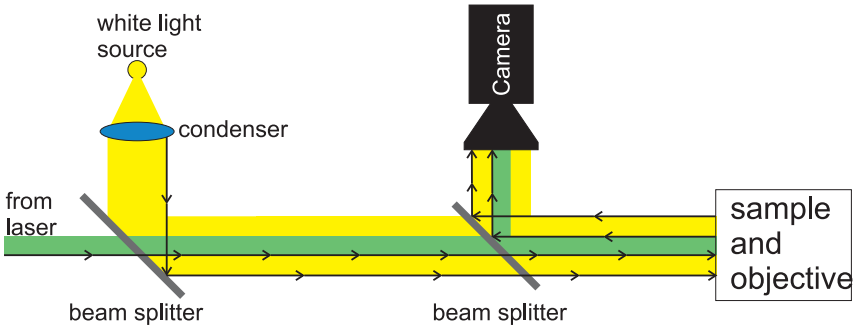

Figure 4.10: Makeup of the imaging system for determination of the laser spot position and size on the sample for adjustment of the focal plane and positioning control.

A schematic of the imaging system is illustrated in figure 4.10. It consists of a white light source a digital camera and two beam splitters. One beam splitter is used to direct the white light onto the sample such that it can be reflected from its surface making it visible for the camera. The second beam splitter is used to redirect a part of the light that has been reflected from the sample surface into the camera where it produces an image of the sample surface and the laser spot.

The reflected and scattered light is collected by the same microscope objective with which the laser beam has been focused onto the sample surface. Due to the nonzero momentum of magnons inelastically scattered light does not return on the same path but will have a certain angle with respect to the incident laser beam. This leads to a momentum cutoff in the magnons that can be detected. Magnons with too large wave-vector lead to a large angle between incident and scattered light hence they cannot be collected by the objective for further analysis which makes them unobservable in the measurement.

The light that has been collected by the objective reaches the same calcite polarizer

again. The part of the it that has not interacted with magnons and hence has a unchanged polarization state gets transmitted, whereas the part of the light that did interact with magnons and whose polarization has changed is reflected by the polarizer and focused into the TFPI.

The basic design of a Fabry Perot interferometer is very simple. It consists of two mirrors with identical reflectance R placed at a distance l parallel to each other. When light is shined in, perpendicular to the surface of the mirrors, it gets reflected between them several times [7] and interferes with itself. As a consequence only photons with certain frequencies will be transmitted, while all others are reflected. The transmission as a function of frequency is given by

$$T(f) = \frac{\tau_0}{1 + \frac{4F^2}{\pi^2} \sin^2\left(\frac{2\pi l \cdot f}{c}\right)} \tag{4.5}$$

with the finesse F which, in the ideal case[8], is given by $F \approx \frac{\pi\sqrt{R}}{1-R}$ with c being the speed of light. It can easily be seen that the transmission is a periodic function of f, hence an unambiguous assignment of a transmission peak to a certain frequency can only be done within the distance of two adjacent transmission peaks. This frequency interval is called the free spectral range (FSR) and is given by $\Delta f = \frac{c}{2l}$. Assuming that the laser frequency is known and that one looks for small deviations from this frequency, the FSR gives the maximum deviation from the frequency that can be measured with the interferometer. The width of each spectral peak δf determines the frequency resolution. Its value can be calculated through

$$\delta f = \frac{cF}{2l} \tag{4.6}$$

It can easily be seen that FSR and resolution depend on each other in an interferometer with given finesse in such a way that a large FSR results in a poor frequency resolution and vice versa. However, the finesse of a mirror pair is limited due to practical reasons like surface roughness, diffraction losses, imperfect alignment etc. In order to get a higher finesse, the beam can be send through the interferometer several times. In the experiment a six pass TFP has been used. It incorporates two mirror pairs. The light is send three times through each of these mirror pairs increasing the finesse and free spectral range of the interferometer. Details can be found in [95, 96, 97, 98]. A general review of BLS is given in [11]. Now by varying the mirror spacing by a small amount, the transmission frequencies can be swept

[7] The quantity of usable reflections is determined by the reflectance of the mirrors.
[8] When all components are perfectly aligned and the mirrors are absolutely flat and parallel to each other.

which makes it possible to record a spectrum of the incident light by relating the amount of transmitted photons to the actual mirror spacing.

The data of mirror spacing, photon counts and lateral position is send to a computer where it is recorded.

4.3.2 Results

As pointed out in section 4.1 the magnon dispersion relation exhibits two degenerate energy minima with opposite momentum. Consequently two different condensates occupy the same spatial region. Their total wave function can be written as

$$|\Psi|^2 = \frac{1}{T}\int_0^T \left[\Psi_+ \sin(k_{gs}z + \omega t) + \Psi_- \sin(-k_{gs}z + \omega t + \Theta(r,t))\right]^2 dt \tag{4.7}$$

Where $\Psi+$ and Ψ_- are amplitudes of the wave functions in the degenerate energy minima located at momenta $\pm k_{gs} = \frac{\pm p_{z,gs}}{\hbar}$. T is the measurement time and $\omega = \frac{E_{gs}}{\hbar}$ is the energy of the ground state. In real measurements the condition $T >> \frac{2\pi}{\omega}$ is always fulfilled.

In BLS experiments the magnon density $n(\vec{r}) = |\Psi(\vec{r})|^2$ can be mapped. A fixed phase Θ should therefore result in a periodic modulation of the ground state magnon density in real space. The periodicity of the density modulation is given by the momentum of the ground state. The momentum depends strongly on the value of the exchange integral J and the thickness of the FM film d. However it is almost independent of the applied external magnetic field B_0 [9].

A value for the momentum has been determined experimentally by Demidov *et.al.*[28], to a value of $p_{z,gs1} = 3.69 \cdot 10^{-28} Ns$[10] in z-direction and with zero momentum in y-direction ,with wave-vector resolved BLS spectroscopy and also in the experiments of section 4.2. The value determined in section 4.2 was $p_{z,gs1} = 5.19 \pm 1.99 \cdot 10^{-28} Ns$[11] in z-direction. The momentum in y-direction has not been measured. Both values measured of $p_{z,GS}$ coincide well within the measurement errors and they also coincide with the theoretically determined momentum of magnons in the ground state.

[9] See section 2.2.1.
[10] Corresponding to a wave number of $k_{z,gs1} = 3.5 \cdot 10^6 m^{-1}$.
[11] Corresponding to a wave number of $k_{z,gs2} = (4.92 \pm 1.89) \cdot 10^6 m^{-1}$.

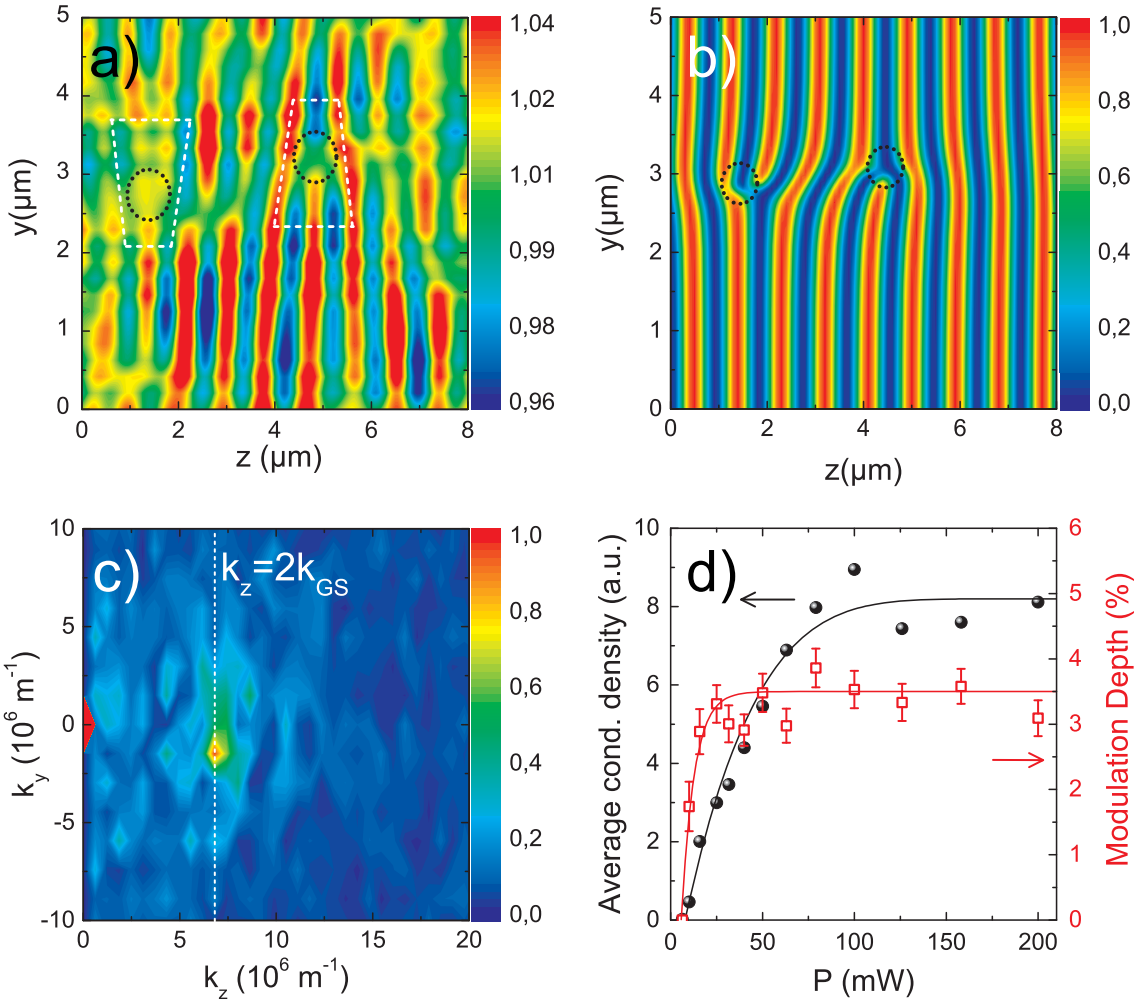

Figure 4.11: Results of the two-dimensional mapping of the ground state magnon density. a) Two dimensional spatial density map of ground state magnon next to the microwave resonator located at $z \approx -25\mu m$. Due to interference between the condensates created at the two degenerate energy minima a periodic pattern can be observed. Dashed circles indicate positions of stationary vortices. b) Density distribution of a mBEC calculated through direct numerical integration of equation 4.8 with parameters $m_{||} = m_{el}$ $m_{\perp} = m_{||}/15$ $\eta = 0.1$ $\gamma = \mu_C = 15\mu eV$ $J = 0.1\mu_C$ $\Gamma_1 = 0.1U_0$ $\Gamma_2 = 0.3U_0$. Γ_1 and Γ_2 are the values for the nonlinear magnon dissipation outside and inside the crystalline defect areas, marked with black dotted cycles, respectively. c) Two dimensional Fourier transform of the spatial density map in **a**. Apart from a huge peak at $k_y = k_z = 0m^{-1}$ which reflects the average condensate density a second peak at $k_y = -1.5 \cdot 10^6 m^{-1}$ $k_z = 6.8 \cdot 10^6 m^{-1}$ is apparent, reflecting the periodicity of the density modulation. d) Average condensate density and periodic pattern modulation depth as a function of pumping power.

Figure 4.11a shows the spatial density distribution of magnons with ground state energy close to the resonator that provides the pumping field. A periodic density variation is apparent. The density map was measured by accumulating spectra at different spatial points. This procedure took approximately a week. Due to this fact it can be excluded that the relative phase Θ has a distinct time dependence, as in this case the interference pattern would be averaged out during measurement. This demonstrates that as long as the condensate is continuously pumped the value of Θ is almost constant with time at each spatial point.

In the same figure stationary defects of the density modulation can be found. They are marked by black dotted circles. Their existence indicates that although Θ has no pronounced time dependence it has a certain spatial dependence. The phase shift around the defect, which can be obtained by following the white dotted path in figure 4.11a, equals 2π. Hence the observed defect is a quantized vortex.

In order to understand the physical origin of the density pattern and the observed defects the condensate has been modeled using a generalized Ginsburg-Landau equation, following an approach previously applied to other non equilibrium condensates [33, 99]. In order to include interactions between the two components of the condensate and to account for their finite lifetime and for injection additional terms are taken into account that describe four magnon scattering processes [31, 30, 100] and dissipation. The system of two coupled differential equations has the following form:

$$i\hbar\frac{\partial}{\partial t}\Psi_{\pm} = \left[-\frac{\hbar^2}{2m_{||}}\frac{\partial^2}{\partial z^2} - \frac{\hbar^2}{m_{\perp}}\frac{\partial^2}{\partial y^2} - \mu_C + U_0|\Psi_{\pm}|^2 + iP(\Psi_{\pm})\right]\Psi_{\pm} + J\Psi_{\mp}^* \qquad (4.8)$$

Due to anisotropy of the magnon dispersion relation in thin films the effective mass of magnons is also anisotropic. This is accounted for by introducing two different effective magnon masses $m_{||}$ and $m_{\perp}$ given by $m_{||} = \hbar\left.\frac{\partial^2 E}{\partial p_z^2}\right|_{\vec{p}_{gs}}$ and $m_{\perp} = \hbar\left.\frac{\partial^2 E}{\partial p_y^2}\right|_{\vec{p}_{gs}}$ respectively.

The parameter U_0 represents the potential that is responsible for interactions within each component of the condensate. The function $P(\Psi_{\pm}) = \gamma_{eff} - i\hbar\eta\frac{\partial}{\partial t} - \Gamma|\Psi_{\pm}|^2$ is a phenomenological description of the flow of magnons into the condensate due to parametric pumping and their dissipation due to magnon-magnon and magnon-phonon interactions. In P γ_{eff} plays the role of an effective gain taking into account magnon flow into the condensate and linear annihilation. In the experiment the spatial region that has been measured was very small compared to the area of parametric pumping. Together with the assumption that linear annihilation is also constant throughout the whole sample, γ can be treated as being independent of space and time. The parameter η accounts for dissipation of condensed magnons via interaction with non condensed and Γ describes the nonlinear

reduction of pumping efficiency at large magnon densities[12]. μ_C is the chemical potential of the Bose-Einstein distribution which is, in the case of BEC, equal to the energy of the ground state. The parameter J describes interactions between the two condensate components and is, in this model, responsible for the phase locking between them[13].

The numerical evaluation of equation 4.8 has been carried out by Natasha Berloff [101]. In order to reproduce the observed stationary defects in the density modulation pattern, crystalline defects in the YIG film were assumed. Although the YIG film that has been used in these experiment posses a high crystallographic quality, crystalline defects can never be inhibited. This makes the assumption plausible. It has been assumed, that at a crystalline defect an additional nonlinear annihilation of magnons occurs within an area equal to the healing length $l_{||,\perp} = \hbar/\sqrt{2m_{||,\perp}\mu_C} \approx 0.2 - 0.5\mu m$. This is modeled by a space dependent $\Gamma = \Gamma(r)$ which is three times larger inside a defect than outside. Starting from random initial configurations for $\Psi_\pm$ the density distribution of the condensate after a time at which it reaches a stationary state is calculated through direct numerical integration of equation 4.8 the result is shown in figure 4.11b.

Magnon masses $m_{||}$ and $m_\perp$ were calculated from the second derivative of the magnon dispersion relation given by equation 2.21 at the ground state. The chemical potential is obtained from a measurement of the ground state energy. All other parameters had to be adjusted in order to reproduce the experimental observations. The striking similarity between figure 4.11a and figure 4.11b demonstrates that expression 4.8 is well suited to reproduce the experimental results. Moreover the calculated picture shows that in the vicinity of the regions where the nonlinear magnon damping is enhanced[14] fork like structures in the interference pattern emerge like the ones observed in the experiment.

This result confirms the assumption that vortices are pinned to defects in the crystalline structure of the medium. This effect is also known from type II superconductors in which vortices are formed when an external magnetic field that is greater than the first critical value is. In an ideal medium[15] these vortices are not stationary and move randomly. When a current is send through the superconductor they follow the direction of the current leading to dissipation in the otherwise dissipationless current flow. If however defects, with enhanced dissipation for Cooper-Pairs, are present in the superconductor, vortices are pinned to them leading to stationary vortices [19].

[12] See section 2.2.2.
[13] J leads to a time independent Θ.
[14] Regions with enhanced nonlinear damping are indicated by black dotted circles in figure 4.11a and 4.11b.
[15] A homogeneous medium with no defects.

Unlike in superconductors vortices in a mBEC are not created through external perturbations[16] instead they are created during the formation of the condensate [102]. In a perfect medium these vortices would vanish after a certain time. Since in our medium defects are present, there is a steady flow of magnons from regions where they are created into the defect area where they are annihilated. This way a vortex that is created during the formation of the condensate can get pinned to this region and becomes a stationary vortex.

The two dimensional Fourier transformation of the interference pattern shown in figure 4.11c reveals two pronounced peaks. One is located at $k_y = k_z = 0$ and reflects the average condensate density. The second peak is located at $k_z = 6.8 \cdot 10^6 m^{-1}$ and $k_y = -1.5 \cdot 10^6 m^{-1}$. This value of k_z is nearly twice as big as expected. This is not surprising; since the BLS signal is proportional to the magnon density squared hence periodicity of the standing wave doubles. Taking this into account it is apparent that there is an excellent agreement with previous measurements. The nonzero value of k_y is attributed to a slight mismatch between the external magnetic field and the z-scanning direction as well as to the influence of topological defects.

In figure 4.11d average condensate density and modulation depth as a function of pumping power are plotted. It is obvious that the modulation depth saturates at lower pumping powers than the average condensate density. Average condensate density saturates due to strong nonlinear dissipation at high magnon densities, while the saturation of the modulation depth is caused by phase locking between the two components of the condensate above the threshold for mBEC. So it is apparent, that Θ is a function of pumping power only close to the mBEC threshold and reaches a constant value as soon as the condensates are established and becomes independent of the actual condensate density.

Another interesting feature is that the modulation depth saturates at a value that is far below 100%. In a system where the two degenerate energy minima are equally occupied and where the phase difference Θ is completely time independent the modulation depth should however reach 100%. There are several reasons why we get a much lower value in the experiments. First of all there is a simple convolution effect. Since the probing laser spot has a diameter that is on the same order of magnitude as the spatial density pattern the modulation depth is reduced by a factor of

$$F = \frac{1}{\sqrt{2\pi}\sigma} \int_{-\infty}^{\infty} \left[\exp\left(-\frac{z^2}{2\sigma^2} \right) \cos(2k_{BEC} z) \right] dz = \exp\left(-2k_{BEC}^2 \sigma^2 \right). \tag{4.9}$$

Although it has been tried to make the probing laser spot size as small as possible it was not possible to reach a purely diffraction limited spot size which is not surprising

[16] Like a magnetic field.

taking into account a thickness of the film of $5 - 6\mu m$. The FWHM of the spot intensity was estimated by moving it over the border between a well reflecting surface and an absorbing one while recording its brightness. With this technique a FWHM of $550nm$ has been determined. This is roughly two times larger than the diffraction limited spot size. Putting this FWHM into equation 4.9 a value of $F \approx 3.5$ can be determined. Hence even when the real modulation depth happens to be 100% a modulation depth of only 28% would have been measured, due to the convolution effect. However there remains a discrepancy between this value and the measured one.

There are two possible explanations at hand for the discrepancy. One could imagine that Θ might not be completely time independent but follows a law

$$\Theta(r,t) = \Theta_0(r) + \Theta_t f(t). \tag{4.10}$$

Here $\Theta_0(r)$ is the space dependent component of $\Theta(r,t)$. $f(t) \in [0,1]$ is a time dependent function and $\Theta_t \in [0,\pi]$. The function $f(t)$ can have any imaginable time dependence. With $\Theta_t = 0$ one would expect a modulation depth that is limited only by convolution, as soon as $\Theta_t \neq 0$ the modulation depth will be reduced until it vanishes completely at $\Theta_t = \pi$ as in this case the interference pattern would be out averaged in a measurement.

Another reason for the reduced modulation depth might be an imbalance in the occupation of the two magnon ground states $\Psi_+ \neq \Psi_-$. The greater the imbalance in occupation the smaller the observed modulation depth. Such an imbalance in the population has been theoretically predicted by Li *et.al.*[103].

4.3.3 Conclusion

It has been demonstrated, that the unique nature of an mBEC, namely its existence in two degenerate energy states manifests itself in a spatially non uniform ground state originating from interference between the two condensate components. The contrast of the interference pattern saturates at lower pumping powers than the average magnon density at a value that is far below 100%. Two possible mechanisms responsible for the small contrast have been identified: A possible phase drifting and an unbalance in the density of the two condensate components. Furthermore stationary quantized vortices have been observed in the interference pattern which are a strong indicator for the superfluidity of the magnon gas and numerical simulations revealed that the vortices are pinned to crystalline defects in the YIG-film.

5 Study of spatially inhomogeneous excitations in a mBEC

While the experiments of the first part deal with the properties of a unperturbed mBEC, the second part concentrates on the properties of dynamic excitations in a mBEC.

The first experiment of the second part reports on the properties of density waves in a magnon gas below and above the threshold for condensation. Important characteristics of these waves like the dispersion relation and penetration depth under the influence of several experimental parameters are in the focus.

The second experiment of the second part deals with the out-coupling of a Bose-Einstein condensed magnon cloud from a spatially confined region into regions with no condensate. The basic properties of this magnon cloud moving in real space are discussed and a simple model that explains most findings quantitatively will be presented.

5.1 Density Waves in a Magnon gas above and below the threshold for mBEC

The properties of density waves in atomic BEC have extensively been studied [104, 105, 106, 107] since their first realization by Anderson *et.al.*[17]. These experiments provided a deep insight into the basic properties of BEC. They confirmed the validity of Bogoliubovs theory, dealing with small perturbations in a weakly interacting Bose gas [104], determined the static structure factor and the upper limit for the critical velocity of the condensate, above which the flow becomes viscid [105], and they demonstrated the vast range of applicability of mean field theory [106]. Additionally, in experiments with varying confinement the effects of parametric resonances could be observed [107], which lead to Faraday waves.

Inspired by the above mentioned experiments a scheme has been developed that enables a stimulation of density waves in mBEC. The following section reports on the experimental technique and the observations that have been made.

5.1.1 Experimental arrangement

As in the previous section the magnon density is measured by means of BLS. Due to different requirements the experimental setup is slightly changed. As it turns out that the wavelengths of the density waves are rather large the demands on spatial resolution are not as high as in the previous section. In contrast to the previous measurement, apart from the spatial and spectral, it is also required to determine the temporal evolution of the magnon density. In order to keep the duration of each measurement small, the signal, originating from interactions between magnons and photons, must be as high as possible.

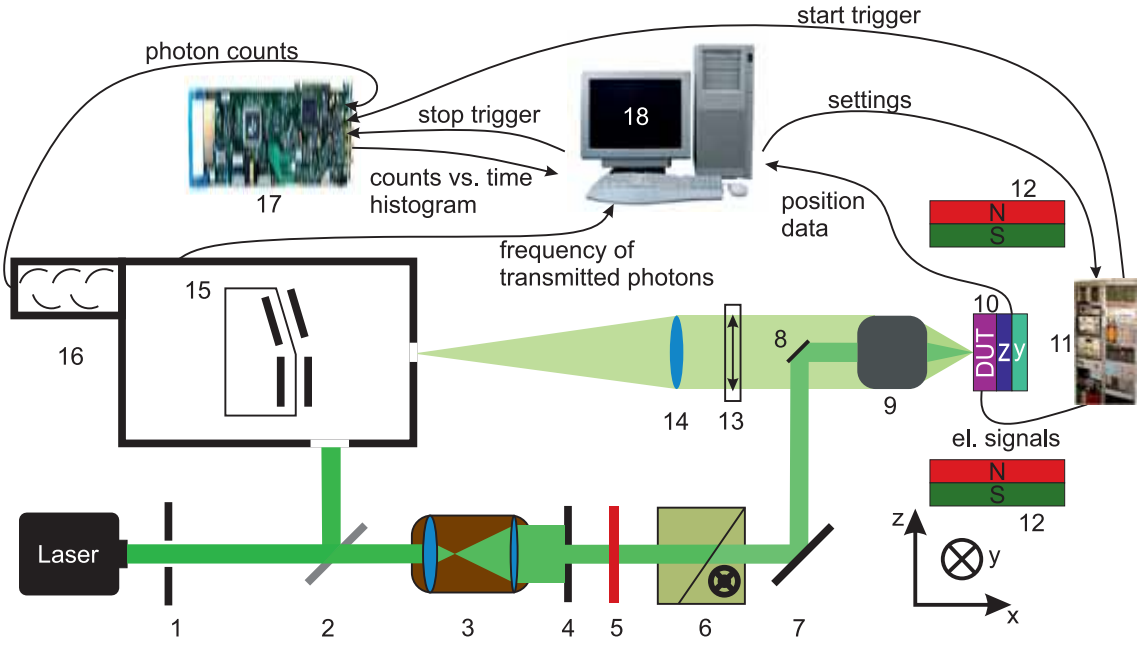

Figure 5.1: Schematic drawing of the experimental setup for time resolved macro BLS measurements. Components: 1. Pinhole 2. Beam splitter 3. Beam expander 4. Pinhole 5. Half wave plate 6. Glann-Taylor polarizer 7. Mirror 8. Mirror 9. Objective 10. Device under test (DUT) together with translation stages for the y- and z- direction 11. Electronic setup 12. Electromagnet 13. Thin film polarizer 14. Collecting lens 15. Scanning Tandem Fabry-Perot interferometer 16. Photomultiplier 17. Multiscaler 18. Computer. Black lines are electric cables.

A schematic of the setup is shown in figure 5.1. Like in the previous experiment, the elements 1-6 are used to direct a reference beam to the FPI, to enhance the uniformity of illumination across the beam diameter, to adjust the power of the beam and to establish a well defined polarization state.

Instead of a microscope objective a camera objective with much larger focal length

is used. The benefits of the larger focal length are better accessibility of the sample and greater focal depth causing an increase in the volume where magnons can interact with photons. However the numerical aperture of the camera objective is comparable to that of the microscope objective hence magnons at the ground state can be detected. The clear aperture of the camera objective is of course much larger than that of the microscope objective; hence the calcite polarizer cannot be used to filter out the elastically scattered photons. A thin film polarizer, with a distinction ratio comparable to calcite polarizers, is used for this task. It can be seen in figure 5.1 that mirror 8 blocks a part of the light that has been collected by the objective. This does not cause any problem because the diameter of this mirror is small compared to the clear aperture of the objective. Additionally, the mirror is placed central to the camera objective, hence only light with small wave vector components in z- and y-direction gets blocked that is mainly elastically scattered. Light that has been scattered by magnons in the ground state is not affected at all. A lens finally focuses the inelastically scattered light into the FPI which is the same as in section 4.3.1.

In contrast to the previous section, the signal from the photomultiplier is not send directly to the computer where it is recorded. Instead the signal is send to a multiscaler. The multiscaler is responsible for the time resolution in the experiment. It records at what time with respect to the start trigger a photon count occurs with an accuracy of better than one nanosecond until he gets a stop trigger signal provided by the computer. The time span between start and stop trigger is usually on the order of a few microseconds. Hence it is much faster than the time the FPI needs to scan the desired range of frequencies which is typically half a second. In this way additional information about the time instant, at which a photon has interacted with a magnon, is gained.

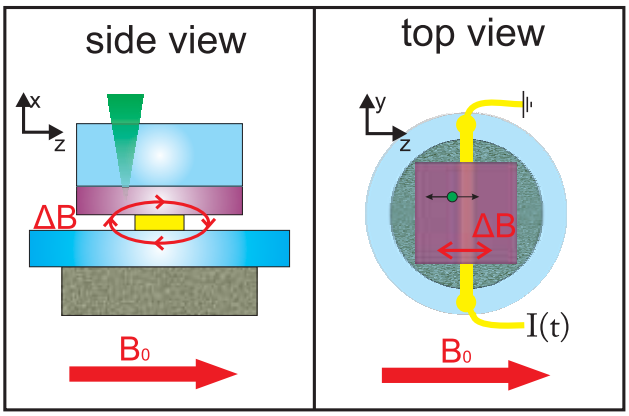

Figure 5.2: Schematic drawing of the sample design utilized to excite density waves in a gas of magnons.

Figure 5.2 shows a schematic of the DUT. A dielectric resonator is used in order to inject addidtional magnons into the YIG film by means of parametric pumping as described in section 4.1. In order to create a field inhomogeneity a sapphire substrate of $200\mu m$ thickness, with a lithographically patterned gold conductor of $10\mu m$ width and a height of $300nm$, is placed on top of the resonator. A $5\mu m$ thick YIG film, on a GGG substrate, is placed on top of the sapphire substrate with gold conductor. A laser beam is used to detect the time, space and frequency dependent magnon density. In this scheme the GGG substrate faces the laser beam, hence the light has to traverse the polished GGG substrate before it reaches the YIG film and gets reflected at the YIG-air boundary. This way the YIG film is in direct contact to the gold conductor and also close to the resonator.

A current that is send through the conductor creates an Oersted field that overlaps with the external magnetic field produced by the electromagnet and creates a inhomogeneity. Due to the direct contact between conductor and YIG film the inhomogeneity is very strong[1] and laterally confined[2] inside the YIG film.

According to equations 2.9 and 2.18 the magnetic field in a FM determines directly the energy of magnons. Hence in an inhomogeneous magnetic field magnons at different positions have distinct energies, therefore the field inhomogeneity acts as a potential which can either attract or repel magnons, leading to a localized density modulation. Because of the comparatively large conductor length perpendicular to the external field waves propagate only parallel to the z-direction hence two dimensions are sufficient to describe the wave propagation. One spatial dimension[3] and one temporal dimension.

[1] There is no inherent boundary for the value of the inhomogeneity created by the wire, however strong currents lead to a significant heating of the structure and can even damage it thus reducing the available amplitude.

[2] The full width at half maximum of the inhomogeneity inside the YIG film has a width of less than $20\mu m$.

[3] The z-direction.

5.1.2 Results

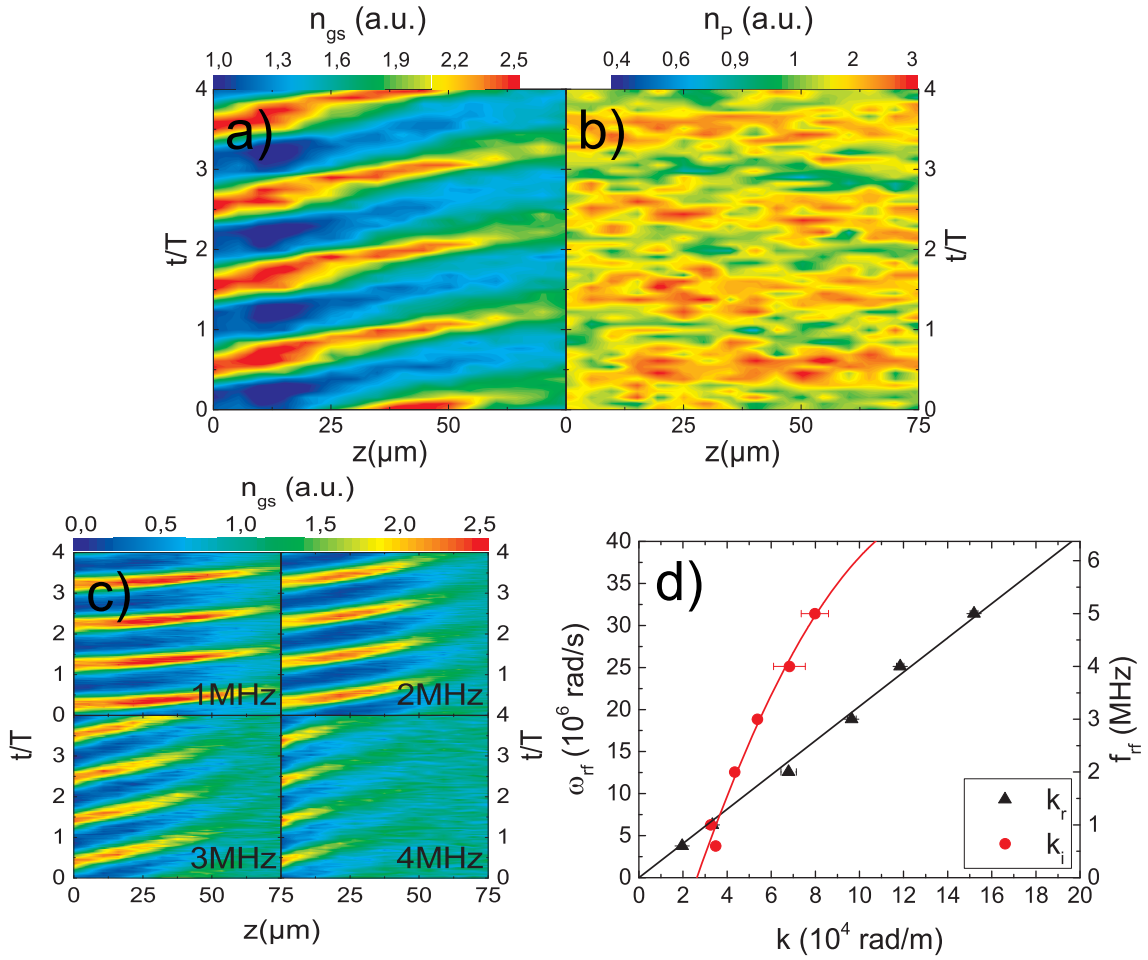

Figure 5.3: Impact of an oscillating, localized inhomogeneity in the external magnetic field on the ground state magnon density in a YIG film, in which magnons with an energy of $E_p = 18.81\mu eV$ are injected above the threshold for mBEC. The film is placed in an external magnetic field with a strength of $B_0 = 128mT$. Time scales are normalized to the period of the oscillating field inhomogeneity. a,b) Time and space dependent magnon density in the **a** ground state and at the **b** parametrically pumped state. The inhomogeneity is located at $z \approx 0\mu m$ oscillating with a frequency of $f_{rf} = 1MHz$ and an amplitude of $\hat{B}_{rf} = 3.8mT$. c) Same as **a** but at various f_{rf} and with $\hat{B}_{rf} = 6.25mT$. d) Dispersion relation for the real k_r and imaginary k_i part of the wave number for waves in the density of ground state magnons $\hat{B}_{rf} = 6.25mT$. The black line is a linear fit through the values of k_r with a slope of $v_{gr} = 204 \pm 4\frac{m}{s}$. The red line is a guide for the eye.

Figure 5.3a shows the space and time dependent, ground state magnon density inside a YIG film, placed in a magnetic field of $B_0 = 128mT$, in which magnons with an energy of $E_p = 18.81\mu eV$ have been injected by a $P = 10W$ pumping field. A current oscillating with a frequency of $f_{rf} = 1MHz$ is send through the conductor located at $z \approx 0\mu m$ producing a peak to peak inhomogeneity in the magnetic field of $\hat{B}_{rf} = 3.8mT$. One can nicely observe a time dependent density modulation at the location of the conductor. However due to interactions between magnons in the ground state the density modulation penetrates into regions further away from the localized perturbation with finite phase velocity. An effect that can not be observed in the parametrically pumped magnons as it is apparent from figure 5.3b. Although signal from the parametrically pumped magnons is very noisy, density modulations with frequency f_{rf} are visible. However in contrast to the density waves in figure 5.3a they appear along the lateral axis with no phase difference; hence it appears as if the phase velocity is infinite. This seems to be rather unlikely, taking into account that the density of primary magnons is rather small hence interactions between them are weak. A better explanation might be that the current in the conductor affects the quality factor of the resonator, leading to an oscillation in the pumping field. It is obvious that such a effect influences the whole resonator and consequently affects the density of primary magnons in the whole YIG film at once.

From figure 5.3c it can be seen that the characteristics of the wavelength λ and penetration depth ρ depend strongly on excitation frequency f_{rf}. Mathematically the waves can be described through

$$n(z,t) = n_0 + \hat{n}\sin(k_r z - \omega t)\cdot\exp(-k_i z) \tag{5.1}$$

with the peak to peak amplitude $2\hat{n}$, the mean condensate density n_0, the real $k_r = \frac{2\pi}{\lambda}$ and imaginary $k_i = \frac{1}{\rho}$ part of the wave number and the angular excitation frequency $\omega = 2\pi f_{rf}$.

The dispersion relation of the real and imaginary part of k is shown in figure 5.3d. A linear dispersion of k_r is apparent. The slope of the linear fit reveals a group velocity of $v_{gr} = 204 \pm 4\frac{m}{s}$. The progression of k_i appears to be nonlinear, albeit k_i also grows with increasing excitation frequency. From this figure it is also apparent that for excitation frequencies below $1MHz$ the wave is already strongly damped before it is able to penetrate into the condensate for more than one wavelength. Hence in this regime the waves are overdamped. At higher excitation frequencies the waves are not overdamped anymore, although their penetration depth decreases. Admittedly a penetration for more than two wavelengths has never been observed.

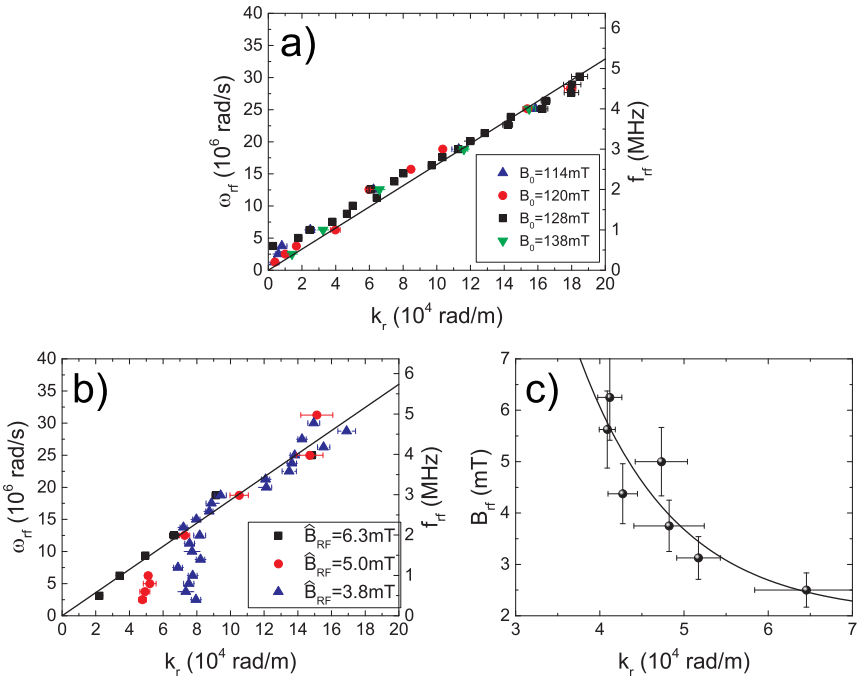

Figure 5.4: Influence of the magnitude of the external magnetic field and the amplitude of the field inhomogeneity on characteristics of waves, in the density of magnons, at the ground state. The large occupation at the ground state was achieved by injecting primary magnons with an energy of $E_p = 18.81\mu eV$ with a pumping field of $P = 10W$. a) Impact of the magnitude of the external magnetic field on the dispersion relation $\hat{B}_{rf} = 6.25mT$. The black line is a linear fit through the data points at $B_0 = 128mT$ with a slope of $v_{gr} = 164 \pm 3\frac{m}{s}$. b) Dispersion relation for different values of the amplitude of the field inhomogeneity $B_0 = 128mT$. The black line is a linear fit through the data points at $\hat{B}_{rf} = 6.25mT$ with a slope of $v_{gr} = 181 \pm 7\frac{m}{s}$ c) Values of k_r at $f_{rf} = 1MHz$ at various amplitudes of the field inhomogeneity. The black line is a guide for the eye.

The impact of the external magnetic field B_0 on the dispersion of k_r is shown in figure 5.4a. A discrepancy in the group velocities in figure 5.3 and 5.4 is attributed to the use of another YIG film. Although the two films had the same dimensions, slight deviations in the parameters during crystal growth can result in substantial changes of material parameters. It is apparent, that the magnitude of magnetic field has little influence on the dispersion in the measured range. The only observable impact can be seen at small excitation frequencies. It seems as though at $B_0 = 128mT$ a gap in the spectrum appears. The rather subtle impact of the external field on wave characteristics is not very surprising. The value of the magnetic field determines the energy difference between primary magnons and the ground state. Since density waves are present exclusively in the magnons at the ground state, the impact on

their characteristics is rather small.

As opposed to the results from figure 5.4a the impact of the field inhomogeneity amplitude and, correspondingly, the amplitude of the wave is much more pronounced. This is apparent from figure 5.4b. At an excitation amplitude of $B_{rf} = 6.25mT$ the dispersion appears to be linear. For $B_{rf} = 5mT$ a kink appears in the dispersion relation at $k_r \approx 5.1 \cdot 10^4 \frac{rad}{m} \quad \omega \approx 6.25 \frac{rad}{m}$. For the kink appears at $B_{rf} = 3.8mT$ at $k_r \approx 7.2 \cdot 10^4 \frac{rad}{m} \quad \omega \approx 13.75 \frac{rad}{m}$.

The impact of varying B_{rf} is most significant at small excitation amplitudes. Therefore the dependence of k_r as a function of the excitation amplitude B_{rf} at an excitation frequency of $f_{rf} = 1MHz$ has been determined. The results are plotted in figure 5.4c. It can be seen that k_r becomes smaller with increasing excitation amplitude following approximately a exponential law. It is interesting to note that the observed nonlinearity is rather unusual, as the effect develops itself with a **decrease** in wave amplitude. For lack of a nonlinear theory that models the interactions between magnons in a Bose-Einstein condensed state no satisfactory explanation can be given for the observed features.

Pumping power P is a critical parameter in experiments dealing with magnon condensates. When it exceeds a certain value a sudden increase in the occupation of the ground state can be observed marking the transition from the uncondensed to the condensed phase. It is apparent from figure 5.5a that under the circumstances of this experiment the transition occurs at a pumping power of $P \approx 1W$[4].

[4]It should be kept in mind that the critical pumping power, which marks the transition from the uncondensed to the condensed phase, is not comparable among experiments with different excitation geometries. The same pumping power can lead to very distinct values of the microwave field at the YIG film, depending on the coupling between the strip line and the resonator, the resonator geometry and quality factor itself and also on the distance between resonator and YIG film although the impact of the latter is rather small.

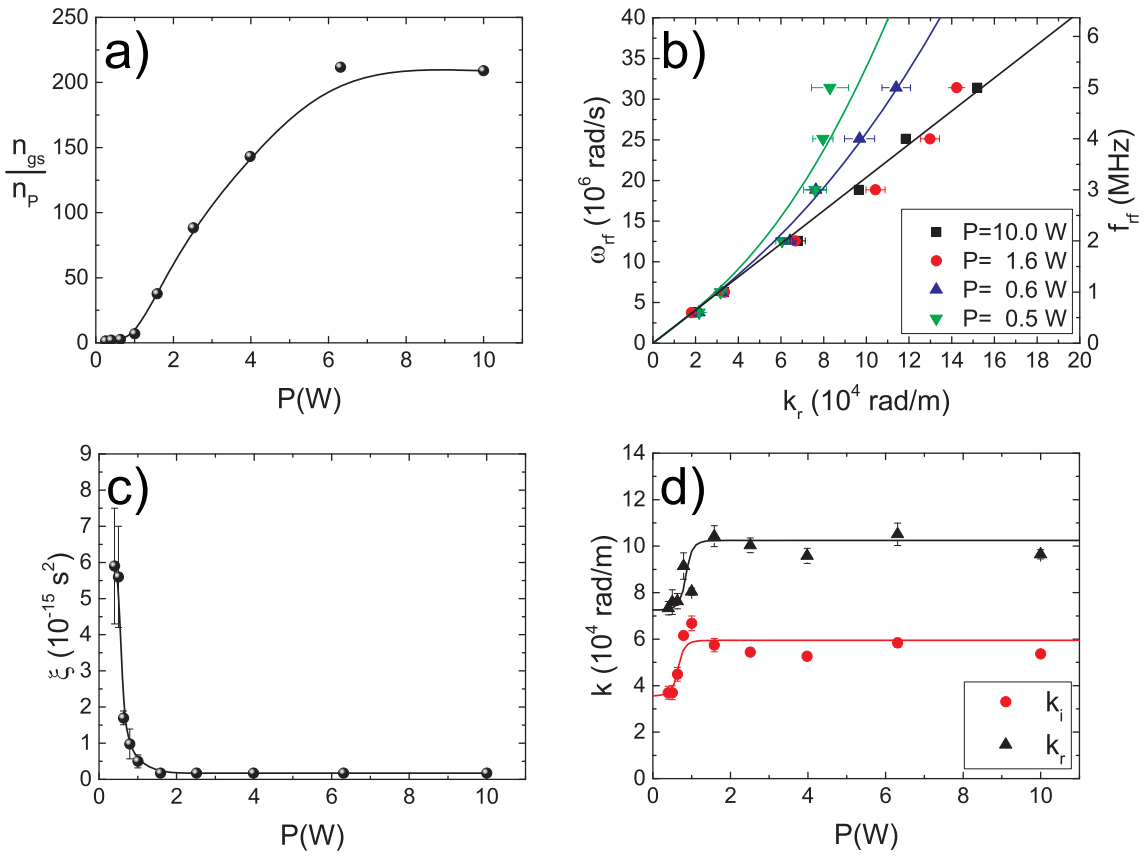

Figure 5.5: Characteristics of waves in the density of magnons at the ground state in a YIG film placed in a magnetic field with a magnitude of $B_0 = 128mT$ where magnons with an energy of $E_p = 18.81\mu eV$ with various values of the pumping power are injected. The field inhomogeneity that is responsible for the excitation of density waves has a amplitude of $\hat{B}_{rf} = 6.25mT$. a) Ratio between the occupation of the ground state and the pumped state as a function of pumping power. The black line is a guide for the eye. b) Dispersion relation for various values of the pumping power. The black line is a linear fit through the data points at $P = 10W$ with a slope of $v_{gr} = 204 \pm 4\frac{m}{s}$. The blue and green line are nonlinear fits, to the data points at $0.5W$ and $0.6W$, whose feature are elucidated in the text. c) Fit parameter ξ for dispersion relations shown in **b**. The plotted values at $P > 2W$ are upper boundaries for the real value of ξ. d) Values of the real k_r and imaginary k_i part of the wave number as a function of pumping power at an excitation frequency of $f_{rf} = 3MHz$. The red and blue lines are a guide for the eye.

Figure 5.5b shows the dispersion for various values of the pumping power P. As long as P is above the threshold for condensation the dispersion stays linear and

does not change its slope even when the pumping power is changed by almost a factor of ten. However below the threshold level the dispersion becomes nonlinear. The dispersions can be well approximated by the function

$$\omega(k) = \sqrt{v_{gr}^2 k^2 + v_{gr}^4 \xi k^4} \tag{5.2}$$

For dispersion relations that display a linear behavior in the considered range, the fit parameter ξ cannot be determined exactly. Instead an upper boundary for this parameter can be determined, based on the fact that a nonlinear behavior has, if ever, to start at wave numbers outside the region plotted in 5.5b. It is apparent that the group velocity v_{gr} is the same for all values of the pumping power and has a value of $v_{gr} = 204 \pm 4\frac{m}{s}$. Figure 5.5c shows the dependence of the parameter ξ on pumping power. A strong decrease of ξ at the threshold for mBEC can bee seen. Further increase in pumping power has no influence on ξ in the observed range.

It is apparent that the pumping power P has little influence on the wave characteristics at small excitation frequency f_{rf}, whereas a clear impact at the threshold for mBEC is observable at high f_{rf}. So as to determine the impact of P on the wave characteristics at high f_{rf} the real and imaginary part of the wave vector at $f_{rf} = 3MHz$ has been determined for various values of P. The results are plotted in figure 5.5d. A strong increase in k_r and k_i can clearly be seen in that figure. Above and below the threshold for mBEC both values however remain constant.

All this findings demonstrate that the dynamics in the magnon system change drastically when the threshold for mBEC is reached. However once the condensate is created a further increase in pumping power does not change the characteristics of wave propagation significantly. This is a mayor difference to atomic condensates. In atomic condensates the speed of density waves depends on the square root of the condensate density. This has been predicted by Bogoliubov [76] and observed by Andrews *et.al.*[104]. Extended theoretical models that take into account the unique features of magnonic system may one day resolve this issue. A major difference between the two systems is that the fraction of condensed magnons with respect to the total magnon number is rather small having a value of below 1%, whereas in atomic condensates it can reach almost 100%. Hence it is expected that the influence of uncondensed magnons on density waves will be quite notable. In this sense an mBEC has less similarity with atomic condensates, but is much closer to liquid helium close to the lambda point. Measurements at cryogenic temperatures, where the condensate fraction is considerably larger, might reveal if the characteristics of density waves change significantly in this case.

5.1.3 Conclusion

In conclusion it has been shown, that density waves can indeed be excited in a magnon gas above and below the threshold for mBEC by means of an inhomogeneity in the external magnetic field. Above the threshold for mBEC these waves exhibit a linear dispersion relation whereas below the threshold the dispersion becomes nonlinear and can be well approximated by a second order polynomial function. Above the threshold for mBEC external magnetic field apparently has hardly any influence on the dispersion. In contrast, the amplitude of the field inhomogeneity has a striking impact and leads to a nonlinearity of the dispersion at small wavenumbers. Due to a lack of theoretical models satisfactory explanations for the observed effects can not be given.

5.2 A Bose Einstein condensed magnon cloud moving in real space

During experiments on density waves in mBEC another interesting effect has been revealed. With a slight change in the experimental arrangement of the previous section a strongly confined condensate with a spatial extend of approx. $50\mu m$ in z-direction could be created. With the aid of a short pulsed field inhomogeneity, at the location of the confined condensate, it was possible to accelerate the magnon cloud and to move it into regions where pumping is not sufficiently high as to allow for mBEC.

This process has some analogy to an atom laser, that has been defined by Wiseman[108] and Robins [109], and observed by Mewes *et.al.*[110] and Bloch *et.al.*[111, 112]. In these experiments the researchers where able to out couple a part of a trapped atomic condensate and to accelerate it via gravity.

Although there is a distinct similarity between the two experiments the effect observed here is not called a magnon laser for reasons that will be pointed out in the following sections.

5.2.1 Experimental arrangement

The basic experimental arrangement including the sample design is identical to that from section 5.1.1. An mBEC is created by injecting additional magnons into a YIG film, with the aid of parametric pumping through the microwave field around a dielectric resonator. The magnetic field can be altered locally by the Oersted field of a current carrying wire located at the center of the resonator. The space and time dependent, frequency resolved magnon density is mapped via a macro BLS setup as shown in figure 5.1.

An important difference with respect to section 5.1.1 is the much lower value of the external magnetic field. The external magnetic field in this experiment has a value of $B_0 = 66mT$ whereas in the previous experiment it had a value of $128mT$. As a consequence the energy difference between primary magnons and the ground state approximately doubles. Thus primary magnons have to scatter more often with each other and with thermal magnons in order to reach the ground state. As a consequence the pumping power threshold for mBEC is significantly increased. Since the microwave field around a dielectric resonator is non uniform, with a maximum at the center and a decrease towards its outer edges, the threshold in pumping power is only reached within a certain area of the YIG film that is much smaller than the dimensions of the resonator. In addition it is possible that the conductor beneath the YIG film also acts as a part of the resonator, causing a strong increasing of the microwave field in its vicinity. This leads to a strongly confined condensate that is

located close to the conductor. Current pulses with a duration of $t = 10ns$ are send through the conductor in order to accelerate the condensate into regions where the threshold for mBEC is not reached.

5.2.2 Results

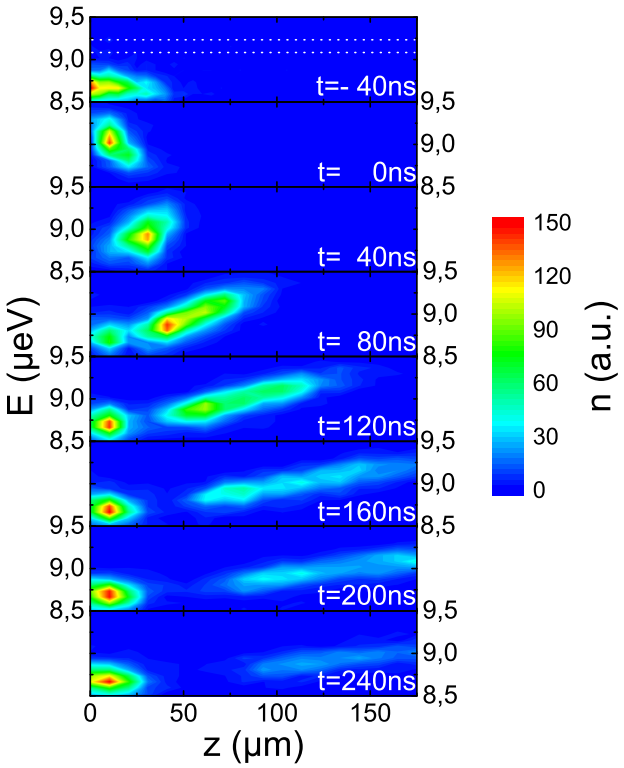

Figure 5.6: Series of space and energy dependent magnon densities at different time instants with respect to the start of the field pulse at $t = 0ns$. The condensate is created through a microwave field with power $P = 10W$ that injects primary magnons with an energy of $E_P = 18.61\mu eV$. The YIG film is placed in a homogeneous magnetic field with a strength of $B_0 = 66mT$ in z-direction. The time difference between adjacent subfigures amounts $\Delta t = 40ns$. Negative times indicate the state of the condensate before the field pulse. The current pulse had a rise and fall time of $2ns$. Subsequent figures show the evolution of the magnon cloud after this short perturbation.

During the experiment a strongly confined mBEC is excited. After a thermalization time, that is typically on the order of one microsecond, a large amount of magnons with ground state energy gathers at $z = 0\mu m$. Figure 5.6 shows a temporal sequence of the lateral magnon density at various energies close to the ground state.

It is apparent from figure 5.6 that at the beginning of the experiment ($t = -40ns$), when the external field is homogeneous, the magnon cloud is located at $z \approx 0\mu m$ and the ground state with an energy of $E_{gs} \approx 8.7\mu eV$ is strongly over-occupied. Whereas the occupation of all other states is much smaller.

A short current pulse that has been send through the conductor beneath the YIG film produces a short localized modification of the external magnetic field. In the experiment the direction of the current has been chosen in such a way that magnetic field is increased inside the YIG film. An increased magnetic field results in a magnon dispersion relation that is shifted to higher energies. As a consequence the magnons in the ground state have to follow the dispersion relation due to the fact that at their original energy no magnon states are available anymore. This effect can nicely be seen in figure 5.6 at $t = 0ns$. The energy of the magnon cloud is shifted by $\Delta E \approx 420neV$ accompanied by a movement of the center of mass by $\Delta z \approx 10\mu m$.

At $t = 80ns$ the influence of the field inhomogeneity is already very small, however it is apparent that the condensate does not drop back into the ground state, instead it stays at elevated energies. Additionally the location of the condensates center of mass changes further.

Even when the inhomogeneity has totally vanished, its impact on the magnon cloud still persists. Two additional features can be seen at $t = 120ns$. One can see that the formally compact magnon cloud starts to spread in real space. The reason at hand for this observation is that magnons which occupy lower energy states move at a smaller velocity, than those occupying higher energy states. The second feature is that a new condensate starts to build up at $z \approx 5\mu m$. This is due to the still ongoing parametric pumping which creates a new condensate at the same position as before, while the "old" condensate is still moving in real space.

On subsequent snapshots a further broadening of the magnon cloud can be observed while it keeps on moving away from the original position. It becomes also apparent, that the magnon density of the magnon cloud becomes smaller. There are two reasons at hand for this. The most obvious one is, that the condensate density becomes smaller due to dissipation into lattice vibrations[5]. The second explanation is that due to the spatial broadening of the cloud the local density becomes smaller. For a better quantification the lateral distribution of magnons at in a specific energy range at different times is plotted in figure 5.7a. The energy range of this cross section is indicated in the upper panel of figure 5.6 by two white dotted, horizontal lines.

[5]Phonons.

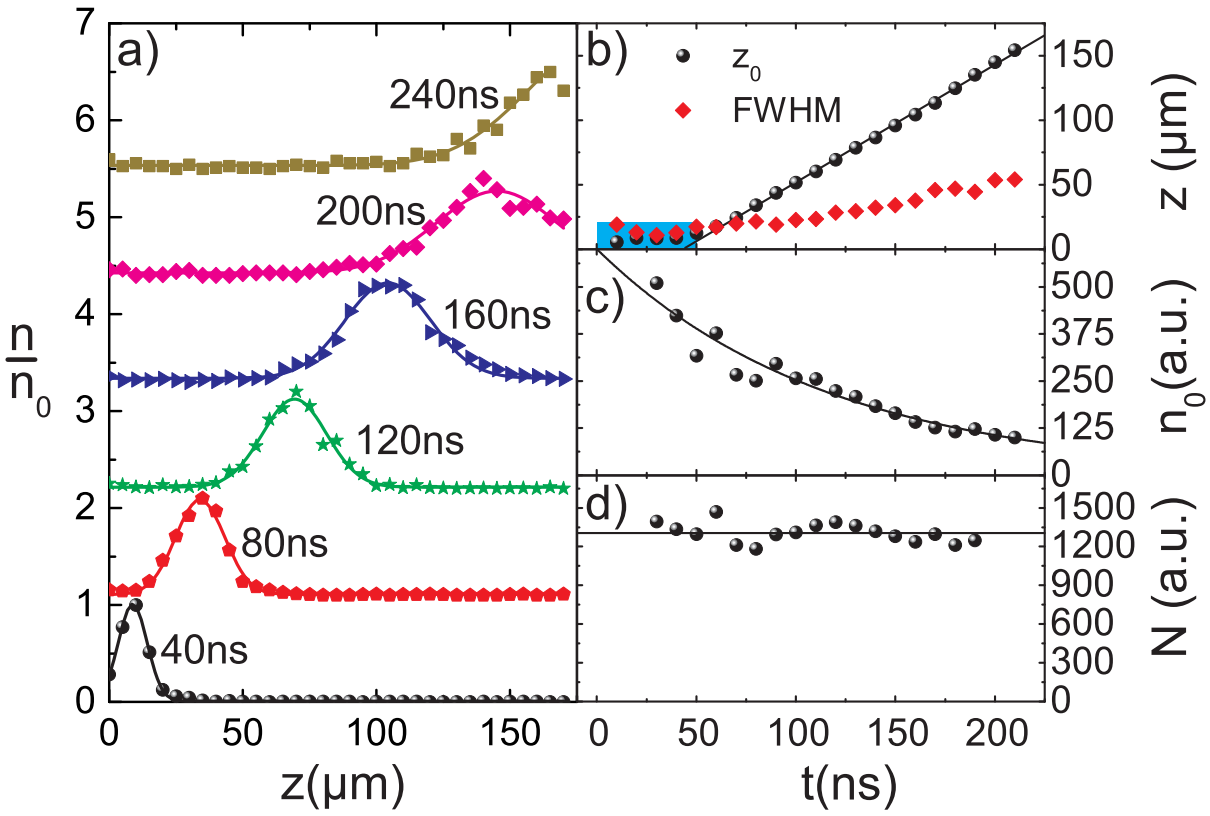

Figure 5.7: Horizontal cross section of figure 5.6 centered at $E \approx 9.156 \mu eV$ with a width of $\delta E \approx 140 neV$. a) Normalized cross section at various time instants b) Center of mass z_0 and FWHM of the magnon distribution as a function of time. The black line is a linear fit through the data points of z_0 at $t \geq 60 ns$. The fit has a slope of $v = 933 \pm 11 \frac{m}{s}$. The temporal and spatial extend of the field inhomogeneity is indicated by a light blue rectangle. c) Maximum magnon density as a function of time. d) Total number of magnons as a function of time.

It was found that the lateral distribution of magnons within the considered energy range can nicely be approximated by a Gaussian distribution function given by

$$n(z) = \frac{N}{\sqrt{2\pi}\sigma} \exp\left\{-\left(\frac{z - z_0}{\sqrt{2}\sigma}\right)^2\right\} \tag{5.3}$$

With total magnon number N[6] and the center of mass z_0. The full width at half maximum (FWHM) is given by $FWHM = \sqrt{8\ln(2)}\sigma$ and the maximum density by $n_0 = \frac{N}{\sqrt{2\pi}\sigma}$.

[6]Magnon density integrated over all spatial points.

The center of mass and FWHM of the magnon density as a function of time are plotted in figure 5.7b. The spatial and temporal extend of the field inhomogeneity produced by the current pulse is indicated through a light blue area in the plot. It can be seen that as the field inhomogeneity is turned off the center off mass starts to move away from the origin with a constant velocity, while the FWHM increases. A very interesting fact is that the condensate keeps moving at a constant velocity even though the influence of the field inhomogeneity has already past.

Along with the broadening of the magnon cloud a decrease of the maximum density can be seen in figure 5.7c. It is apparent that the broadening and the accompanying decrease in maximum density are due to the different velocity of magnons from different energies. However a surprising fact is that the total density is almost constant during propagation although the magnon cloud has left the region where the pumping field is above threshold (see figure 5.7d).

There is a straightforward explanation for the observed effects. Figure 5.8a shows the dispersion relation at $z = 0\mu m$ before a current is send through the conductor. Due to parametric pumping, above the threshold for mBEC, and subsequent thermalization the ground state is strongly over-occupied. This is indicated by a blue dot. The energy of primary magnons lies above $9.5\mu eV$ and is not displayed here. When a current is send through the conductor the dispersion relation is locally shifted to higher energies. The condensate is forced to follow the modified dispersion relation as below the ground state no magnon states exist as can be seen in figure 5.8b. Figure 5.8c in turn shows the situation on the falling edge of the current pulse. In this case the dispersion relation starts to shift to lower energies again. However now there is no need for the condensate to remain in the ground state. When the dispersion relation is shifted towards lower energies, new magnon states become available for the condensate. Due to scattering processes the energy of some magnons from the condensate becomes lower while their wave vector remains the same, thus they occupy the new ground state. However this is not the only possibility. Some of the condensate remains at the same energy, while its wave vector is being changed due to scattering with other magnons. Of course most magnons change energy and wave vector. Finally when no current flux is present in the conductor, most of the condensate is smeared over the dispersion relation between the original ground state and the ground state energy of the shifted dispersion relation.

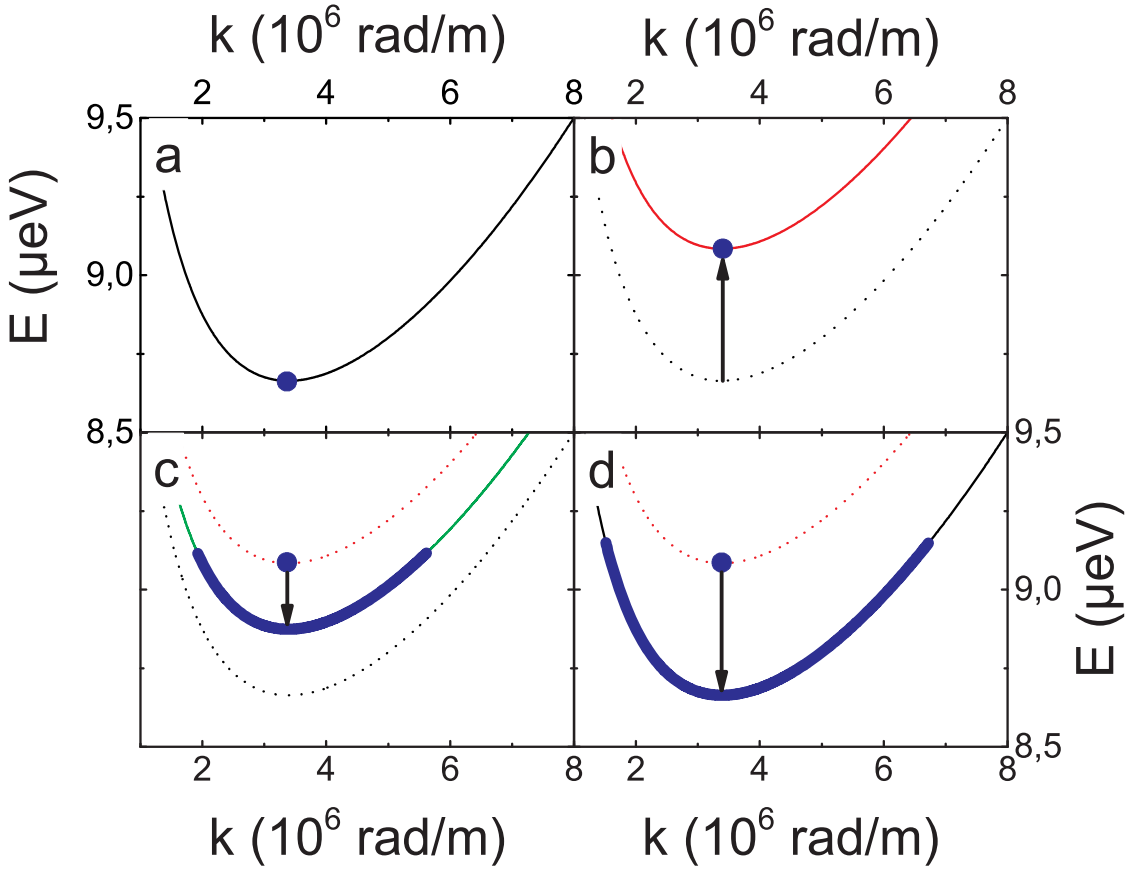

Figure 5.8: Magnon dispersion relations in YIG close to the ground state a) Dispersion relation in a homogeneous magnetic field of $B_0 = 66mT$. The blue dot marks the strongly over-occupied ground state. b) Black line and blue dot: Same as in **a**. Red line: Shifted dispersion relation at $z = 0\mu m$ when a current is send through the conductor. c) Black line, red line an blue dot: Same as in **b**. Green line: Intermediate dispersion relation on the falling edge of the current pulse. The blue highlighted part of the green curve marks accessible magnon states for magnons from the condensate. d) Black line, red line and blue dot: Same as in **b**. The blue highlighted part of the black curve marks accessible magnon states for magnons from the condensate.

The slope of a dispersion relation determines the group velocity of particles $v_{gr} = \frac{d\omega}{dk}$. The group velocity is a quantity that describes the velocity of particles in real space in contrast to the phase velosity $v_{ph} = \frac{\omega}{k}$ which determines the rate at which the phase of the corresponding wave propagates. Hence the group velocity is connected with a flux of particles and energy while the phase velocity can be nonzero even when no particle or energy flux is present. The slope of the dispersion relation at the ground state is zero, hence a condensate at the ground state does not move

in real space. However when a part of the condensate is brought to higher wave numbers where the slope of the dispersion is non-zero it attains a group velocity and starts to move. Apparently this would explain the observed effect. It is worth noticing that all the dynamics happen on the lowest thickness mode, as the energy of the next mode is too high to be reached by the currents used here.

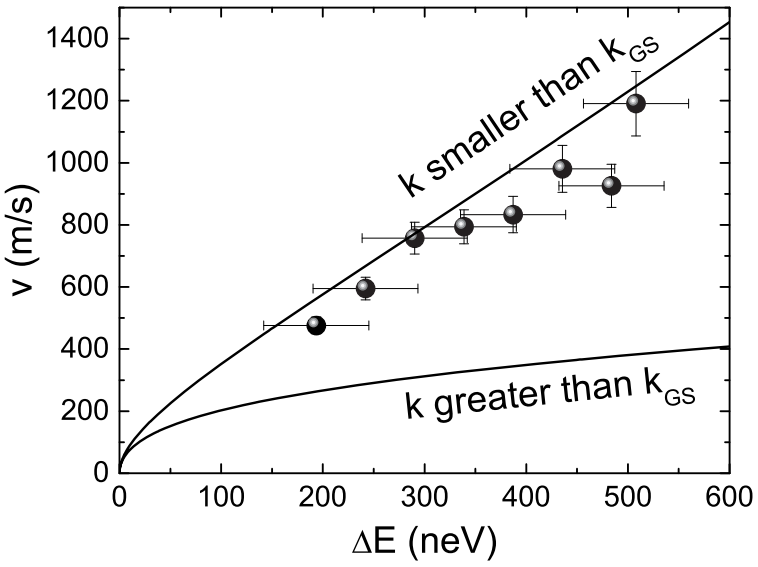

Figure 5.9: Black line: Group velocity of magnons at different energies with respect to the ground state energy E_{gs}. The dots are measured values of the moving condensate clouds velocity.

The group velocity of magnons at different energies with respect to the ground state energy $\Delta E = E - E_{GS}$, based on equation 2.21, is plotted in figure 5.9 as a black line. Due to the asymmetry of the dispersion relation there exist two possible group velocities for each ΔE depending on whether the wave vector is smaller or greater than that of the ground state. The black dots represent measured values of the velocity of the magnon cloud at various values of ΔE. It is apparent that the presented model nicely reproduces the observed velocities. On the other hand, it also can be seen that the wave vector of moving magnons has become smaller than that of the ground state and no movement of magnons with greater wave vector can be observed. There is a simple reason for this finding. The experimental setup applied here can only detect magnons up to a certain critical wave vector determined by the numerical aperture of the used objective. In this particular experiment the critical wave vector has a value of $k_c \approx 3.9 \cdot 10^6 \frac{rad}{m}$ hence magnons with a higher wave number than that of the ground state can not be observed with this setup even

though they might exist.

5.2.3 Conclusion

It has been demonstrated that an mBEC can be set into motion in real space. The effect has some analogy to an atom laser [108, 109, 110, 111, 112]. However in contrast to atom lasers the spectrum of the out coupled magnons is not monochromatic instead it spreads over a certain range defined by the magnitude of the field inhomogeneity. Hence the whole emitted condensate beam cannot be coherent, although it is still possible that each frequency component of the out coupled condensate is coherent. On the other hand the above mentioned features are also observed in nonlinear optics, where intense light fields in a nonlinear medium create short pulses of light with a broad frequency range, a effect called supercontinuum generation [113].

Bibliography

[1] Bloch, F. Zur theorie des ferromagnetismus. *Zeitschrift für Physik A Hadrons and Nuclei* **61**, 206 (1930). URL http://dx.doi.org/10.1007/BF01339661. 1, 28, 50

[2] Griffiths, J. H. E. Anomalous high-frequency resistance of ferromagnetic metals. *Nature* **158**, 670 (1946). URL http://dx.doi.org/10.1038/158670a0. 1

[3] Bloembergen, N. & Damon, R. W. Relaxation effects in ferromagnetic resonance. *Phys. Rev.* **85**, 699–699 (1952). URL http://dx.doi.org/10.1103/PhysRev.85.699. 1

[4] Anderson, P. W. & Suhl, H. Instability in the motion of ferromagnets at high microwave power levels. *Phys. Rev.* **100**, 1788–1789 (1955). URL http://dx.doi.org/10.1103/PhysRev.100.1788. 1

[5] Suhl, H. The theory of ferromagnetic resonance at high signal powers. *J. Phys. Chem. Solids* **1**, 209–227 (1957). URL http://dx.doi.org/10.1016/0022-3697(57)90010-0. 1, 17, 22

[6] Sparks, M. Ferromagnetic resonance in thin films. i. theory of normal-mode frequencies. *Phys. Rev. B* **1**, 3831–3856 (1970). URL http://dx.doi.org/10.1103/PhysRevB.1.3831. 1

[7] Sparks, M. *Ferromagnetic Relaxation Theory* (McGraw-Hill, 1964). 1, 25, 27, 30, 32

[8] Sparks, M. Effect of exchange on magnetostatic modes. *Phys. Rev. Lett.* **24**, 1178–1180 (1970). URL http://dx.doi.org/10.1103/PhysRevLett.24.1178. 1

[9] Fleury, P., Porto, S., Cheesman, L. & Guggenheim. Light scattering by spin waves in fef_2. *Phys. Rev. Lett.* **17**, 84 (1966). URL http://dx.doi.org/10.1103/PhysRevLett.17.84. 1

[10] Sandercock, J. Some recent applications of brillouin scattering in solid state physics. In Queisser, H. (ed.) *Festkörperprobleme 15*, vol. 15 of *Advances*

in Solid State Physics, 183–202 (Springer Berlin / Heidelberg, 1975). URL http://dx.doi.org/10.1007/BFb0107378. 1

[11] Borovik-Romanov, A. & Kreines, N. Brillouin-mandelstam scattering from thermal and excited magnons. *Phys. Rep.* **81**, 351 (1982). URL http://dx.doi.org/10.1016/0370-1573(82)90118-1. 1, 82

[12] Holstein, T. & Primakoff, H. Field dependence of the intrinsic domain magnetization of a ferromagnet. *Phys. Rev.* **58**, 1098–1113 (1940). URL http://dx.doi.org/10.1103/PhysRev.58.1098. 1, 23, 28

[13] Dyson, F. General theory of spin-wave interactions. *Phys. Rev.* **102**, 1217 (1956). URL http://dx.doi.org/10.1103/PhysRev.102.1217. 1, 28

[14] Oguchi, T. Theory of spin-wave interactions in ferro- and antiferromagnetism. *Phys. Rev.* **117**, 117 (1960). URL http://dx.doi.org/10.1103/PhysRev.117.117. 1, 28

[15] Bose, S. Plancks gesetz und lichtquantenhypothese. *Z. f. Phys.* **26**, 178 (1924). URL http://dx.doi.org/10.1007/BF01327326. 1, 41, 48, 50

[16] Einstein, A. Quantentheorie des einatomigen idealen gases zweite abhandlung. *Sber. Preuss. Akad. d. Wiss.* **1** (1925). 1, 41, 49, 50

[17] Anderson, M., Ensher, J., Matthews, M., Wieman, C. & Cornell, E. Observation of bose-einstein condensation in a dilute atomic vapor. *Science* **269**, 198 (1995). URL http://dx.doi.org/10.1103/PhysRevLett.82.3008. 1, 55, 89

[18] Davis, K. *et al.* Bose einstein condensation in a gas of sodium atoms. *Phys. Rev. Lett.* **75**, 3969 (1995). URL http://dx.doi.org/10.1103/PhysRevLett.75.3969. 1, 55

[19] Buckel, W. & Kleiner, R. *Superconductivity* (Wiley-VCH, 2004). 1, 56, 58, 61, 86

[20] Keesom, W. & Keesom, A. New measurements on the specific heat of liquid helium. *Proc. Amsterdam* **34**, 605 (1931). 1, 55

[21] Kalafati, Y. & Safonov, V. Possibility of bose condensation of magnons excited by incoherent pump. *JETP Lett.* **50**, 149 (1989). URL http://www.jetpletters.ac.ru/ps/1126/article_17065.shtml. 2, 58

[22] Kalafati, Y. & Safonov, V. Theory of bose condensation of magnons excited by noise. *JMMM* **123**, 184 (1993). URL http://dx.doi.org/10.1016/0304-8853(93)90030-6. 2, 58

[23] Melkov, G., Safonov, V., Taranenko, A. & Sholom, S. Kinetic instability and bose condensation of nonequilibrium magnons. *JMMM* **132**, 180 (1994). URL http://dx.doi.org/10.1016/0304-8853(94)90311-5. 2, 58

[24] Demokritov, S. *et al.* Bose-einstein condensation of quasi equilibrium magnons at room temperature under pumping. *nature* **443**, 430 (2006). URL http://dx.doi.org/10.1038/nature05117. 2, 54, 59, 61, 63, 64

[25] Dzyapko, O., Demidov, V., Demokritov, S., Melkov, G. & Slavin, A. Direct observation of bose–einstein condensation in a parametrically driven gas of magnons. *N. J. Phys.* **9**, 64 (2007). URL http://dx.doi.org/10.1088/1367-2630/9/3/064. 2, 61

[26] Demokritov, S., Demidov, V., Dzyapko, O., Melkov, G. & Slavin, A. Quantum coherence due to bose–einstein condensation of parametrically driven magnons. *New J. Phys.* **10**, 045029 (2008). URL http://dx.doi.org/10.1088/1367-2630/10/4/045029. 2, 59, 61, 64, 71

[27] Demidov, V., Dzyapko, O., Demokritov, S., Melkov, G. & Slavin, A. Observation of spontaneous coherence in bose-einstein condensate of magnons. *Phys. Rev. Lett.* **100**, 047205 (2008). URL http://dx.doi.org/10.1103/PhysRevLett.100.047205. 2, 59, 61

[28] Demidov, V. E. *et al.* Magnon kinetics and bose-einstein condensation studied in phase space. *Phys. Rev. Lett.* **101**, 257201 (2008). URL http://link.aps.org/doi/10.1103/PhysRevLett.101.257201. 2, 59, 61, 73, 83

[29] Chumak, A. *et al.* Bose-einstein condensation of magnons under incoherent pumping. *Phys. Rev. Lett* **102**, 187205 (2009). URL http://dx.doi.org/10.1103/PhysRevLett.102.187205. 2, 59

[30] Tupitsyn, I., Stamp, P. & Burin, A. Stability of bose-einstein condensates of hot magnons in yttrium iron garnet films. *Phys. Rev. Lett* **100**, 257202 (2008). URL http://dx.doi.org/10.1103/PhysRevLett.100.257202. 2, 59, 75, 85

[31] Rezende, S. M. Theory of coherence in bose-einstein condensation phenomena in a microwave-driven interacting magnon gas. *Phys. Rev. B* **79**, 174411 (2009). URL http://dx.doi.org/10.1103/PhysRevB.79.174411. 2, 61, 85

[32] Rezende, S. Wave function of a microwave-driven bose-einstein magnon condensate. *Phys. Rev. B* **81**, 020414(R) (2010). URL http://dx.doi.org/10.1103/PhysRevB.81.020414. 2

[33] Malomed, B., Dzyapko, O., Demidov, V. & Demokritov, S. Ginzburg-landau model of bose-einstein condensation of magnons. *Phys. Rev. B* **81**, 024418 (2010). URL http://dx.doi.org/10.1103/PhysRevB.81.024418. 2, 59, 85

[34] Haken, H. & Wolf, H. *The Physics of Atoms and Quanta* (Springer, 2005). 5, 31

[35] Kittel, C. *Introduction to solid state physics* (WILEY, 2005). 7, 31

[36] Stoehr, J. & Siegmann, H. *Magnetism from Fundamentals to Nanoscale Dynamics* (Springer, 2006). 7

[37] Gurevich, A. & Melkov, G. *Magnetization Oscillations and Waves* (CRC-Press, 1996). 10, 11, 22, 32

[38] Herring, C. & Kittel, C. On the theory of spin waves in ferromagnetic media. *Phys. Rev.* **81**, 869–880 (1951). URL http://dx.doi.org/10.1103/PhysRev.81.869. 11

[39] Damon, R. & Eshbach, J. Magnetostatic modes of a ferromagnet slab. *J. Phys. Chem. Solids* **19**, 308–320 (1961). URL http://dx.doi.org/10.1016/0022-3697(61)90041-5. 13

[40] Kalinikos, B. A. & Slavin, A. N. Theory of dipole-exchange spin wave spectrum for ferromagnetic films with mixed exchange boundary conditions. *J. Phys. C: Solid State Phys.* **19**, 7013 (1986). URL http://dx.doi.org/10.1088/0022-3719/19/35/014. 14

[41] Kalinikos, B. Excitation of propagating spin waves in ferromagnetic films. *IEE Proc. H* **127**, 4 (1980). URL http://dx.doi.org/10.1049/ip-h-1:19800002. 14

[42] Louisell, W. *Coupled Mode and Parametric Electronics* (WILEY, 1960). 18

[43] Wiese, G., Kabos, P. & Patton, C. Subsidiary-absorption spin-wave-instability process in yttrium iron garnet thin films: Couples lateral standing modes, critical modes, and the kink effect. *Phys. Rev. B* **51**, 15085 (1995). URL http://dx.doi.org/10.1103/PhysRevB.51.15085. 19

[44] Zakharov, V., L'vov, V. & Starobinets, S. Spin-wave turbulence beyond the parametric excitation threshold. *Sov. Phys. Usp.* **17**, 896 (1974). URL http://dx.doi.org/10.1070/PU1975v017n06ABEH004404. 22

[45] Nolting, W. *Grundkurs Theoretische Physik Quantenmechanik - Methoden und Anwendungen* (Springer, 2012). 29

[46] Abrahams, E. & Kittel, C. Spin-lattice relaxation in ferromagnets. *Phys. Rev.* **88**, 1200 (1952). URL http://dx.doi.org/10.1103/PhysRev.88.1200. 31

[47] Akhiezer, A., Bar'yakhtar, V. & Peletminskii, S. *Spin Waves* (North-Holland, 1968). 31

[48] Freiser, M. A survey of magnetooptic effects. *IEEE Trans. Mag.* **4**, 152 (1968). URL http://dx.doi.org/10.1109/TMAG.1968.1066210. 35

[49] Cheeseman, I. The structure of the long wave absorption edge of insulating crystals. *Proc. Phys. Soc. A* **65**, 25 (1952). URL http://dx.doi.org/10.1088/0370-1298/65/1/304. 35

[50] Wettling, M., Cottam, M. & Sandercock, J. The relation between one-magnon light scattering and the complex magneto-optic effects in yig. *J. Phys. C* **8**, 211 (2012). URL http://dx.doi.org/10.1088/0022-3719/8/2/014. 35, 37, 38, 40

[51] Loudon, R. Theory of the temperature dependence of first-order light scattering by ordered spin systems. *J. Phys. C* **3**, 872 (1970). URL http://dx.doi.org/10.1088/0022-3719/3/4/016. 36, 37

[52] Gall, H. L. & Jamet, J. Theory of the elastic and inelastic scattering of light by magnetic crystals. *Phys. Stat. Sol. B* **46**, 467 (1971). URL http://dx.doi.org/10.1002/pssb.2220460202. 37

[53] Landau, L. D. & Lifshitz, E. M. *Electrodynamics of continuous media* (Pergamon Press, 1960). 37

[54] Cochran, J. & Dutcher, J. Calculation of the intensity of light scattered from magnons in thin films. *J. Magn. Magn. Mat.* **73**, 299 (1988). URL http://dx.doi.org/10.1016/0304-8853(88)90095-9. 39

[55] Camley, R., Rahman, T. & Mills, D. Theory of light scattering by the spin-wave excitations of thin ferromagnetic films. *Phys. Rev. B* **23**, 1226 (1981). URL http://dx.doi.org/10.1103/PhysRevB.23.1226. 39

[56] Planck, M. Über das gesetz der energieverteilung im normalspektrum. *Annalen der Physik* **4**, 553 (1901). URL http://theochem.kuchem.kyoto-u.ac.jp/Ando/planck1901.pdf. 41

[57] Nolting, W. *Grundkurs Theoretische Physik 6 Statistische Physik* (Springer, 2007). 44, 48

[58] Drude, P. Zur elektronentheorie der metalle. *Annalen der Physik* **306**, 566 (1900). URL http://dx.doi.org/10.1002/andp.19003060312. 45

[59] Pauli, W. The connection between spin and statistics. *Phys. Rev.* **58**, 716 (1940). URL http://dx.doi.org/10.1103/PhysRev.58.716. 46

[60] Fließbach, T. *Quantenmechanik* (Springer Spektrum, 2008). 46

[61] Fermi, E. Zur quantelung des idealen einatomigen gases. *Z. f. Phys.* **36**, 902 (1926). URL http://dx.doi.org/10.1007/BF01400221. 48

[62] Dirac, P. On the theory of quantum mechanics. *Proc. R. Soc. Lond. A* **112**, 762 (1926). URL http://dx.doi.org/10.1098/rspa.1926.0133. 48

[63] Neumann, T., Serga, A. & Hillebrands, B. Probing of a parametrically pumped magnon gas with a nonresonant packet of travelling spin waves. *Appl. Phy. Lett.* **93**, 252501 (2008). URL http://dx.doi.org/10.1063/1.3050530. 55

[64] van Delft, D. & Kes, P. The discovery of superconductivity. *Physics Today* **63**, 38 (2010). URL http://dx.doi.org/10.1063/1.3490499. 55

[65] Bardeen, J., Cooper, L. & Schrieffer, J. Microscopic theory of superconductivity. *Phys. Rev* **106**, 162 (1957). URL http://dx.doi.org/10.1103/PhysRev.106.162. 55, 57

[66] Kapitza, P. Viscosity of liquid helium below the lambda point. *Nature* **141**, 74 (1938). URL http://dx.doi.org/10.1038/141074a0. 55, 56

[67] Landau, L. Theory of the superfluidity of helium ii. *Phys. Rev.* **60**, 356 (1941). URL http://dx.doi.org/10.1103/PhysRev.60.356. 55

[68] Donnelly, R. *Quantized vortices in Helium II* (Cambridge University Press, 1991). 56

[69] Matthews, M. *et al.* Vortices in a bose-einstein condensate. *Phys. Rev. Lett.* **83**, 2498 (1999). URL http://dx.doi.org/10.1103/PhysRevLett.83.2498. 56

[70] Allen, J. & Jones, H. New phenomena connected with heat flow in helium ii. *Nature* **141**, 243 (1938). URL http://www.nature.com/physics/looking-back/superfluid2/index.html. 56

[71] Sato, Y. & Packard, R. Superfluid helium quantum interference devices: physics and applications. *Reports on Progress in Physics* **75**, 016401 (2012). URL http://dx.doi.org/10.1088/0034-4885/75/1/016401. 56, 61

[72] Jaklevic, R., Lambe, J., Silver, A. & Mercereau, J. Quantum interference effects in josephson tunneling. *Phys. Rev. Lett.* **12**, 159 (1964). URL http://dx.doi.org/10.1103/PhysRevLett.12.159. 56, 61

[73] Andrews, M. *et al.* Observation of interference between two bose condensates. *Science* **275**, 637 (1997). URL http://dx.doi.org/10.1126/science.275.5300.637. 56, 61

[74] Kasprzak, J. *et al.* Bose–einstein condensation of exciton polaritons. *Nature* **443**, 409 (2006). URL http://dx.doi.org/10.1038/nature05131. 56, 61

[75] Moskalenko, S. & Snoke, D. *Bose Einstein Condensation of Excitons and Biexcitons and Coherent Nonlinear Optics with Excitons* (Cambridge University Press, 2000). 56

[76] Pitaevskii, L. & Stringari, S. *Bose-Einstein condensation* (Clarendon Press Oxford, 2003). 57, 98

[77] Daunt, J. & Smith, R. The problem of liquid helium - some recent aspects. *Rev. Mod. Phys.* **26**, 172 (1954). URL http://dx.doi.org/10.1103/RevModPhys.26.172. 58

[78] Maris, H. Hydrodynamics of superfluid helium below 0.6k i. viscosity of the normal fluid. *Phys. Rev. A* **8**, 1980 (1973). URL http://dx.doi.org/10.1103/PhysRevA.8.1980. 58

[79] Maris, H. Hydrodynamics of superfluid helium below 0.6k ii. velocity and attenuation of ultrasonic waves. *Phys. Rev. A* **8**, 2629 (1973). URL http://dx.doi.org/10.1103/PhysRevA.8.2629. 58

[80] Maris, H. Hydrodynamics of superfluid helium below 0.6k iii. propagation of temperature waves. *Phys. Rev. A* **9**, 1412 (1974). URL http://dx.doi.org/10.1103/PhysRevA.9.1412. 58

[81] Lavrinenko, A., L'vov, V., Melkov, G. & Cherepanov, V. "kinetic" instability of a strongly nonequilibrium system of spin waves and tunable radiation of a ferrite. *JETP* **81**, 1022 (1981). URL http://www.jetp.ac.ru/cgi-bin/e/index/e/54/3/p542?a=list. 58

[82] Snoke, D. & Wolfe, J. Population dynamics of a bose gas near saturation. *Phys. Rev. B* **39**, 4030 (1989). URL http://dx.doi.org/10.1103/PhysRevB.39.4030. 58

[83] Kalafati, Y. & Safonov, V. Theory of quasiequilibrium effects in a system of magnons excited by incoherent pumping. *JETP* **73**, 836 (1991). URL http://www.jetp.ac.ru/cgi-bin/e/index/e/73/5/p836?a=list. 58

[84] Dzyapko, O., Demidov, V., Demokritov, S., Melkov, G. & Slavin, A. Quasiequilibrium gas of magnons with a nonzero chemical potential: A way to bose-einstein condensation. *J. Appl. Phys.* **101**, 09C103 (2007). URL http://dx.doi.org/10.1063/1.2693891. 59, 61, 64

[85] Demidov, V., Dzyapko, O., Demokritov, S., Melkov, G. & Slavin, A. Thermalization of a parametrically driven magnon gas leading to bose-einstein condensation. *Phys. Rev. Lett.* **99**, 037205 (2007). URL http://dx.doi.org/10.1103/PhysRevLett.99.037205. 59, 61, 64, 74

[86] Dzyapko, O., Demidov, V., Demokritov, S., Melkov, A. & Safonov, V. L. Monochromatic microwave radiation from the system of strongly excited magnons. *Appl. Phys. Lett.* **92**, 162510 (2008). URL http://dx.doi.org/10.1063/1.2910653. 59, 61, 74

[87] Leggett, A. Bose-einstein condensation in the alkali gases: Some fundamental concepts. *Rev. Mod. Phys.* **73**, 307 (2001). URL http://dx.doi.org/10.1103/RevModPhys.73.307. 60

[88] Levinstein, H., Licht, S., Landorf, R. & Blank, S. Growth of high quality garnet thin films from supercooled melts. *Appl. Phys. Lett.* **719**, 3486 (1971). URL http://dx.doi.org/10.1063/1.1653784. 62

[89] Giess, E., Kuptsis, J. & White, E. Liquid phase epitaxial growth of magnetic garnet films by isothermal dipping in a horizontal plane with axial rotation. *J. Crys. Growth* **16**, 36 (1972). URL http://dx.doi.org/10.1016/0022-0248(72)90083-8. 62

[90] Cherepanov, V., Kolokolov, I. & L'vov, V. The saga of yig: Spectra, thermodynamics, interaction and relaxation of magnons in a complex magnet. *Phys. Rep.* **229**, 81 (1993). URL http://dx.doi.org/10.1016/0370-1573(93)90107-O. 63, 76

[91] Dzyapko, O. *et al.* Excitation of two spatially separated bose-einstein condensates of magnons. *Phys. Rev. B* **80**, 060401(R) (2009). URL http://dx.doi.org/10.1103/PhysRevB.80.060401. 63, 73

[92] L'vov, V. *Wave Turbulence under Parametric Excitation* (Springer, 1994). 64

[93] Wettling, W., Andlauer, B., Koidl, P., Schneider, J. & Tolksdorf, W. Optical absorption and faraday rotation in yttrium iron garnet. *Phys. Stat. Sol. (b)* **59**, 63 (1973). URL http://dx.doi.org/10.1002/pssb.2220590105. 68

[94] Nikogosyan, D. Beta barium borate (bbo) a review of its properties and applications. *Appl. Phys. A* **52**, 359–368 (1991). URL http://dx.doi.org/10.1007/BF00323647. 69

[95] Hillebrands, B. Progress in multipass tandem fabry–perot interferometry: I. a fully automated, easy to use, self-aligning spectrometer with increased stability and flexibility. *Rev. Sci. Inst.* **70**, 1589 (1999). URL http://dx.doi.org/10.1063/1.1149637. 82

[96] Mock, R., Hillebrands, B. & Sandercock, R. Construction and performance of a brillouin scattering set-up using a triple-pass tandem fabry-perot interferometer. *J. Phys. E* **20**, 656 (1986). URL http://dx.doi.org/10.1088/0022-3735/20/6/017. 82

[97] Demokritov, S. O., Hillebrands, B. & Slavin, A. N. Brillouin light scattering studies of confined spin waves: linear and nonlinear confinement. *Phys. Rep.* **348**, 441 (2001). URL http://dx.doi.org/10.1016/S0370-1573(00)00116-2. 82

[98] Demokritov, S. & Demidov, V. Micro-brillouin light scattering spectroscopy of magnetic nanostructures. *IEEE Trans. Magn.* **44**, 6–12 (2008). URL http://dx.doi.org/10.1109/TMAG.2007.910227. 82

[99] Borgh, M. O., Keeling, J. & Berloff, N. G. Spatial pattern formation and polarization dynamics of a nonequilibrium spinor polariton condensate. *Phys. Rev. B* **81**, 235302 (2010). URL http://dx.doi.org/10.1103/PhysRevB.81.235302. 85

[100] Troncoso, R. & Núnez, A. Dynamics and spontaneous coherence of magnons in ferromagnetic thin films. *J. Phys.: Cond. Mat.* **24**, 036006 (2012). URL http://dx.doi.org/10.1088/0953-8984/24/3/036006. 85

[101] Nowik-Boltyk, P., Dzyapko, O., Demidov, V., Berloff, N. & Demokritov, S. Spatially non-uniform ground state and quantized vortices in a two-component bose-einstein condensate of magnons. *Nat. Sci. Rep.* **2** (2012). URL http://dx.doi.org/10.1038/srep00482. 86

[102] Berloff, N. & Svistunov, B. Scenario of strongly nonequilibrated bose-einstein condensation. *Phys. Rev. A* **66**, 013603 (2002). URL http://dx.doi.org/10.1103/PhysRevA.66.013603. 87

[103] Li, F., Saslow, W. & Pokrovsky, V. Phase diagram for magnon condensate in yttrium iron garnet film. *Nat. Sci. Rep.* **3**, 1372 (2013). URL http://dx.doi.org/10.1038/srep01372. 88

[104] Andrews, M. *et al.* Propagation of sound in a bose-einstein condensate. *Phys. Rev. Lett.* **79**, 553 (1997). URL http://dx.doi.org/10.1103/PhysRevLett.79.553. 89, 98

[105] Steinhauer, J., Ozeri, R., Katz, N. & Davidson, N. Excitation spectrum of a bose-einstein condensate. *Phys. Rev. Lett.* **88**, 120407 (2002). URL http://dx.doi.org/10.1103/PhysRevLett.88.120407. 89

[106] Simula, T. *et al.* Observations on sound propagation in rapidly rotating bose-einstein condensates. *Phys. Rev. Lett.* **94**, 080404 (2005). URL http://dx.doi.org/10.1103/PhysRevLett.94.080404. 89

[107] Engels, P., Atherton, C. & Hoefer, M. Observation of faraday waves in a bose-einstein condensate. *Phys. Rev. Lett.* **98**, 095301 (2007). URL http://dx.doi.org/10.1103/PhysRevLett.98.095301. 89

[108] Wiseman, H. Defining the (atom) laser. *Phys. Rev. A* **56**, 2068 (2009). URL http://dx.doi.org/10.1103/PhysRevA.56.2068. 100, 107

[109] Robins, N., Altin, P., Debs, J. & Close, J. Atom lasers: Production, properties and prospects for precision inertial measurement. *Phys. Rep.* **529**, 265 (2013). URL http://dx.doi.org/10.1016/j.physrep.2013.03.006. 100, 107

[110] Mewes, M.-O. *et al.* Output coupler for bose-einstein condensed atoms. *Phys. Rev. Lett.* **78**, 582 (1997). URL http://dx.doi.org/10.1103/PhysRevLett.78.582. 100, 107

[111] Bloch, I., Hänsch, T. & Esslinger, T. Atom laser with a cw output coupler. *Phys. Rev. Lett.* **82**, 3008 (1999). URL http://dx.doi.org/10.1103/PhysRevLett.82.3008. 100, 107

[112] Bloch, I., Köhl, M., Greiner, M., Hänsch, T. & Esslinger, T. Optics with an atom laser beam. *Phys. Rev. Lett.* **81**, 030401 (2001). URL http://dx.doi.org/10.1103/PhysRevLett.87.030401. 100, 107

[113] Hundertmark, H. *et al.* Supercontinuum generation with 200 pj laser pulses in an extruded sf6 fiber at 1560 nm. *Optics Express* **11**, 3196 (2003). URL http://dx.doi.org/10.1364/OE.11.003196. 107

Acknowledgements

First of all I would like to thank my doctoral adviser Prof.Dr. Sergej Demokritov for the possibility to be a part of his group and for his support and advice during my studies.

Special thanks go to Dr. Oleksandr Dzyapko who introduced me into the topic of magnon Bose Einstein condensation. He had always an open ear for my questions and problems and helped me in many ways. I owe him a lot of fruitful discussions about physics. Without his guidance I would have been completely lost.

I also thank Dr. Vladislav Demidov who was always there for me to answer all my question regarding magnetization dynamics and measurement technique.

I would also like to thank the other two postdocs Dr. Johann Jersch and Dr. Matthias Buchmeier for their help and support.

I am also grateful to Prof. Reinhold Kleiner and Prof. Dieter Kölle my supervisors for the Diploma thesis at the University of Tübingen who gave me access to their facilities in order to prepare samples for my Ph.D. studies. Additional thanks go to Christoph Back, Markus Turad and Matthias Lange for their support during sample preparation.

A big thanks goes to my parents Jerzy and Bozena Nowik-Boltyk who have always reminded me that education is one of the greatest goods and without whose support I would probably be a completely different person.

And a very special thanks go to my wife Ewa and to my son Luke Nowik-Boltyk for their love and for the joy they brought into my life.

Curriculum Vitae

Personal Data

Name	Patryk Nowik-Boltyk
Date of Birth	03.11.1983
Place of Birth	Graudziadz, Poland
Nationality	German
Name of Parents	Jerzy and Bozena Nowik-Boltyk

Education

1990-1994	Grundschule Berg-Fidel, Münster
1994-2000	Immanuel Kant Gymnasium Münster
2000-2004	Quenstedt Gymnasium Mössingen
2004	Higher Education Entrance Qualification

Higher Education

2004-2010	Study of Physics at the Physics Department of the Eberhard Karls Universität Tübingen
2010	Diploma in Physics. Title of Diploma thesis: *Magnetic Tunnel Junctions from Manganate Heterostructures*

Ph.D. Studies

Since 2010	Ph.D. studies at the Institute for Applied Physics of the Westfälische Wilhelms Universität Münster in the "Nonlinear Magnetization Dynamics" group of Prof. Dr. Sergej O. Demokritov